PULSE DETONATION ENGINE THRUST TUBE HEAT EXCHANGER FOR FLASH VAPORIZATION AND SUPERCRITICAL HEATING OF JP-8

THESIS

Christen L. Miser, Captain, USAF

AFIT/GAE/ENY/05-M11

DEPARTMENT OF THE AIR FORCE
AIR UNIVERSITY

AIR FORCE INSTITUTE OF TECHNOLOGY

Wright-Patterson Air Force Base, Ohio

The views expressed in this thesis are those of the author and do not reflect the official policy or position of the United States Air Force, Department of Defense, or the United States Government.

AFIT/GAE/ENY/05-M11

PULSE DETONATION ENGINE THRUST TUBE HEAT EXCHANGER FOR FLASH VAPORIZATION AND SUPERCRITICAL HEATING OF JP-8

THESIS

Presented to the Faculty

Department of Aeronautics and Astronautics

Graduate School of Engineering and Management

Air Force Institute of Technology

Air University

Air Education and Training Command

In Partial Fulfillment of the Requirements for the

Degree of Master of Science in Aeronautical Engineering

Christen L. Miser, B.S.

Captain USAF

March 2005

AFIT/GAE/ENY/05-M11

PULSE DETONATION ENGINE THRUST TUBE HEAT EXCHANGER FOR FLASH VAPORIZATION AND SUPERCRITICAL HEATING OF JP-8

Christen L. Miser, BS
Captain, USAF

Approved:

/signed/	08 Mar 05
Paul I. King (Chairman)	date
/signed/	09 Mar 05
Ralph A. Anthenien (Member)	date
/signed/	08 Mar 05
Milton E. Franke (Member)	date

Abstract

Research has shown that performance of liquid hydrocarbon fueled pulse detonation engines is limited by the time required to evaporate liquid fuel droplets within the mixture. Vaporization of liquid fuels prior to injection has been shown to decrease ignition times and also increases fuel efficiency; however, the size and efficiency of the vaporization system used are not feasible for use in future pulse detonation aircraft concepts. The purpose of this research is to harness the waste heat of pulse detonation engine thrust tubes to generate a steady-state, self-sustained flash vaporization and supercritical heating system using JP-8 as the working fluid and fuel.

Using a pulse detonation engine thrust tube mounted heat exchanger, the successful flash vaporization of JP-8 has been demonstrated. Additional testing demonstrated the successful heating of JP-8 to supercritical conditions with fuel injection temperatures over 760 K. All JP-8 flash vaporization and supercritical heating tests were sustained by the heated fuel and run to steady-state conditions. Heat addition rates to the fuel of up to 7.7 kW were achieved during superheated testing. A method for experimentally determining supercritical fluid density is presented based on the findings of the supercritical heating tests.

Acknowledgements

I would like thank my thesis advisor Dr. Paul King for the opportunity to work with PDE and the continuous support, knowledge, and time to make it through this work. Thank you to my committee members Dr. Ralph Anthenien and Dr. Milton Franke for taking the time nudge me onto the correct path when I wandered astray. Special thanks to Dr. Anthenien for the heat transfer help during non-office hours.

Without my sponsor Dr. Fred Schauer none of this would have happened. Thank you for supporting my work and allowing me to push the envelope. Many thanks to Dr. John Hoke for the heat transfer help and promoting me through the D-Bay ranks. To Royce Bradley I am extremely indebted for his wisdom, knowledge, creative acquisition, and occasional admonishment. Thank you to my right hand man Curtis Rice. Whether we were turning wrenches or running near off condition you're always there to help. Thank you to Dave Baker and Dwight Fox for their incredible workmanship.

Thank you to Colin Tucker for showing me the ropes and providing the foundation for everything I accomplished. My appreciation goes out to Jeffrey Stutrud for the software to make sense of the mountains of data. Thank you to Dr. Tim Edwards for all of the fuels support, resources, and most importantly the fuel. Thanks to Thanh Chu for trying to keep me safely within reason and regulations. Thank you to Mike Mcleish for continually being a voice of reason. We made it. Thank you to my successor, Timothy Helfrich for the helping with the testing. I gave you the key, you have to open the door. Last but not least thank you to my faculty and friends at AFIT. Going back to school couldn't have been a more rewarding experience in class and out.

Table of Contents

Page

Page

List of Figures

Page

Page

Page

Page

Page

List of Tables

Page

List of Symbols

Acronyms

AIAA	American Institute of Aeronautics and Astronautics
AFRL	Air Force Research Laboratory
AFRL/PR	Air Force Research Laboratory Propulsion Directorate
ASME	American Society of Mechanical Engineers
CJ	Chapman-Jouguet
CRC	Coordinating Research Council
DDT	Deflagration to detonation transition
FN	Flow number
FVS	Flash vaporization system
NASA	National Air and Space Administration
NIST	Nation Institute of Standards and Technology
NPT	National Pipe Thread
PDE	Pulse detonation engine
RO	Reverse osmosis
SS	Steady-state

Greek Symbols

ρ	Density [kg/m^3]
γ	Ratio of specific heats
ϕ	Equivalence ratio
σ	Stefan-Boltzmann constant [5.67*10-8 $W/(m^2\text{-}K^4)$]
ε	Emissivity
β	Expansion coefficient [1/K]
ν	Kinematic viscosity [m^2/s]
μ	Dynamic viscosity [$(N\text{-}s)/m^2$]
α	Thermal diffusivity [m^2/s]

Symbols

A	Area [m^2]
a	Speed of sound (m/s)
C	Carbon
c_p	Specific heat [kJ/(kg-K)]
g	Acceleration due to gravity [m^2/s]
Gr	Grashof number
H	Hydrogen
h	Heat transfer coefficient [W/(m^2-K)]
k	Thermal conductivity [W/(m-K)]
M	Mach number
MW	Molecular weight [kmol/kg]
O	Oxygen
N	Nitrogen
Per	Perimeter [m]
P	Pressure [Pa]
Pr	Prandtl number
q	Heat transfer rate per unit length [kW/m]
Q	Heat transfer rate [kW]
R	Gas constant [kJ/(kg-K)]
Ra	Rayleigh number
Re	Reynolds number
R_{univ}	Universal gas constant [8.314 kJ/(kmol-K)]
T	Temperature [K]
u	Velocity [m/s]
Vol	Volume (m^3)

Subscripts

1	State one, reactants
2	State two, products
inlet	Heat exchanger inlet
outlet	Heat exchanger outlet
fuel	Fuel
air	Air
water	Water
mix	Fuel-air mixture
sto	Stoichiometric
dot	Time rate of change of quantity
sur	Property of AFRL SUPERTRAPP JP-8 surrogate
o	Outer tube for single tube configuration
i	Inner tube for single tube configuration
film	Film condition, average of outer tube and ambient
rad	Radiation
fc	Free convection
dia	diameter
amb	Ambient
plain_tube	Plain tube
tube	Property for tube
flame	Average condition inside PDE tube
cal	Calormetric
ii	Inner tube inner surface
io	Inner tube outer surface
oi	Outer tube inner surface
oo	Outer tube outer surface
in	In to the system
out	Out of the system
trans	Transmitted to the system
fluid	Heat exchanger fluid

PULSE DETONATION ENGINE THRUST TUBE HEAT EXCHANGER FOR FLASH VAPORIZATION AND SUPERCRITICAL HEATING OF JP-8

I. Introduction

Study of detonations have been recorded since the work of Hoffman in the 1940s (Hoffman, 1940). However, until the late 1980s the study of detonations and the pulse detonation engine as a means of propulsion had seen limited interest. Since the late 1980's there has been an explosion in pulse detonation engine research rooted in the higher thermal efficiencies of the constant volume process which detonations closely emulate. It has been understood for sometime that the constant volume process has thermal efficiencies much higher than that of constant pressure processes (Eidelman, 1991) used in most of today's current aeronautical propulsion systems.

In addition to the high thermal efficiency of pulse detonation engines, benefits include low cost, mechanical simplicity, few moving parts, scalability, and a wide range of operation. Expected applications of pulse detonation engines include cruise missiles and unmanned aerial vehicles. Hybrid concepts using pulsed detonation engines as an afterburner in turbojet engines or as an additional thrust source in the bypass of turbine engines are being studied. Other research efforts include combined engine concepts where pulse detonation engines are used up to hypersonic velocities at which time scramjets engines are utilized (Kailasanath, 2003). Space applications include pulse detonation rocket engines which are currently being researched and tested by Air Force Research Laboratory and NASA (Kailasanath, 2003)

Motivation

While the prospective applications of pulse detonation engines are extensive, there are numerous technological and logistical hurdles that must be overcome before pulse detonation engines may transition from the experimental environment to operational use.

The majority of pulse detonation research uses hydrogen or gaseous hydrocarbon fuels (Glassman, 1996:224). These fuels are readily available, provide excellent repeatability, and the gaseous state of the fuel contributes to excellent detonability characteristics. Conversely, the use of liquid hydrocarbon fuels has been extremely limited due to the difficulty in obtaining detonations. While there has been limited success in using liquid hydrocarbons and various aviation fuels, the complexity of the systems used has prevented the integration of liquid fuels as the standard for experimental pulsed detonation research. As the maturity of pulse detonation engine technology advances, the integration of liquid hydrocarbon fuels is paramount to the success of the pulse detonation engine as a viable propulsion system.

Additionally, the United States Air Force and Navy have invested significant funding and research into pulse detonation research in hopes of high military payoff for use in a wide array of aerospace military applications. If any of these applications are to come to fruition, the use of military grade turbine fuels such as JP-8 and JP-10 will be essential. The processes and additives meant to enhance the stability of these fuels provide additional complications by further decreasing the detonability of the fuel.

Problem Statement

Recent research has shown that the difficulties of using liquid hydrocarbon fuels and even military grade turbine fuels in pulse detonation engines are surmountable by the use of complex atomization and mixing methods or by the use of flash vaporization systems. The use of an external electrically powered flash vaporization system was successfully employed to flash vaporize JP-8 (Tucker, 2004) While these systems demonstrated the use of the liquid hydrocarbon fuels of interest, the feasibility of incorporating such systems on aircraft designs are not practical. The focus of this research is to further the development of a practical fuel vaporization and supercritical heating system that will allow the use of military grade turbine fuels in pulsed detonation engines without the use of complex fuel atomization or injection methods and without the use of an external power source.

Previous Flash Vaporization Systems

This research is being completed as a direct follow on to works completed by Dr. Colin Tucker and sponsored by Air Force Research Laboratories Pulse Detonation Research Facility (Tucker, 2004). In the previous flash vaporization system, a 20 kW external electric heater in a nitrogen inert furnace was used to statically heat pressurized JP-8 to temperatures well above the auto-ignition temperatures of the fuel. The heated fuel was pressure fed through fuel nozzles allowing a premixed flash vaporized fuel/air mixture.

Tucker's work demonstrated the first successful detonation of JP-8 in a working pulse detonation engine. The research was also successful in measuring the quantitative

benefits of flash vaporizing the fuel, in addition to characterizing the required parameters necessary to achieve flash vaporization in liquid hydrocarbon fuels, specifically JP-8. To the author's knowledge, no documented flash vaporization system has been used in pulse detonation research prior to Tucker's work.

Pulse Detonation Heat Transfer Research

There have been a number of papers written on the heat losses and heat loads in pulse detonations engines (Radulescu, 2004; Hoke, 2003; Eidelman, 2000; Paxson, 2004). The focus of these papers has been to determine the heat loads and the effect on performance due to heat losses. To the author's knowledge none of these papers have used liquid hydrocarbons as the detonating fuel or emphasized the possibility of using the heat losses as a potential energy source.

Hoke et al. (Hoke, 2003) performed a calorimetrical heat load analysis to determine how heat load varied as a function of multiple operating parameters. These tests provided insight into heat loads generated with hydrogen detonations and with shorter tube lengths than those required for liquid hydrocarbon fuels. Analytical work by Radulescu et al. studied the effect of heat losses on performance and how the heat losses varied as a function of the length of tube to tube diameter (Radulescu, 2004). Eidelman et al. developed simulations to model wall temperature and heat transfer as a function various design parameters using hydrogen as the fuel (Eidelman, 2004). Paxson and Perkins studied the cooling required for a hybrid engine with pulsed detonation tubes acting as the afterburner in gas turbine based engine (Paxson, 2004). It was their conclusion that the cooling required drastically reduced the performance benefit of the

hybrid engine concept. The cooling methods used were forced or free air convection and varying engine parameters rather than using the fuel as a heat sink.

Research Goals

It is the primary goal of this research to use the waste heat generated by the pulse detonation engine cycle to develop a steady-state, self-staining, flash-vaporization and supercritical heating system for military grade JP-8 turbine fuel. The safety risks and experimental uncertainties in such a venture require many intermediate goals to be met to ensure the feasibility and safety of meeting the primary objective. The following is a list of the intermediate goals met in order to achieve the primary goal.

1. Determine if sufficient waste heat is available to flash vaporize and superheat military grade JP-8 turbine fuel
2. Design and construct a PDE tube mounted heat exchanger and flash vaporization system
3. Complete water-cooled tests using hydrogen as the detonation fuel to determine heat transfer and prove design concept
4. Complete aviation gasoline and JP-8 detonation tests without the use of the heat exchanger to determine thrust tube heat transfer and axial temperature profiles
5. Complete water-cooled tests using aviation gasoline as the detonation fuel to determine further heat transfer estimates
6. Complete safety approval process for using a JP-8 cooled heat exchanger

7. Conduct JP-8 cooled heat exchanger tests using heated JP-8 as the detonation fuel.

8. Determine and test at operating condition where steady-state, self-sustained, flash vaporization of JP-8 occurs using a JP-8 cooled heat exchanger using heated JP-8 as the detonation fuel.

9. Determine and test at operating condition where steady-state, self-sustaining, supercritical heating of JP-8 occurs using a JP-8 cooled heat exchanger using heated JP-8 as the detonation fuel.

Chapter Summary

The high thermal efficiencies of pulse detonation engine propulsion systems have drawn significant attention in the research community. One of the largest challenges in the advancement of pulse detonations engine technologies and fielding of pulse detonation engine powered vehicles is the transition from the use of gaseous fuels to liquid hydrocarbons. A complex flash vaporization system has been demonstrated as a viable method for using liquid hydrocarbon fuels It is the purpose of this work to use a PDE tube mounted heat exchanger harnessing the waste heat to develop a flash vaporization and supercritical JP-8 fuel heating system.

Organization

Chapter I served as a brief introduction to pulse detonation engine technology. In addition the motivation, problem statement, and goals for this work are discussed. Chapter II provides the engineering foundation for this research beginning with the explanation of the detonations and the concept of a pulse detonation engine. The

development of JP-8 property data and the heat transfer methods used are also presented. In Chapter III, the facility, pulse detonation engine, instrumentation, and test configurations are discussed. Chapter IV provides the results and analysis of experimental data and an experimental method for determining supercritical density. Chapter V discusses the conclusions from the previous chapters and provides recommendations for further research.

II. Background

Detonation Overview

When a tube open at both ends is filled with an explosive fuel-air mixture and ignited at either end the flame front will progress into the flammable mixture. The products of the reaction behind the flame front have a higher temperature and specific volume in comparison to the unburned mixture. However, because the tube is open at both ends the local pressure rise created by the increase in specific volume is allowed equalize with the ambient environment and the flame travels at the steady rate at which it can burn the reactants. The flame front in this reaction is a deflagration wave.

When a tube closed a one end is filled with an explosive fuel-air mixture and ignited at the closed end the flame front will progress into the flammable mixture. The products of the reaction trailing the flame front have a higher temperature and specific volume than the unburned mixture. The increase in specific volume creates a compression wave that travels at the speed of sound until it reaches the flame front causing the flame to accelerate. As the flame continues to burn the compression waves are continually emanated by the increase in specific volume behind the wave. The compression waves also create an increase in temperature and consequently an increase in the speed of sound which causes each compression wave to catch up to the previous waves and coalesce at the flame front further increasing the speed of flame front. The increase in the flame speed also generates turbulence in the flame which causes further acceleration in the flame front.

If the tube is long enough the acceleration of the flame front will continue until a shock is formed from the coalescing compression waves. The shock wave generated is strong enough to ignite the mixture ahead of the flame front. The reaction behind the shock front continuously sends forward compression waves preventing the shock wave from decaying. This self-sustaining shock wave coupled with its following reaction front is termed a detonation wave.

Typical ratios of detonations and deflagrations are presented in Table 1 for comparison, with state one and state two represented in Figure 1. Note that the detonation pressure ratio is an order of magnitude greater than deflagrations waves and also that the detonation waves travel at Mach numbers several orders of magnitudes higher than deflagration waves.

Table 1. Typical detonation and deflagration property ratios (Glassman, 1996:223)

	Usual magnitude of ratio	
Ratio	Detonation	Deflagration
u1/a1	5 - 10	0.0001 - 0.03
u2/u1	0.4 - 0.7	4 - 16
P2/P1	13 - 55	0.98 - 0.976
T2/T1	8 - 21	4 - 16
$\rho 1/\rho 2$	1.4 - 2.6	0.06 - 0.25

Detonation Background

Consider a one dimensional combustion wave that travels through a channel from left to right. Relative to the wave, the reactants moving into the wave at a velocity, u_1, and the products are leaving the wave at a velocity, u_2, as shown in Figure 1.

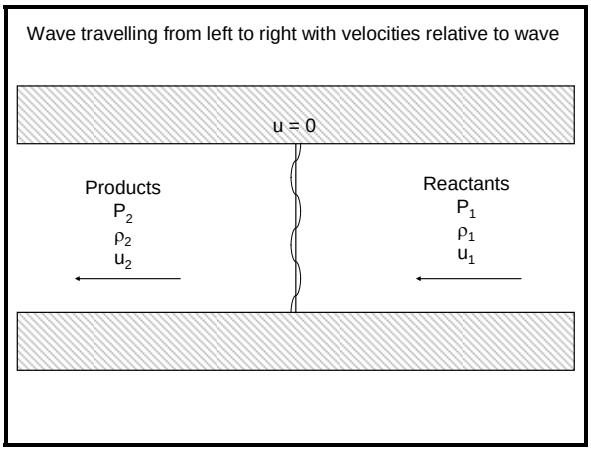

Figure 1. One dimensional combustion wave traveling through channel with velocities relative to the wave front

The one dimensional conservation of mass, momentum, and energy equations are

$$\rho_1 \cdot u_1 = \rho_2 \cdot u_2 \tag{1}$$

$$P_1 + \rho_1 \cdot u_1^2 = P_2 + \rho_2 \cdot u_2^2 \tag{2}$$

$$c_p \cdot T_1 + \frac{1}{2} \cdot u_1^2 + q = c_p \cdot T_2 + \frac{1}{2} \cdot u_2^2 \tag{3}$$

If the ideal gas law and constant gas constant can be assumed for both the reactants and the products then

$$P_1 = \rho_1 \cdot R \cdot T_1 \tag{4}$$

$$P_2 = \rho_2 \cdot R \cdot T_2 \tag{5}$$

Additionally the speed of sound and Mach number relations are

$$M_1 = \frac{u_1}{a_1} \tag{6}$$

$$M_2 = \frac{u_2}{a_2} \tag{7}$$

$$a_1 = \sqrt{\gamma \cdot R \cdot T_1} = \sqrt{\frac{\gamma \cdot P_1}{\rho_1}} \tag{8}$$

$$a_2 = \sqrt{\gamma \cdot R \cdot T_2} = \sqrt{\frac{\gamma \cdot P_2}{\rho_2}} \tag{9}$$

By substitution and re-arranging the above equations (Glassman, 1996:228) it can be shown that

$$q = \frac{\gamma}{\gamma - 1} \cdot \left(\frac{p_2}{\rho_2} - \frac{p_1}{\rho_1} \right) - \frac{1}{2} \cdot \left[(p_2 - p_1) \cdot \left(\frac{1}{\rho_1} + \frac{1}{\rho_2} \right) \right] \tag{10}$$

Equation (10) is known as the Hugoniot equation. Assuming values for density and pressure at state one and assigning a value for q, the possible solutions for the pressure and density of state two can be determined by setting a range variable for one of the unknowns and solving for the other. In this manner the Hugoniot curve is generated as shown in Figure 2.

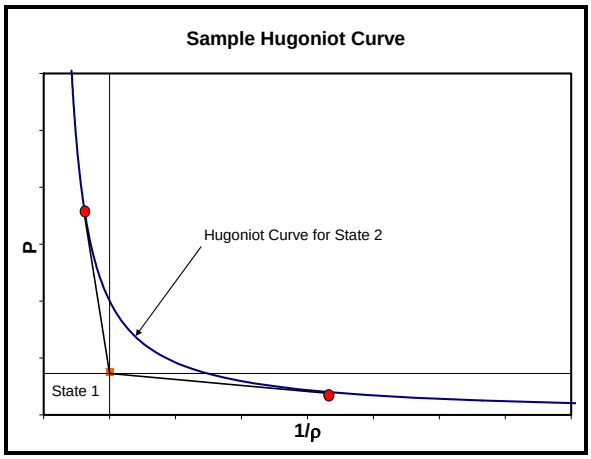

Figure 2. Pressure versus inverse density for initial state and Hugoniot curve for state 2

By drawing parallel lines to each axis through state one and also drawing lines from state one to the tangents of the Hugoniot curve for state two, the curve can be segmented into five portions. Only certain portions of the Hugoniot curve represent solutions that are physically possible. These portions can be further differentiated into steady-state and transient solutions represented in Figure 3. Only one steady-state solution occurs at pressures greater than the initial state. This point is known as the Chapman-Jouguet (CJ) point and corresponds to a self-sustained detonation. The dashed region above the CJ point refers to a strong detonation which is an unstable condition that will equalize to the CJ point. The dashed region below the CJ point refers to a weak detonation. For this solution to exist extremely fast chemical kinetics are required. The kinetics of liquid hydrocarbon fuels, such as JP-8, does not permit this solution. The solutions to the right of the state one refer to deflagrations. (Glassman, 1996:232-235)

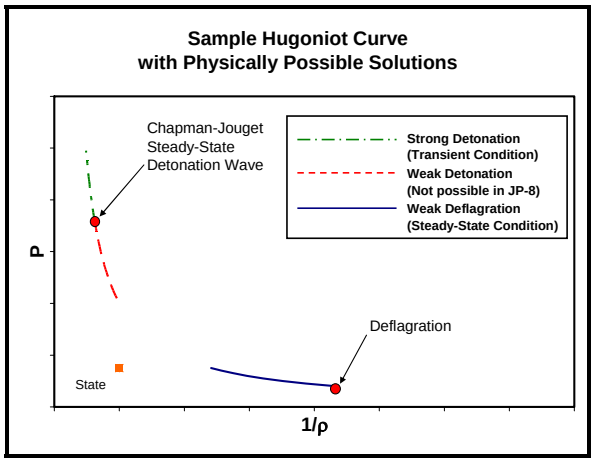

Figure 3. Pressure versus inverse density for initial state and Hugoniot curve with physically possible solutions for state two

For propulsion purposes the CJ point is the desired steady-state solution. Of the possible solutions the CJ point corresponds to the state with the minimum entropy (Glassman, 1996:236) and reaches supersonic detonation wave velocities with large pressure ratios. The wave speed of the CJ point has become one of the governing metrics for determining when detonations are present. The CJ wave speed for most hydrocarbon-air mixtures with equivalence ratios from 1.0 – 2.0 are between 1700 m/s and 2000 m/s (Glassman, 1996;247)

Pulse Detonation Engine Cycle

The generalized pulse detonation engine (PDE) cycle is composed of fill, detonation, and purge processes represented in Figure 4, Figure 5, and Figure 6 respectively. In the fill process a valve is opened filling the PDE tube with an explosive fuel-air mixture. The ratio of the fuel-air mixture volume to the tube volume is referred to as the fill fraction. A fill fraction of one represents the entire tube filled with a fuel-air mixture while a fill fraction of 0.5 indicates half of the tube is filled. For the purpose of

this work the fill fraction was kept at one. When the fill process is complete the fill valve is closed.

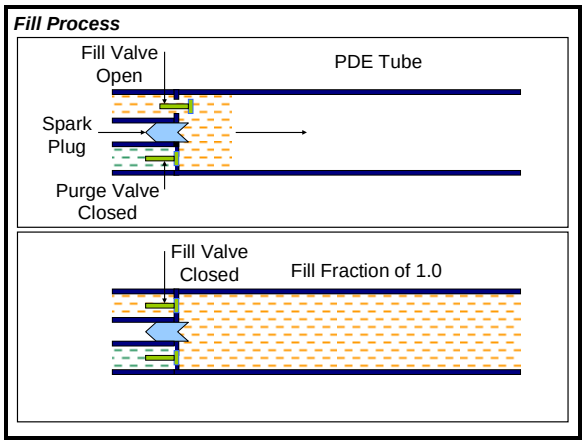

Figure 4. Generalized PDE fill process with valve opening to fill the PDE tube with fuel-air mixture

The detonation process is typically thermally initiated. For this work the ignition energy was provided by an automotive spark ignition system. The ignition begins a deflagration at the closed end of the tube which transitions to a detonation by the process mentioned earlier in this chapter. The transition from a deflagration to a detonation is known as the detonation to deflagration transition (DDT). The time and distance required to achieve DDT are to be minimized for optimum PDE performance. Thrust for the PDE is generated during blowdown when the products are exhausted by the finite change in momentum and also due to the pressure ratio at the exit area.

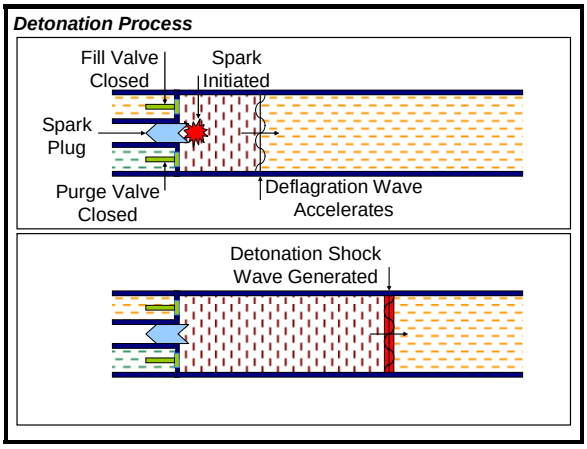

Figure 5. Spark initiated PDE detonation process with transition from deflagration wave to detonation wave

In the purge process the purge valve opens and fills the tube with a non-explosive air mixture to purge the exhaust products from the tube. The purge air also cools the PDE tube and remaining products. The purpose of the purge process is to prevent a standing flame from occurring that would lead to a backfire. The purge fraction is the ratio of purge air volume to the PDE tube volume. The purge fraction for this work was 0.5. Once the tube has been filled with the designated purge fraction the purge valve is closed and the PDE cycle is repeated.

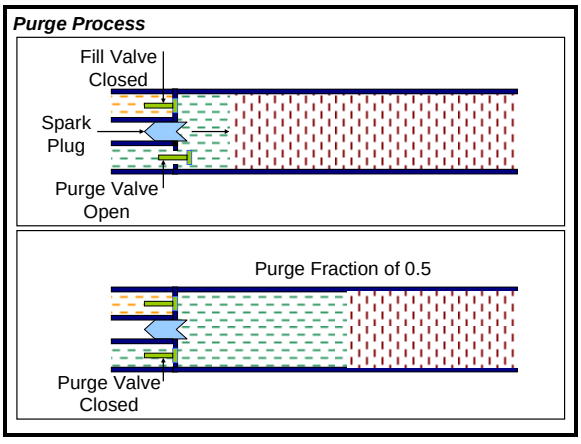

Figure 6. Generalized PDE purge process with valve opening to purge the PDE tube with air

Flash Vaporization

Flash vaporization is a process that occurs between two states. The initial state required for flash vaporization is characterized by a fluid at an elevated temperature and pressure. The second state is characterized by a significantly lower pressure and constant enthalpy if the process is assumed adiabatic. If the pressure drop occurs rapidly the fluid passes through the vapor dome and the final state of the substance will be a vapor. The state flash vaporization temperature is defined as the temperature that intersects the state pressure with the saturated vapor line. The process from state one to state two is represented in the pressure-enthalpy diagram for the AFRL SUPERTRAPP JP-8 surrogate in Figure 7. The development of the data for this figure is presented later in this chapter.

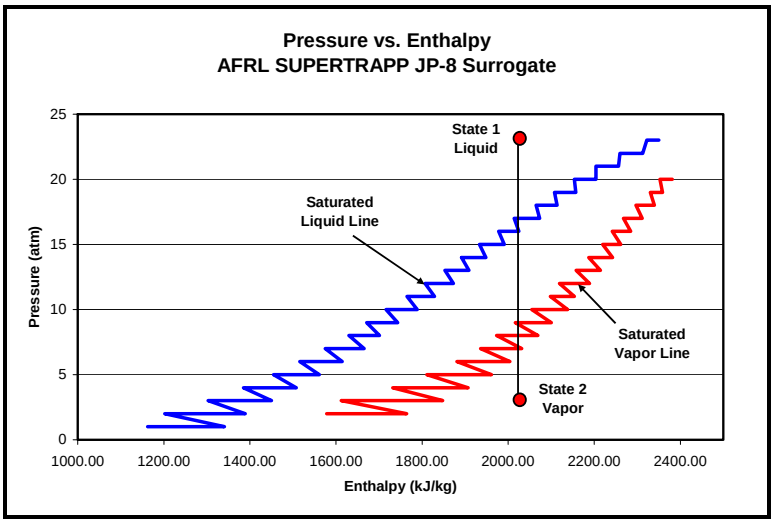

Figure 7. Pressure versus enthalpy diagram of AFRL SUPERTRAPP JP-8 surrogate with vapor dome and flash vaporization process path

In the PDE engine the fuel is injected into an air stream through the use of fuel nozzles. The pressure after the injection point may be assumed to be at ambient pressure. Assuming the pressurized heated liquid fuel is at or above the saturated vapor

temperature for ambient pressure; the pressure drop that occurs across the nozzles will flash vaporize the fuel locally in the fuel stream. If the air stream is not at a temperature at or above the dew point temperature of the mixture, some of the fuel in the mixture will re-condense.

The concept of local flash vaporization and mixture dew point temperature is illustrated in a generic mixture temperature versus fuel temperature diagram shown in Figure 8. In two cases the air is heated prior to fuel injection to air temperatures T_{air1} and T_{air2} with $T_{air1}>T_{air2}$. For the fuel temperature range the mixture temperature for the case with T_{air2} does not exceed dew point temperature of the mixture (T_{dpmix}) and does not completely vaporize the mixture, but it does locally flash vaporize the fuel at fuel temperatures greater than or equal to the fuel flash vaporization temperature (T_{fvfuel}). Over the same range of fuel temperature for the case with T_{air1} the mixture temperature surpasses the mixture dew point temperature and the fuel mixture becomes completely vaporized.

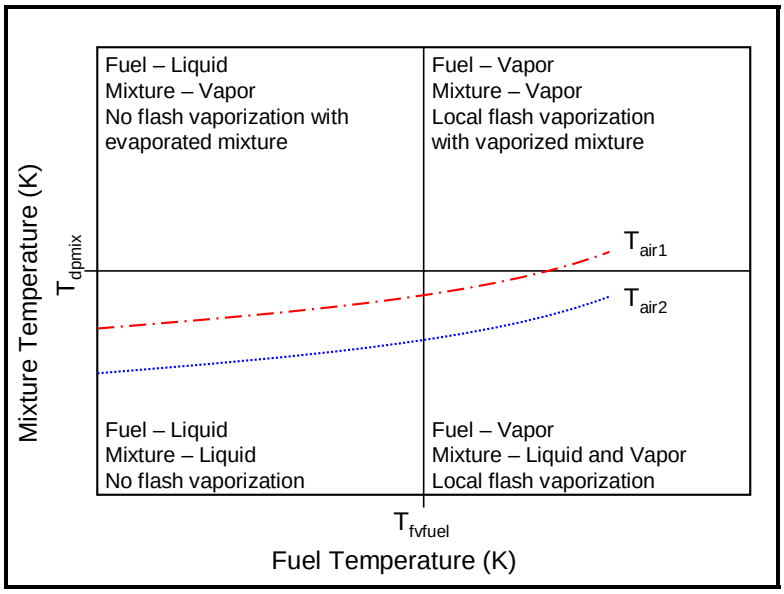

Figure 8. Mixture temperature versus fuel temperature for two air temperatures at constant air pressure

The mixture temperature versus JP-8 fuel temperature for various air temperatures is presented in Figure 9. This data was generated analytically and experimentally verified (Tucker, 2005). For JP-8 the mixture temperature required for a completely vaporization is 400 K (Tucker, 2005). The JP-8 flash vaporization temperature shown in Figure 9 is 530 K.

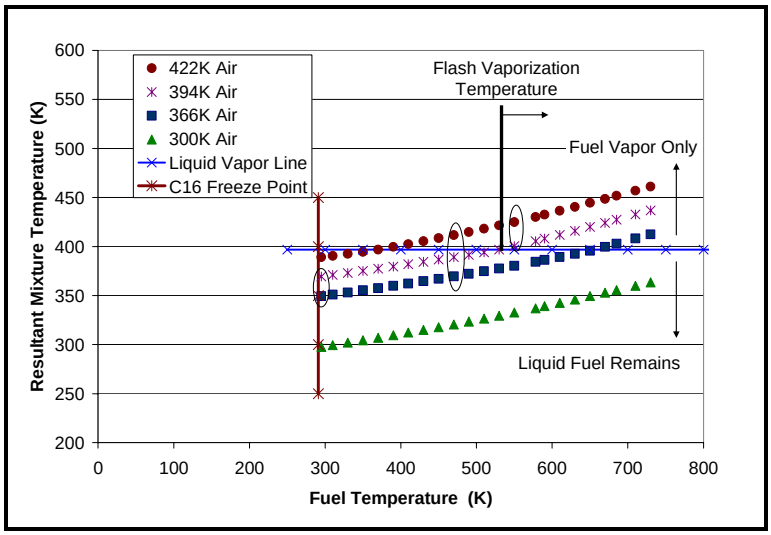

Figure 9. Stoichiometric JP-8 surrogate air mixture liquid vapor equilibrium in the intake manifold for 4 air temperatures at 2 bar. (Tucker, 2005)

Supercritical JP-8

The critical point is the point where the slope of the vapor dome is zero as shown in Figure 10. The critical pressure and temperature are values that intersect at the critical point. For pressures and temperatures greater than or equal to the critical pressure and temperature the substance can no longer be considered a liquid or vapor. At these values the substance is referred to as supercritical. The pressure-temperature diagram used for JP-8 is presented in Figure 10. The development of the figure is presented in the following section. The critical pressure and critical temperature of JP-8 are 23.3 atm and 683 K respectively (Szetela, 1981).

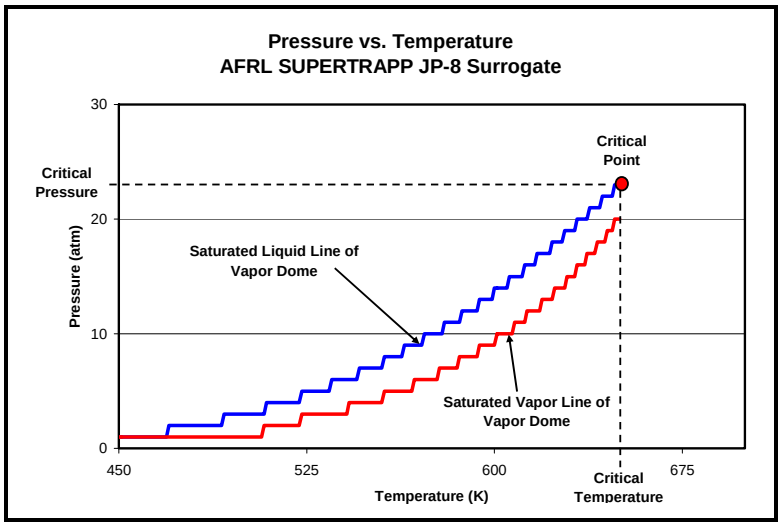

Figure 10. Pressure versus temperature diagram of AFRL SUPERTRAPP JP-8 surrogate with vapor dome and critical point

JP-8 Thermodynamic Properties Data

The flash vaporization system design and analysis required the thermodynamic property data of JP-8 from room temperature to supercritical temperature ranges of up to 800 K. The lower temperature property data can be obtained from the CRC Handbook of Aviation Fuel Properties (CRC, 2004). Unfortunately, the property data is only provided for temperatures up to 393 K for JP-8. To the author's knowledge, there is no complete set of thermodynamic data for JP-8 above this temperature that includes density, specific heat, viscosity, and thermal conductivity.

The lack of high temperature JP-8 property data is attributed to two reasons. First and foremost, there has not been a widespread need for data at these temperatures. In most engineering applications it is not necessary, or desirable, to operate with fuel at supercritical temperatures and pressures. Second there are no current methods to determine the fuel properties at these temperatures and pressures. The enthalpy and specific heat of high temperature fuels may be determined by heat transfer tests but

without the other key thermodynamic properties there is limited benefit. As a result of this work an experimental method for determining high temperature fuel density is presented.

Since JP-8 is not a pure substance it also difficult to model the fuel based on its chemical makeup. To model characteristics or properties of JP-8 a surrogate was used. A surrogate is a mixture of hydrocarbons that are pure substances for which the chemistry is known. The surrogate is developed to mimic certain characteristics or properties of the fuels.

PPDS2 and SUPERTRAPP are two known software packages that predict the thermophysical property data based on a surrogate mixture. PPDS2 is a commercially available thermophysical properties calculation engine and associated databanks for obtaining the thermodynamic, transport and phase equilibria properties for fluids and fluid mixtures (PPDS, 2005). SUPERTRAPP is a product of the National Institute of Standards and Technology (NIST). SUPERTRAPP is an interactive computer database for the prediction of thermodynamic and transport properties of fluid mixtures (NIST, 2003).

For this work SUPERTRAPP was used to develop the required thermodynamic property data for a surrogate JP-8 mixture. The surrogate used in the development of the data was provided by Air Force Research Laboratory Propulsion Directorate (AFRL/PR). The surrogate composition, hereto referred to as the AFRL SUPERTRAPP JP-8 surrogate, is presented in Table 2.

Table 2. AFRL SUPERTRAPP JP-8 surrogate composition (Spadaccini, 1998)

Component	SUPERTRAPP Synonym	Mole Fraction	Mass Fraction
methylcyclohexane	MCC6	0.065	0.042
meta-xylene	MXYL	0.07	0.049
ethylcyclohexane	ECC6	0.067	0.050
n-decane	C10	0.157	0.147
butylbenzene	C4BNZ	0.056	0.050
isobutylbenzene	IC4BNZ	0.056	0.050
nampthalene	NAPH	0.058	0.049
n-dodecane	C12	0.175	0.207
1-methylnapthalene	1MNAPH	0.052	0.049
n-tetradecane	C14	0.113	0.156
n-hexadecane	C16	0.066	0.104
2,5-dimethylhexane	25DMH	0.065	0.049

The determination to use the AFRL surrogate was based on agreement with the CRC Handbook of Aviation Fuel Properties in the available temperature range and with other surrogate model data available at the limited pressures and temperatures available. The comparison surrogate data was also provided by AFRL/PR. The first comparison surrogate data was compiled in SUPERTRAPP based on a surrogate developed by Schulz (Henegan and Schulz, 1993). The second surrogate data was compiled in PPDS2 based on a proprietary surrogate. Both of these data sets were generated for a pressure of 6.895 MPa.

The AFRL SUPERTRAPP data generated compared well with low temperature CRC data and with the two comparison surrogate data sets at the prescribed pressure of 6.895 MPa as shown in Figure 11.

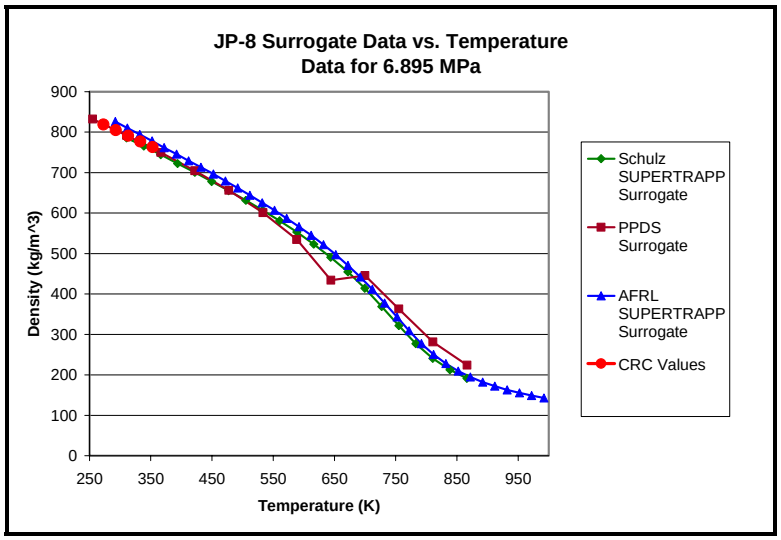

Figure 11. Modelled JP-8 surrogate density at 6.895 MPa and CRC JP-8 comparison

The AFRL SUPERTRAPP surrogate presented in Table 2 met the measures of success prescribed and is used for all design calculations and analysis. The surrogate shall be referred to as the AFRL surrogate for the remainder of this document. Density, specific heat, viscosity, and thermal conductivity tables were generated for temperatures ranging from 273-998 K and pressures ranging from 1-85 atm using the AFRL surrogate in SUPERTRAPP. Using the state information provided by SUPERTRAPP the vapor pressure curve was also generated. All AFRL surrogate data generated by SUPERTRAPP is provided in Appendix A.

Power Required

For steady-state conditions with no work and negligible contributions from velocity and elevation, the specific energy required to heat JP-8 over a temperature differential can be determined from the reduced form of the energy equation (Incropera and DeWitt, 1996:399)

$$q = \int_{T_{inlet}}^{T_{outlet}} c_p(T)\, dT \tag{11}$$

Graphically this equation represents the area under the curve between any two temperatures on a specific heat versus temperature curve. With the specific heat data generated for the AFRL SUPERTRAPP JP-8 surrogate the finite difference method was used to determine the specific energy required between any two temperatures. For the purpose of this work the cold temperature was conservatively set to 290 K. The hot temperature chosen for the initial heat exchanger design was 530 K. The heat of combustion of the JP-8 used in the tests was 43.3 MJ/kg. From Eq. 11 the specific energy required is 554 kJ/kg or 1.3% of the energy available in the fuel.

To determine the power required, the mass flow must be calculated. The mass flow calculation is determined from the engine operating parameters and the chemistry of the fuel-air mixture. The engine operating parameters provide the volumetric flow rate and mixture chemistry provides the correlation to mass flow rate.

The volumetric flow of the fuel-air mixture is a dependent on engine frequency, fill fraction, number of PDE tubes, and tube volume. Engine frequency is a user input parameter and for design purposes is constant at 15 Hz. The tube volume for one 1.829 m tube with a 5.25 cm diameter is 0.004 m^3. Mechanical limitations of the current PDE engine require a two-tube configuration for liquid fuel operation. Since only one heat exchanger is to be installed during the tests for this work the mass flow requirements will be based on a two-tube configuration. Fill fraction was unity for this work. The total volumetric flow of the engine is then determined by

$$\frac{d(Vol)}{dt} = (Frequency)\cdot(Tube\_Volume)\cdot(Fill\_Fraction)\cdot(Number\_of\_Tubes) \tag{12}$$

The equivalence ratio is the ratio of the design or test fuel-air mixture divided by the ratio of fuel-air mixture for stoichiometric conditions (Glassman, 1996:21). An equivalence ratio of unity is termed stoichiometric. A stoichiometric mixture is the ideal ratio of fuel and air so that all of the air and all of the fuel are consumed in the reaction.

$$\phi = \frac{\left(\frac{m_{fuel}}{m_{air}}\right)_{act}}{\left(\frac{m_{fuel}}{m_{air}}\right)_{sto}} \tag{13}$$

Equivalence ratios of greater than one indicate there is not sufficient air to allow for complete combustion of the fuel and is referred to as rich. Equivalence ratios of less than one indicate there is excess air for the fuel present and is referred to as lean.

Since JP-8 is not a pure substance the chemical formula for its composition is unknown and in most cases proprietary to the manufacturer. The chemical formula is approximated as $C_{10.9}H_{20.9}$. To determine the stoichiometric ratio of JP-8 and air the following chemical equation must be balanced for Y, A, B, and C.

$$1\cdot\left(C_{10.9}H_{20.9}\right) + Y\cdot\left(O_2 + \frac{79}{21}\cdot N_2\right) = A\cdot\left(C\cdot O_2\right) + B\cdot\left(H_2\cdot O\right) + C\cdot\left(N_2\right) \tag{14}$$

Solving for A, B, C, and Y yeilds

$$A = 10.900 \quad B = 10.450 \quad Y = 16.125 \quad C = 60.66$$

The mass of the fuel and air are obtained by multiplying the molar values above by the molecular weight. The stoichiometric ratios of air-fuel and fuel-air mixture for JP-8 are obtained

$$\left(\frac{m_{air}}{m_{fuel}}\right)_{sto} = 14.575 \tag{15}$$

$$\left(\frac{m_{fuel}}{m_{air}}\right)_{sto} = 0.069 \tag{16}$$

With the desired equivalence ratio, stoichiometric fuel-air mixture, volumetric flow rate and assuming steady-state conditions with ideal gas law for air, the volumetric and mass flow for the air and fuel can be determined from

$$V_{dot\_mix} = V_{dot\_air} + V_{dot\_fuel} \tag{17}$$

$$\frac{m_{dot\_fuel}}{m_{dot\_air}} = \phi \cdot \left[\left(\frac{m_{fuel}}{m_{air}}\right)_{sto}\right] \tag{18}$$

$$m_{dot\_air} = \frac{V_{dot\_air} \cdot P_{amb}}{\frac{R_{univ}}{MW_{air}} \cdot T_{mix}} \tag{19}$$

$$m_{dot\_fuel} = V_{dot\_fuel} \cdot \rho_{sur} \tag{20}$$

The fuel mass flow multiplied by the specific energy yields the power required to heat the fuel through the desire temperature range.

$$Power\_Required = m_{dot\_fuel} \cdot Specific\_Energy \tag{21}$$

The specified and calculated heat exchanger design parameters are presented in Table 3.

Table 3. Heat Exchanger Design Parameters

Frequency	15 Hz
Single Tube Volume	0.004 m^3
Number of Tubes	2
Fill Fraction	1
Equivalence Ratio	1.05
Inlet Temperature	290 K
Outlet Temperature	530 K
Specific Energy Required	554 kJ/kg
Fuel Mass Flow	0.443 kg/min
Heat Exchanger Power Required	4.082 kW

PDE Heat Transfer Coefficient and Inner Tube Temperature

Approximate values for the average heat transfer coefficient and the average internal tube temperature were required to begin the heat exchanger design. Due to the high temperatures, vibrations, and impulses generated in the PDE tube these values could not be experimentally determined. These values were extrapolated from experimental data from previous hydrogen-air tests for both plain tube steady-state external tube temperatures and calorimetric heat transfer testing with a water-cooled heat exchanger (Hoke, 2003). Using the experimental data the heat transfer rates were calculated. Using conservation of energy the heat transfer rates are used to calculate the inner wall temperatures. With the heat transfer and inner wall temperature for both tests the heat transfer coefficient and inner tube temperature may be solved for as the two unknowns.

For the referenced plain tube tests the steady-state external wall temperature at the hottest section of the tube was 1005 K. The heat transfer per unit length was calculated based on free convection and radiation losses. The complete calculations can be found in Appendix B. All material and air properties were calculated based on table values and linearly interpolated to the film temperature (Incropera and DeWitt, 1996:326) defined as

$$T_{film} = \frac{\left(T_o + T_{amb}\right)}{2} \tag{22}$$

Where

T_o = External surface temperature (K)

T_{amb} = Ambient temperature

Radiation losses were calculated based on heat transfer to a black body (Incropera and Dewitt, 1996:10)

$$q_{rad} = \varepsilon \cdot \sigma \cdot d_o \cdot \pi \cdot \left(T_o^{\,4} - T_{amb}^{\,4}\right) \tag{23}$$

Where

ε = Emissivity of the tube material from property table

$\sigma = 5.67 \times 10^{-8} \frac{kg}{s^3 K^4}$ (Stefan-Boltzmann constant)

dia_o = Outer tube diameter (m)

Convective losses due to free convection (Incropera and DeWitt, 1996:8) are determined by

$$q_{fc} = h_{fc} \cdot \pi \cdot d_o \cdot \left(T_o - T_{amb}\right) \tag{24}$$

Where

q_{fc} = Heat transfer due to free convection (W/m)

h_{fc} = Free convection heat transfer coefficient [W/(m^2-K)]

The free convection heat transfer coefficient (Incropera and DeWitt, 1996:307) is calculated by

$$h_{fc} = \frac{Nu_{fc} \cdot k_{amb}}{dia_o} \tag{25}$$

Where

k_{amb} = Thermal conductivity of the air [W/(m-K)]

Nu_{fc} = Nusselt number for free convection

The Nussult number for free convection is determined by the Churchill and Chu correlation (Incropera and DeWitt, 1996:465) for a long horizontal cylinder

$$Nu_{fc} = \left[0.6 + \frac{0.387 \cdot Ra^{\frac{1}{6}}}{\left[1 + \left(\frac{0.559}{Pr_{fc}} \right)^{\frac{9}{16}} \right]^{\frac{8}{27}}} \right]^2 \tag{26}$$

The Raleigh number (Incropera and DeWitt, 1996:456) is determined from

$$Ra = \frac{g \cdot \beta \cdot \left(T_o - T_{amb} \right) \cdot dia_o^{\,3}}{\nu \cdot \alpha} \tag{27}$$

Where

$\beta = \frac{1}{T_{film}}$ Expansion coefficient for ideal gas (1/K)

$g = 9.8\frac{m}{s^2}$ Acceleration due to gravity

ν = Kinematic viscosity ($m^2/2$)

α = Thermal diffusivity ($m^2/2$)

The summation of the radiation and free convection losses equals the total heat loss

$$q_{plain\_tube} = q_{rad} + q_{fc}$$

For steady-state conditions the heat transfer to the ambient environment must the same as the heat transfer through the wall. The tube is considered a radial system and the conduction through the tube wall (Incropera and DeWitt, 1996:91) may be represented as

$$q_{plain\_tube} = \frac{2 \cdot \pi \cdot k_{tube} \cdot \left(T_o - T_{i\_plain\_tube}\right)}{\ln\left(\frac{dia_i}{dia_o}\right)} \tag{28}$$

Where

k_{tube} = Thermal conductivity of the tube wall [W/(m-K)]

T_i = Average temperature on the inside of the PDE tube (K)

dia_i = Inner PDE tube diameter (m)

The inner surface temperature may be determined knowing all other terms.

For the calorimetric water cooled heat exchanger tests the temperature increases were on the order of 13 K. Over this temperature range the specific heat for water may be assumed constant and the total heat transfer (Incropera and DeWitt, 1996:399) can be determined from

$$Q_{cal} = m_{dot\_water} \cdot c_{p\_water} \cdot \left(T_{outlet} - T_{inlet}\right) \tag{29}$$

Where

Q_{cal} = Heat transfer from calorimetric heat exchanger tests (W)

c_{p_water} = Specific heat of the water (J/[kg-K])

T_{inlet} = Heat exchanger inlet temperature (K)

T_{outlet} = Heat exchanger outlet temperature (K)

By using a modified form of Equation 28, the inner surface temperature for the calorimetric water-cooled heat exchanger tests.

$$Q_{cal} = \frac{2 \cdot \pi \cdot k_{tube} \cdot L \cdot \left(T_o - T_{i\_cal}\right)}{\ln\left(\frac{dia_i}{dia_o}\right)} \tag{30}$$

Where

L = Length of the heat exchanger (m)

Knowing the heat transfer and inner tube temperature for the free convection/radiation test and the water cooled test there are now two equations and two unknowns allowing for the average heat transfer coefficient (h_{flame}) and inner tube temperature (T_{flame}) to be solved for

$$[redacted] \tag{31}$$

$$Q_{cal} = h_{flame} \cdot \pi \cdot dia_{inner} \cdot L \cdot \left(T_{flame} - T_{i\_cal}\right) \tag{32}$$

The calculated heat transfer coefficient and inside tube temperature were calculated to be

$$h_{flame} = 175 \frac{W}{m^2 \cdot K} \qquad T_{flame} = 1131 K \tag{33}$$

Heat Exchanger Design

The heat exchanger designed for this work was a concentric tube counter-flow heat exchanger. This type of heat exchanger was chosen based on ease of incorporating into the PDE tube, size, simplicity, ease of manufacture, and the high heat transfer efficiency possible by having the fuel in contact with the heat transfer source. The heat exchanger was designed based on calculations for both water and JP-8 as the working fluid. The general methodology and assumptions used to design the heat exchanger are presented in the following paragraphs. The actual calculations for both working fluids are presented in Appendix B.

The heat exchanger design is based on a one-dimensional, steady-state, uniform flow, radial system using a finite difference method. A representation of a heat exchanger segment and cutaway view is presented in Figure 12.

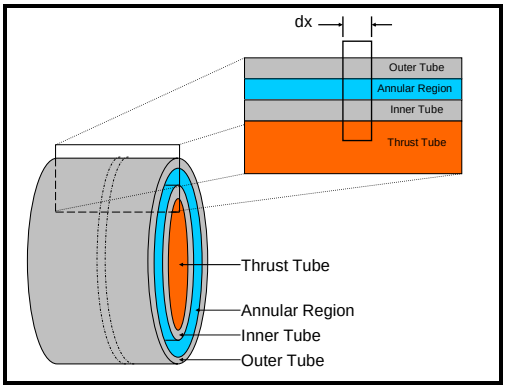

Figure 12. Representative concentric tube heat exchanger segment with cutaway view and finite slice for finite difference method

Looking at a finite slice of the segmented heat exchanger, indicated as dx, a graphical representation of the finite difference method is presented in Figure 13.

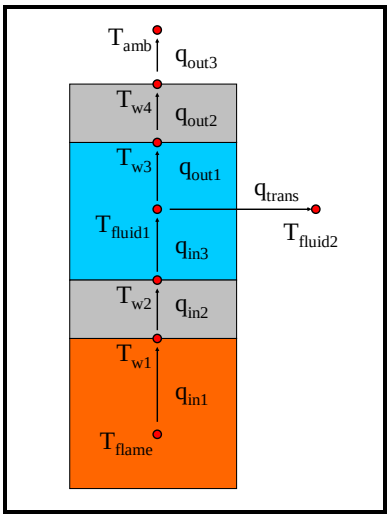

Figure 13. Finite difference method representation of finite slice dx of concentric tube heat exchanger

Heat is transferred to the working fluid by convection from the inside of the PDE tube to the inner tube wall. Heat is then conducted through the inner tube wall. The heat is transferred to the working fluid by convection from the tube wall. The heat is then rejected to the ambient environment or transmitted in the form of a temperature increase to the next finite slice fluid element. The rejected heat is transferred by convection to the outer tube wall, conducted through the outer tube wall and rejected to the ambient environment by free convection and radiation.

The heat transfer equations between each temperature node in Figure 13 may be represented as

$$q_{in1} = h_{flame} \cdot \pi \cdot dia_{ii} \cdot dx \cdot \left(T_{flame} - T_{w1}\right) \tag{34}$$

$$q_{in2} = \frac{2 \cdot \pi \cdot dx \cdot k \cdot \left(T_{w1} - T_{w2}\right)}{\ln\left(\frac{dia_{io}}{dia_{ii}}\right)} \tag{35}$$

$$q_{in3} = h_{fluid} \cdot \pi \cdot dia_{ii} \cdot dx \cdot \left(T_{w2} - T_{fluid}\right) \tag{36}$$

$$q_{out1} = h_{fluid} \cdot \pi \cdot dia_{oi} \cdot dx \cdot \left(T_{fluid} - T_{w3}\right) \tag{37}$$

$$q_{out2} = \frac{2 \cdot \pi \cdot dx \cdot k \cdot \left(T_{w3} - T_{w4}\right)}{\ln\left(\frac{dia_{oo}}{dia_{oi}}\right)} \tag{38}$$

$$q_{out3} = \left[h_{fc} \cdot \pi \cdot dia_{oo} \cdot dx \cdot \left(T_{w4} - T_{amb}\right)\right] + \left[\varepsilon \cdot \sigma \cdot \pi \cdot dia_{oo} \cdot dx \cdot \left(T_{w4}^{4} - T_{amb}^{4}\right)\right] \tag{39}$$

$$q_{trans} = m_{dot\_fluid} \cdot c_{p\_fluid} \cdot \left(T_{fluid2} - T_{fluid1}\right) \tag{40}$$

If the initial inlet temperature is used for the first finite slice then there are ten unknowns

T_{w1} T_{w2} T_{w3} T_{w4} T_{fluid2} q_{trans} q_{in1} q_{in2} q_{in3} q_{out1} q_{out2} q_{out3}

From conservation of energy

$$q_{in1} = q_{in2} = q_{in3} \tag{41}$$

$$q_{out1} = q_{out2} = q_{out3} \tag{42}$$

$$q_{in1} = q_{trans} + q_{out1} \tag{43}$$

Equations (17)-(21) represent ten equations for the ten unknowns allowing the determination of all temperatures and heat transfers for the finite slice. The temperature of fluid in the following finite slice is also calculated permitting the same set of equations to be solved for as each subsequent finite slice.

The finite difference method begins with the inlet temperature as the fluid temperature. The next fluid element temperature is calculated as an unknown and the

cycle begins over again for the next finite slice. This continues until the desired outlet temperature is achieved. The number of cycles required multiplied by the slice size represents the length of the heat exchanger required.

Turbulent flow effects on the heat transfer coefficient of the working fluid are accounted for in the model, as are material and fluid property variations as a function of temperature. While too extensive to discuss in this chapter the interested reader is referred to Appendix B for the final calculations for the method used.

Other Design Considerations

To match the current PDE tubes, the inner tube of the heat exchanger was limited to 2" stainless steel pipe. Using the existing 2" pipe geometry and threading on the heat exchanger inner tube ensured that the heat exchanger could easily be moved along the axial length to adjust the heat transfer to the fluid.

The annular region thickness was the primary consideration in determining the outside tube diameter. It was desired to have the smallest annular region possible to reduce residence time and minimize the amount of hot fuel in the heat exchanger while maximizing the surface contact area with the heated inner tube. The outer tube selection was limited to the selection of the pipe stock available and manufacturing capabilities. With these criteria in mind 2.5" stainless steel schedule 10 tube was selected for the outer tube which provided a 3.302 mm annular thickness.

A concern in the early design process was that boiling may occur in regions prone to stagnation. To prevent stagnation, a helical rod was incorporated into the design. It was believed that installing the helical rod would force the flow in a helical path from the

inlet to the exit preventing any hot spots and cold spots. It is shown in the chapter four that the helical rod did not work as intended due to buoyancy in the working fluid.

III. Facilities and Instrumentation

Pulsed Detonation Research Facility

This research was conducted at the Pulse Detonation Research Facility located at Building 71A, D Bay, Wright-Patterson Air Force Base, Ohio. The Pulse Detonation Research Facility is a component of the Air Force Research Laboratory Propulsion Directorate (AFRL/PR).

This facility was originally designed and constructed for turbojet testing, and has since been modified to support pulse detonation research. The major components of the facility include the test cell, control room, and fuel room. The 21,200 m^3 test cell features a static thrust stand capable of measuring thrust of up to 267,000 N (Schauer, 2001:3). For pulse detonation research, the thrust values and the size of the research equipment does not necessitate the use of the high capacity static thrust stand. A smaller damped thrust stand has been installed above the static thrust stand. It is on the small damped thrust stand that all pulse detonation research is completed. During testing the products are ejected into an exhaust tunnel and vented to the atmosphere. The test cell is explosion proof and is separated from the control room and the fuel room by 0.61 m thick concrete walls.

The control room is located adjacent to the test cell. Personnel are not permitted in the test cell during testing. To monitor the test cell, a number of closed circuit cameras are placed throughout the test cell and fuel room. All testing is controlled by use of a facility specific control panel and LabView control software run from a control computer. Real-time data is recorded by the LabView control software run from the control

computer, while high-speed data is recorded by a second computer also running additional LabView software.

The fuel room, located adjacent to the control room and the test cell, provides a low point ventilation system, liquid fuel storage, and fuel conditioning equipment. All liquid fuels are processed, stored, conditioned, and pressure fed from the fuel room to the test cell.

Air Supply System

Compressed air for the PDE is provided by one of two Ingersoll-Rand Pac Air Compressors (Model No. PA 300V). Each 261 kW compressor provides 40 m^3/min at a rated operating pressure of 689 kPa. Air from the compressors is stored in a 4.5 m^3 collection tank fabricated by Buckeye Fabrication Co. Inc., Dayton Ohio (Serial Number 10894). From the collection tank the air is piped into the test cell.

The main supply line is split into two separate lines under the test stand for the fill and purge supply lines, indicated in Figure 14. A large range of air mass flow rates are possible by the use of fixed diameter orifice plates in line with the fill and purge supply lines. For the purpose of this work an 8.99 mm diameter orifice plate was used in the purge supply line and a 12.7 mm diameter orifice plate was used in the fill supply line. During testing, air mass flow rate is controlled from the control computer by Tescom Electropneumatic PID Controllers (Model No. ER 1200) which actuate dome loader type pressure regulators upstream of the orifice plates. Surge tanks are located down stream of the orifice plates to prevent compression waves generated in the valve system from disrupting the flow at the orifice plates.

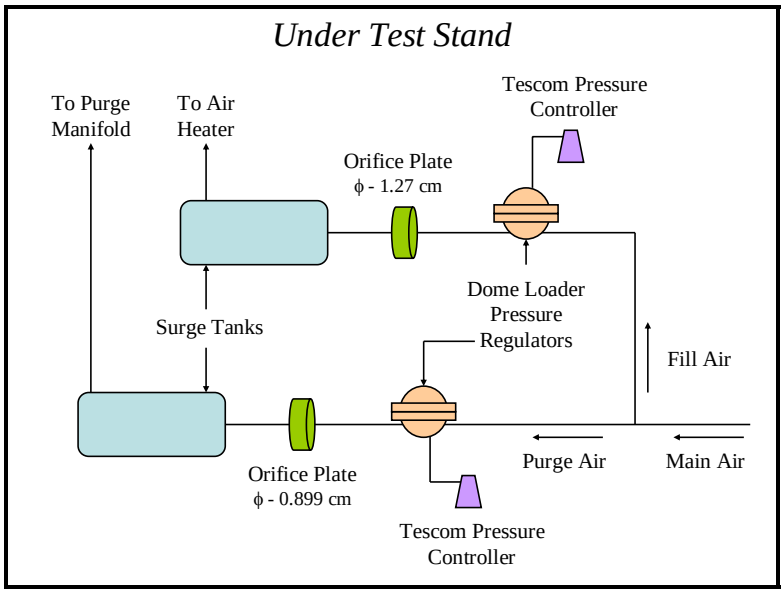

Figure 14. Diagram of PDE main air supply split to fill and purge air supply lines with associated hardware

The purge air enters the test stand and is piped into the purge manifold for use in the PDE. The fill air enters the test stand where it flows through a 15 kW Chromalox Circulation Heater (P/N 053-500870-187). The air temperature can be adjusted by setting the upper temperature limit on the Chromalox temperature controller (Model No. 2104) on the facility control panel or by adjusting a setting on the control computer. After exiting the heater, the fill air is mixed with the fuel and enters the fill manifold for use in the PDE.

Hydrogen Fuel Supply System

The hydrogen fuel supply is provided by a hydrogen tuber trailer located outside of the research facility. The trailer holds 38 individual hydrogen bottles each with a starting pressure of 16.55 MPa. The total water volume of the trailer is 15.69 m^3. During testing, individuals bottles are used until the bottle pressure falls below the pressure

required for a given test condition, at which time a new bottle is opened. This continues until the entire hydrogen trailer has been emptied at which time the trailer is replaced.

The hydrogen enters the research facility through the test cell. The hydrogen is routed under the test stand through a series of manual and pneumatic ball valves. The pneumatic ball valves provide the ability to turn the hydrogen flow on or off during testing from the facility control computer. The hydrogen mass flow rate is determined by a Flow-Dyne critical flow nozzle (P/N N08006-SA). During testing, the hydrogen mass flow rate is regulated from the control computer by a Tescom Electronic Pressure Controller (Model No. ER3000) and TESCOM Pressure Regulator (Model No. 44-1313-2122A200) upstream of the critical flow nozzle. A surge tank is located downstream of the critical flow nozzle to prevent shock waves generated in the valve system from disrupting the flow at the critical flow nozzle.

For this research the hydrogen was injected prior to the inlet manifold by means of a T-section in the air supply line located at the exit of the air heater 2.5 m upstream of the injection valve. Due to the gaseous state of the hydrogen, nozzles or mixing devices were not needed in the referenced tests. Instead the turbulent nature of the airflow and fuel injection, in addition to the flow path are sufficient to ensure a near homogenous mixture.

Liquid Fuel Supply System

The two liquid hydrocarbon fuels used for this work were aviation gasoline and JP-8 military turbine fuel, hereto referred to as avgas and JP-8 respectively. Avgas was used due to its availability, detonability, and numerous similarities to JP-8, which is the

primary fuel of interest for this work. The similarity in the fuel system for these fuels is near identical and hence will be presented in such a fashion with any pertinent differences noted. For JP-8 flash vaporization and supercritical heating tests the JP-8 requires conditioning which is discussed in the following section. This section will explain the fuel system as if the fuel has already been conditioned or does not require conditioning.

Avgas is directly available from the fuel farm adjacent to the facility and is pumped directly from the fuel farm to the fuel room. JP-8 is obtained locally from AFRL/PR Fuels Branch and stored in 18.93 L fuel containers until use.

For testing, the fuel was placed in a 41.64 L stainless steel general purpose pressure vessel (S/N 28108-007). The fuel is pressure fed by a standard nitrogen bottle to two 9.46 L Greer hydraulic accumulators (Model No.30A-2½A) rated to 20.86 MPa. The accumulators are pressurized by a standard nitrogen bottle and high pressure regulator. The accumulators use a rubber diaphragm that to separate the nitrogen source from the fuels and is compatible with the fuels used in this work (Tucker, 2005). The fuel fill and pressurization schematic are present in Figure 15.

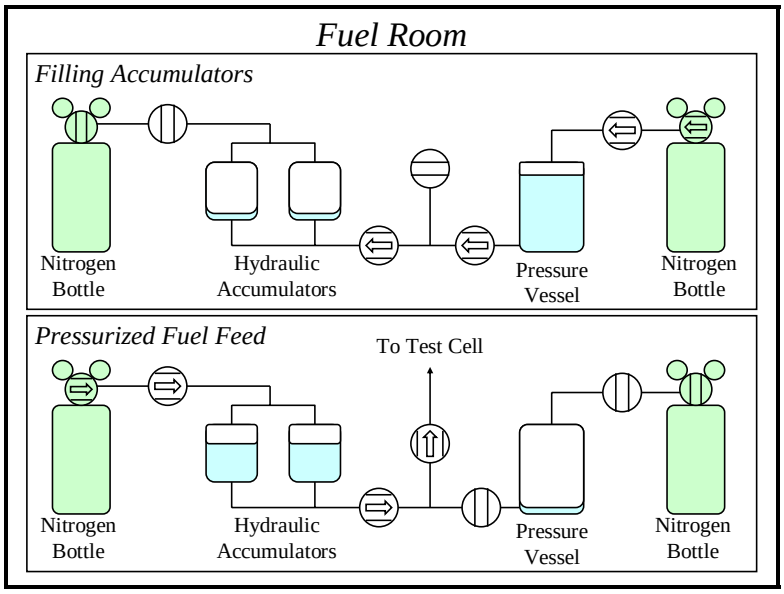

Figure 15. Diagram of fuel room configuration and process of filling the accumulators and also pressuring the accumulators providing pressurized fuel for testing

The fuel line out of the fuel room is opened by manual ball valves allowing a flow path to a point underneath the test stand. At this point two manual ball valves control one of two flow paths. The first is a flow meter bypass used for system pressurization. The second path is through a Flow Technology turbine volumetric flow meter (Model No. FT4-8AEU2-LEAT5). A thermocouple immediately after the flow meter permits temperature compensation in fuel density for fuel mass flow to be calculated by the control computer. From the flow meter, the fuel line traverses the underside of the test stand to a pneumatic valve actuated from the control computer. This valve is referred to as the last chance valve and controls the flow of fuel during test. After the last chance valve the fuel line enters the test stand. The diagram of the flow meter and flow meter bypass are presented in Figure 16.

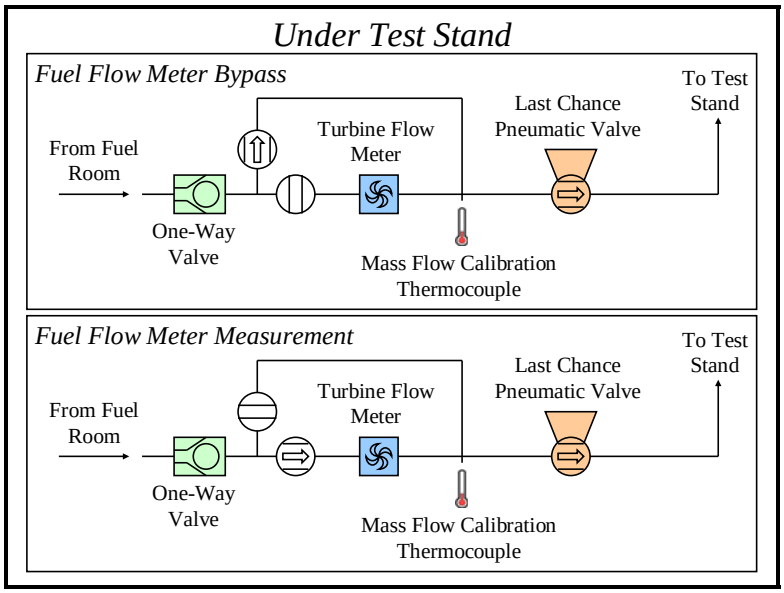

Figure 16. Diagram of fuel flow meter and flow meter bypass system with last chance valve

For testing without fuel heating, the fuel line was routed to the fuel inlet manifold. For fuel heating tests the fuel entered the flash vaporization system, discussed in a following section, and terminated in the fuel inlet manifold. The fuel inlet manifold consists of two spray bars that have been welded into the fill air manifold as shown in Figure 17. Each spray bar is drilled and tapped with five threaded holes that accept the Delavan fuel flow nozzles. The number of nozzles and flow number of the nozzles used varied from test to test depending on the fuel, fuel pressure, and mass flow requirements.

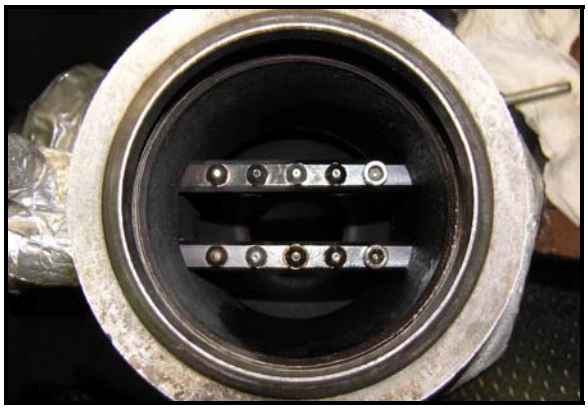

Figure 17. Upstream view into the fill air manifold of the fuel inlet manifold with spray bars Delavan fuel flow nozzles

Fuel Conditioning

For heated JP-8 tests, fuel conditioning is required to minimize carbon deposits in the flash vaporization system due to the dissolved oxygen reacting with the fuel. Fuel condition begins with placing the JP-8 in a 41.64 L general purpose pressure vessel. A coiled piece of stainless steel tubing in the bottom of the vessel with numerous small diameter holes drilled in it is attached to a piece of tubing that exits the pressure vessel and is connected to a standard nitrogen bottle and regulator. A ball valve on the top of the pressure vessel is vents the tank to the outside atmosphere. The nitrogen pressure is raised until bubbling through the coils is audibly detected. After the proper volume of nitrogen (Tucker, 2005) has been bubbled through the JP-8, the vent to atmosphere is closed and the holding tank is pressurized. At this point the JP-8 may be used to fill the fuel system as mentioned in the previous section.

Figure 18. Top view of fuel conditioning holding tank with nitrogen bubbling coiled tube at the tank bottom

Ignition System

The ignition system timing is determined by the angular position of the camshaft in the PDE. The camshaft position is read by a BEI optical encoder (Model H25, S/N

Y0013039) and sent to the control computer. An ignition delay may be set in the control computer by the user and is often required to prevent backfiring. With the encoder input and the user defined ignition delay the control computer will determines the ignition timing and sends a signal to the ignition relay box. The relay box sends the signal to 12 VDC MSD Digital DIS-4 Ignition system. The ignition system releases 105-115 mJ per spark. For each fire cycle the control computer commands four sparks signals per tube for total ignition energy of 420-460 mJ per tube per cycle.

The spark plugs used are a modified NGK plug that has the grounding electrode removed and a small piece of tube welded to the end of the spark plug. The cylinder provides the grounding capability for the spark and a small non-turbulent environment for explosive reaction to develop.

Pulse Detonation Engine

The PDE used for this research uses the head from a General Motors Quad 4 head with dual overhead camshafts shown in Figure 19. The camshafts are belt driven by a variable speed 14.9 kW Baldor electrical motor (Model No. M4102T, S/N C0303240142). Motor control and frequency are provided by the control computer. Instead of the intake and exhaust cycles typical in automotive engines, the valve system in the PDE corresponds to fill and purge cycles respectively. On the fill cycle, the intake valves open allowing a fuel-air mixture to flow into the PDE. Likewise, on the purge cycle the exhaust valves open allowing purge air to flow into the PDE engine. The valve train is lubricated by automotive oil which is pumped into the head from an external reservoir and electric oil pump. The cooling water is provided by a closed loop radiator

cooling system, which is pumped through the existing head cooling water ports by use of an external electric water pump.

Figure 19. GM Quad 4 head being used as PDE valve train for fill air manifold (top) and purge manifold (bottom)

PDE tube mounting plates are attached to the head with the existing head bolts. The mounting plates are 1.27 cm stainless steel plate that mount flush with the head and are sealed by the use of a stock head gasket. In general, the mounting plates are threaded to accept male 2" national pipe thread (NPT).

When using liquid hydrocarbon fuels it is necessary to use detonation initiating devices to achieve detonations in reasonable lengths of tube. Numerous types of detonation tripping devices exist, however for this research a structurally enhanced shchelkin spiral (Shchelkin, 1940) was and is shown in Figure 20. The spiral is installed prior to the mounting plates and held in place once by the mounting plates. The PDE tube is then slid over the spiral and screwed into the mounting plate.

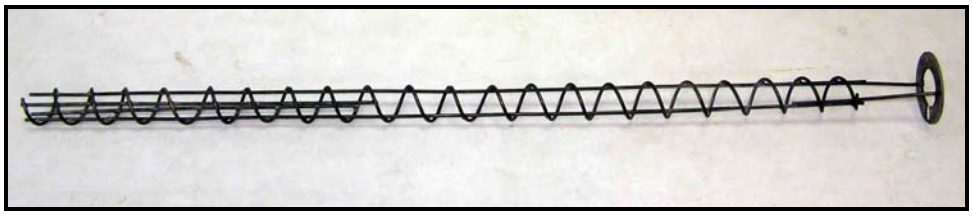

Figure 20. Shelkin Like Spiral with Structural Support

The PDE tubes used for this research were 1.829 m long and fabricated from 2" stainless steel schedule 40 pipe sections joined with 2" NPT collars. During tests with a heat exchanger installed, various pipe sections were used to allow axial positioning of the heat exchanger while maintaining the tube length of 1.829 m.

Heat Exchanger Configuration

For this research two heat exchangers were developed. The first heat exchanger used was designed based on assumptions and heat transfer calculations discussed in the previous chapter and presented in Appendix B. After multiple tests it was realized that a smaller second heat exchanger was required due to the high heat transfers and to validate theories developed using the first heat exchanger. The first heat exchanger was 76.2 cm long and the second heat exchanger was 38.1 cm long; and therefore the heat exchangers shall be referred to as the long heat exchanger and the short heat exchanger for the remainder of this document.

The long heat exchanger is a 76.2 cm long concentric tube configuration with the inner tube constructed from 2" stainless steel schedule 40 pipe and the outer tube constructed from 2 1/2" stainless steel schedule 10 pipe. It would seem counter-intuitive that a thinner walled pipe would be used on the outside given the high pressures in the heat exchanger, however the annular region in between the two tubes was the critical

concern in the design as long as the heat exchanger could pass structural design considerations.

The two pipes were welded to 6.35 mm stainless steel end plates allowing equal annular spacing of 3.302 mm around the perimeter. In an attempt to prevent stagnation of the fluids within the heat exchanger a 3.175 mm diameter stainless steel rod was spot welded to the inner tube in a helical path with six full turns. The helical rod is shown welded to the inner tube in Figure 21. The helical rod did not ensure a fluid tight flow barrier, but it was hypothesized that the helix would force a helical flow path and a more even temperature distribution throughout the length of the heat exchanger flow path would be developed. The outer tube had two 1/4" Swagelok unions welded at opposite ends and 180 degree radially offset. These fittings corresponded to the fluid inlet and outlet positions.

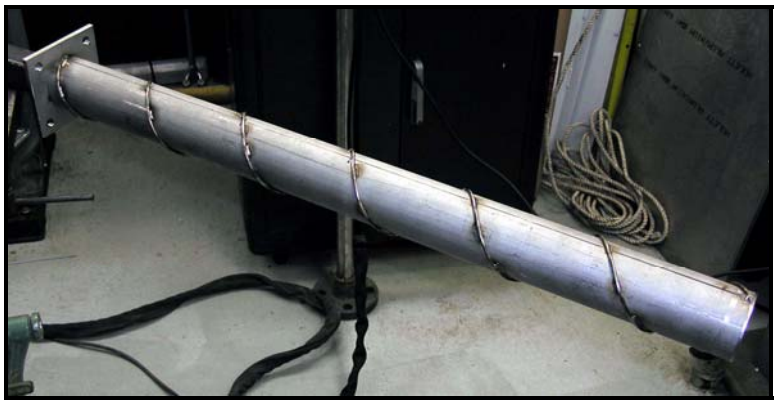

Figure 21. Construction of the long heat exchanger with helical rod welded in place

To mount the heat exchanger to existing PDE tubes, two 15.24 cm extensions were fabricated from 2" stainless steel schedule 40 pipe. At one end of the extension a 6.35 mm stainless steel endplate for mounting to the heat exchanger is welded in place. The other end of the extension is threaded with male 2" NPT mate for mounting to the

PDE head or to other PDE tube sections with female 2” NPT pipe collars as shown in Figure 22. In each extension two 3/8”-24 stainless steel bolts are welded three inches apart from one another for wave speed measurement.

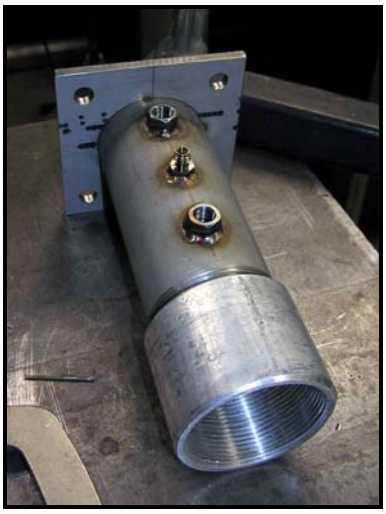

Figure 22. Heat exchanger connecting extension with end plate for heat exchanger installation, instrumentation ports, and male 2” NPT connected to female 2” pipe collar

The short heat exchanger was also a concentric tube configuration. The inner tube is fabricated of 2” stainless steel schedule 10 pipe and the outer tube is 2.5” stainless steel schedule 10 pipe. The short heat exchanger was 38.1 cm long. The short heat exchanger did not have the helical flow coil installed. The same size inlet and outlet fittings were used and installed at opposite ends of the tube and 180 degrees radially offset. 1/8” swagelok fittings were installed at the 12.7 cm and 25.4 cm axial positions and radially aligned with the outlet. These fittings were used to insert thermocouples into the flow. The short heat exchanger utilized the same endplate construction and connecting extensions used in the long heat exchanger. The short heat exchanger is presented in Figure 23.

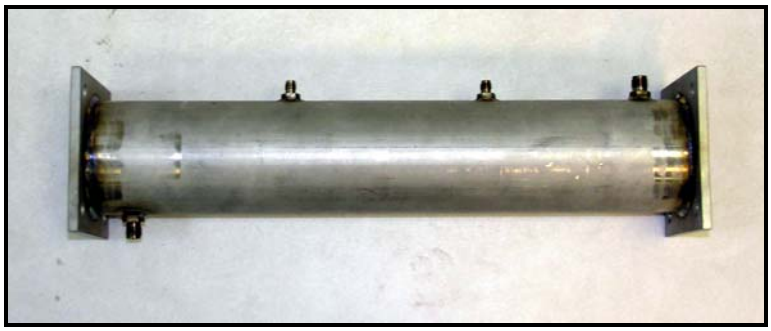

Figure 23. Profile view of short heat exchanger with inlet and outlet ports at opposing ends and two spaced thermocouple flow ports on the outlet side

Both heat exchangers were hydrostatically pressure tested in accordance with ASME B31.3. The rated working pressure for both heat exchangers is 5.516 MPa at 588 K.

Water Flash Vaporization System

Safety requirements necessitated that initial tests be completed using water for flash vaporization. This served as a proof-of-concept for a JP-8 flash vaporization system (FVS). These tests also provided insight into the heat transfer rates and flow characteristics of the FVS and heat exchangers.

The water FVS consists of a standard nitrogen bottle, water reservoir, one of the two previously mentioned heat exchangers, high temperature/pressure ball valve, thermocouples, pressure transducer, and all associated tubing and fittings required to properly connect all components. All components in the FVS are connected by ¼" stainless steel tubing connected with varying types of ¼" stainless steel Swagelok compression fittings.

Reverse osmosis (RO) water was used in all tests using water as the heated fluid. RO water was obtained locally and transported by 18.93 L container. The water reservoir

is a locally manufactured 2.134 m long, 2” stainless steel schedule 80 pipe with end caps welded in place. The reservoir provided 3.785 L capacity and is rated to a working pressure of 10.342 MPa. The filled reservoir is pressurized by means of a standard nitrogen bottle and high pressure regulator. The water is pressurized up to 6.895 MPa and pressure fed to the heat exchanger inlet.

An Omega 13.79 MPa pressure transducer (Model No. PX02K1-2KG5T) at the heat exchanger outlet monitors static pressure. The water flows from the heat exchanger to a pneumatically operated Bonetti stainless steel ball valve (Model No. 941-NPT-600-31) rated to 4.72 MPa at 823 K. The pneumatic valve provided water flow control during test from the control computer. A diagram of the water FVS is presented in Figure 24.

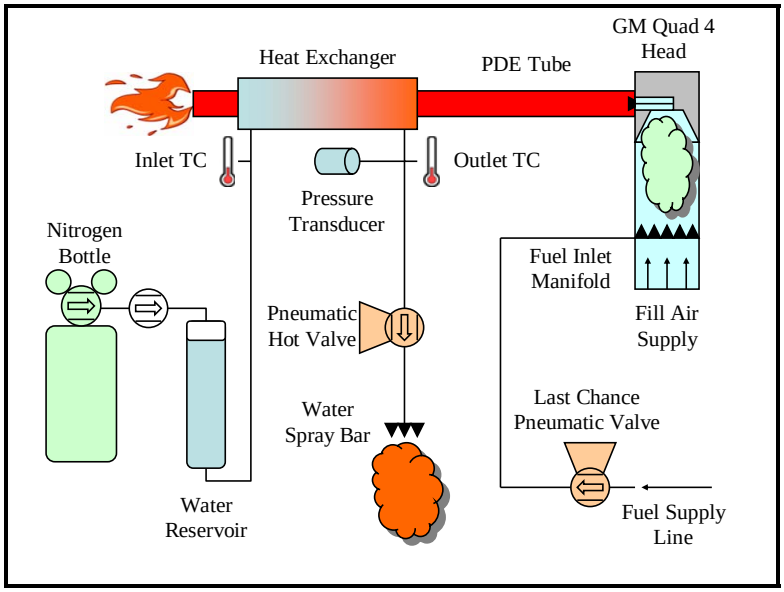

Figure 24. Diagram of PDE engine with water FVS and instrumentation installed

After passing through the hot valve the heated water is exhausted to the test cell atmosphere by use of a spray bar using the same type of Delavan spray nozzles used in the fuel system. A picture of the spray bar with nozzles installed is present in Figure 25.

The spray bar was manufactured out of 19.05 mm stainless steel hexagon bar stock. The spray bar was drilled and ported for five spray nozzles. A 1/4" Swagelok union was welded to provide an inlet for the hot water supply from the FVS. The exhausted heated water is vaporized after crossing the nozzles and experiencing the pressure drop to ambient atmosphere.

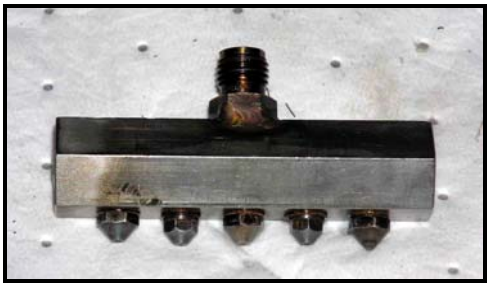

Figure 25. Water spray bar with Delavan spray nozzles installed

Water mass flow was measured by exhausting the water into an 18.927 L stainless steel general purpose pressure vessel (S/N 109702-024). The water vapor was ejected into the vessel which was partially filled with water to a level above the spray nozzles. The vessel had a small fitting less than one centimeter that vented the vessel to atmosphere. The mass losses to the environment due to steam leaving the vessel were assumed to be negligible. The vessel hung from a 1334 N capacity BLH load cell (Type U3XXA, S/N 36557). Load cell data is sent to the control computer.

JP-8 Flash Vaporization System

The JP-8 FVS consists of a pneumatic fuel control, a nitrogen bottle for purging the hot fuel from the system, a pneumatic control for nitrogen purge, a check valve for the nitrogen purge, one of the two previously mentioned heat exchangers, thermocouples, pressure transducer, and all associated tubing and fittings required to properly connect the

components. All components in the JP-8 FVS are connected by stainless steel tubing fastened with varying types of stainless steel Swagelok compression fittings, unless otherwise noted. The purpose of the nitrogen purge is to maintain FVS pressurization and purge the remaining JP-8 in the FVS after the fuel supply has been shut off.

The JP-8 FVS begins at the last chance valve under the test stand. Immediately after the last chance valve a tee connection introduces the nitrogen purge into the system. The nitrogen purge is controlled by a pneumatic ball valve and inline check valve. The nitrogen purge pneumatic valve controls the flow of the nitrogen and the check valve ensures that the nitrogen purge will initiate if the fuel pressure drops below the nitrogen pressure set point. For the purpose of this work the nitrogen purge was set values above the critical pressure of JP-8.

The flow path enters the test stand through a manual ball valve where the flow is routed to the heat exchanger inlet. An Omega pressure transducer rated to 13.79 MPa is placed at the heat exchanger outlet to monitor static pressure. From the heat exchanger outlet the flow traveled through an insulated fuel line which is terminated in the fuel inlet manifold. The JP-8 FVS diagram is presented in Figure 26.

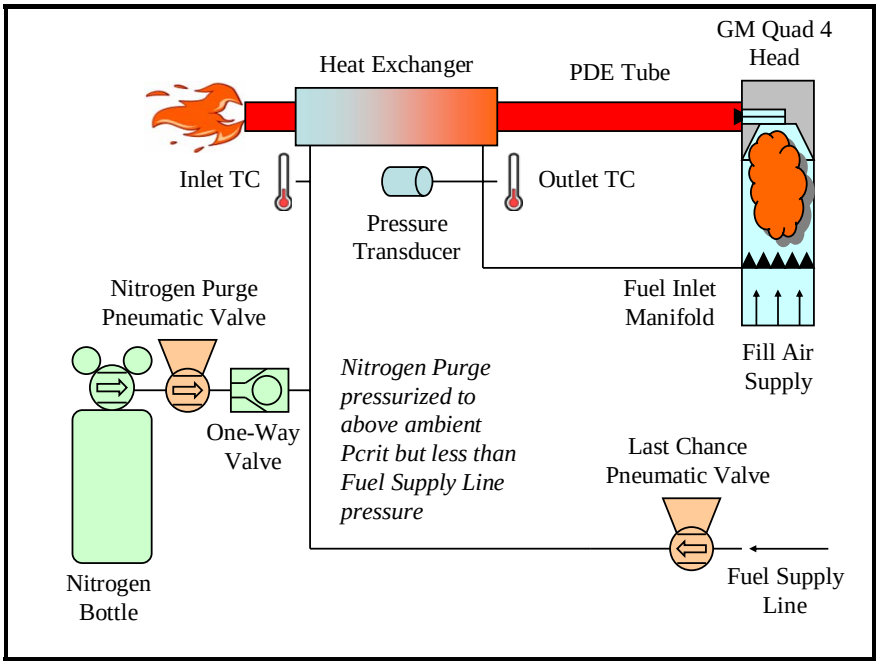

Figure 26. Diagram of PDE engine with JP-8 FVS and instrumentation installed

Temperature Instrumentation

Inlet and outlet heat exchanger flow temperatures were measured using J-Type thermocouples placed at the centerline supply lines. The measurements were taken 7.62 cm upstream and downstream of the heat exchanger entrance and exhaust respectively. Internal heat exchanger flow temperatures were measured by 1/8" J-Type thermocouples placed in the middle of the annular region of the heat exchanger.

During JP-8 heated fuel tests the fuel manifold inlet temperatures were read by a J-Type thermocouple placed at the centerline of the supply line 7.62 cm upstream of the fuel manifold inlet. The fuel line was insulated during these tests and the temperature losses from the thermocouple reading to fuel nozzles was assumed to be negligible.

Air flow temperature measurements were taken by J-type thermocouples 0.5 m upstream of the fuel inlet manifold. Fuel-air mixture temperature was recorded by a J-type thermocouple 0.25 m downstream of the fuel inlet manifold.

External PDE tube wall temperatures were measured by J-type thermocouples mounted externally by compression clamps to the PDE tube. Figure 27 shows the use of external thermocouples in addition to flow, inlet, and outlet thermocouples installed on the short heat exchanger.

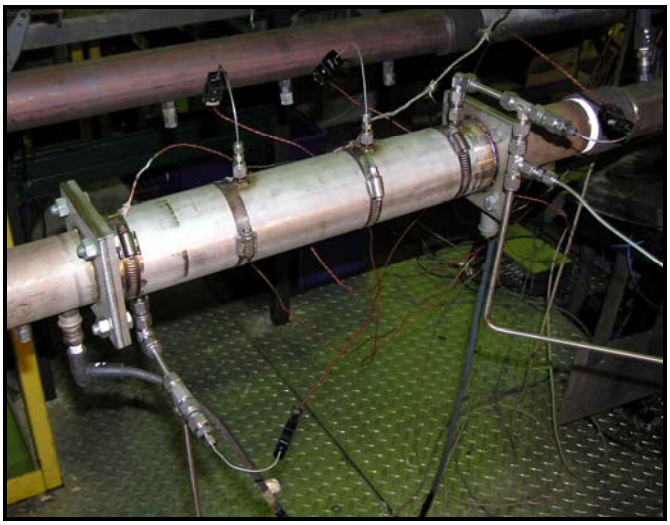

Figure 27. Short heat exchanger installed with surface, flow, inlet, and outlet thermocouples

Facility Control Software

The Labview PDE Facility Control and Data Acquisition software provides realtime control and data acquisition of all PDE operating parameters. The software controls engine frequency, purge and fill air mass flow rates, purge and fill fraction, ignition delay, spark control, and fuel flow control, just to name a few. The software provides real-time monitoring of all of the control parameters in addition a multitude of air/fuel pressure and temperatures.

Test Configuration for PDE Tube Tests without Heat Exchanger

Plain tube tests were completed with avgas-air and JP-8-air detonations to determine steady-state external wall temperature, heat transfer rates, and wavespeed data as functions of axial position. Two 1.829 m PDE tubes with 1.219 m shelkin like spirals were used for these tests. For the avgas test, fill air was heated to 321 K and the equivalence ratio was varied between 0.95-1.26. For the JP-8 test, fill air was heated to 394 K and the equivalence ratio was varied between 1.05-1.26. Engine operating frequency was maintained at 15 Hz and an 8 ms ignition delay was used. Ion probes and external thermocouples locations are shown in Table 4.

Table 4. Plain tube test ion probe and thermocouple locations

Ion Probe and External Thermcouple	Axial PDE Tube Location (cm)
1	19.69
2	46.99
3	73.82
4	105.89
5	121.76
6	137.01
7	154.62
8	169.86

Water FVS with Hydrogen-Air Detonation Configuration

Water FVS tests with hydrogen-air detonations were completed with long heat exchanger. For hydrogen fueled tests one1.829 m PDE tube, with heat exchanger, was used. The spiral for the hydrogen fueled tests was .305 m long. The hydrogen-air mixture was maintained at an equivalence ratio of 1.0 with an engine frequency of 10 Hz, and ignition delay of 6 ms.

Water FVS with Avgas-Air Detonation Configuration

Water FVS tests with avgas-air detonations were completed with long and short heat exchanger. For avgas fueled tests two 1.829 m PDE tubes were used, each with a 1.219 m spiral. Only one heat exchanger was incorporated for all tests.

JP-8 FVS Configuration

JP-8 FVS tests were completed with long and short heat exchanger. Two1.829 m PDE tubes were used, each with a 1.219 m spiral. Only one heat exchanger was incorporated for all tests. A photograph representing a two-tube test configuration with the long heat exchanger installed at the hot section is shown in Figure 28. Inlet and outlet thermocouples can be seen in addition to PDE tube ion probes.

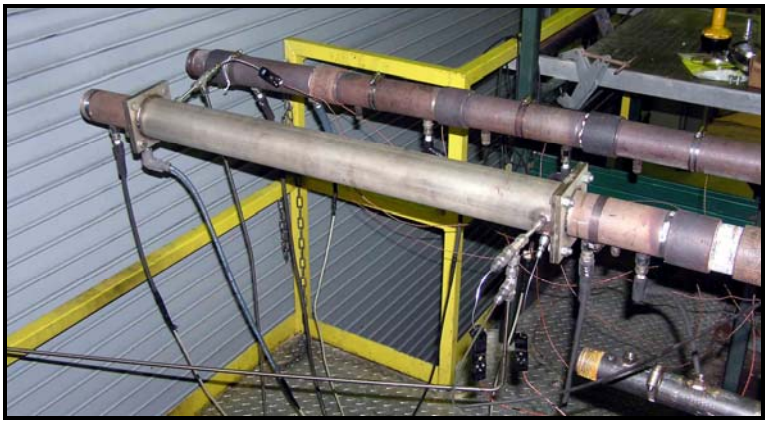

Figure 28. Generic two-tube configuration with instrumented long heat exchanger installed on closest PDE tube with the inlet at the end of the tube and the outlet toward the front of the tube

IV. Results and Analysis

Determination of Water Mass Flow Rate

Water mass flow rate was determined by ejecting the heated water into a holding tank that was hung from a load cell. The slope of the load cell recordings with time provided the mass flow rate for water tests. A sample image of the load cell recordings and how mass flow rate is calculated is shown in Figure 29.

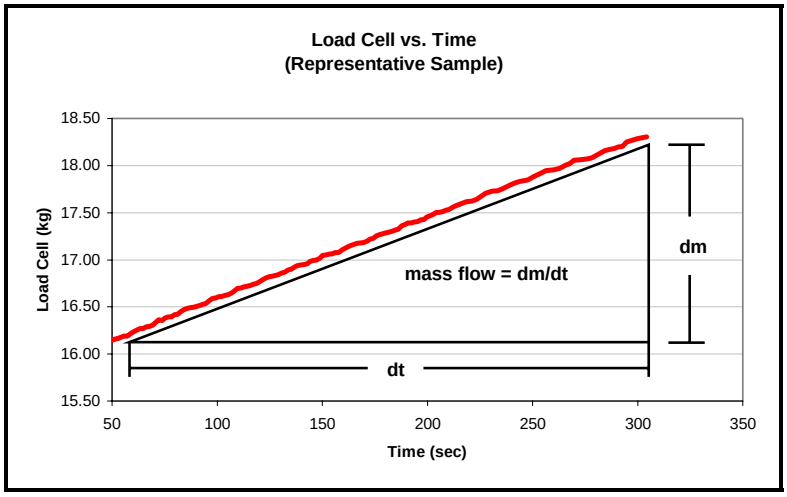

Figure 29. Sample mass flow calculation based on slope of load cell versus time

Heat Transfer Calculation

For heat exchanger tests, the heat transfer rate to the working fluid was determined from the mass flow, the specific heat of the working fluid, and the inlet/outlet temperatures. Mass flow was determined by the method in the previous paragraph for water FVS tests and using flow meter data for JP-8 FVS tests. If specific heat is assumed to be constant the determination of heat transfer rate is governed by

$$q := m_{dot} \cdot c_p \cdot \left(T_{outlet} - T_{inlet}\right) \tag{44}$$

Due to the elevated temperatures achieved in the heat exchanger, specific heat may no longer be assumed constant and must be accounted for as a function of temperature. An approximation of specific heat was obtained by using the specific heat value for the average temperature between the inlet and outlet temperature. This specific heat value is obtained by linearly interpolating the average temperature with the fluid property values. The calculations for the heat exchanger tests are presented in Appendix E.

During the plain tube tests the measured external tube wall temperature and ambient temperature were used to calculate the heat transfer rate from the tube to ambient environment by free convection and radiation calculation. The heat transfer rate changes with axial tube length due to the varying temperature profile; therefore, heat transfer rate is calculated as a function of length. The method used to calculate the heat transfer rate is presented in Appendix C.

Wave Speed Calculation

Wave speed is determined by ion probe and time data collected from the high speed data computer. The ion probes are continuously supplied with 4.5 volts. When a wave travels past the ion probe, a circuit is completed causing a steep decrease in the recorded voltage as shown in Figure 30 and Figure 31. The energizing system quickly recharges the electrode before the next ignition event occurs.

The time the wave passes a probe is determined by the threshold value below the source voltage when the circuit is completed. A threshold value of 4.45 volts was used. This value was chosen because it is outside of the noise level of the voltage reading but

within the range to obtain weak wave events (See Figure 31). The voltage drop for a measurable wave event is a nearly linear function allowing for linear interpolation of data points. The first data sample after the threshold value and the point prior to the threshold value are used to interpolate the time of the wave event. The analyzed time data has a data resolution of 50 microseconds. The code used to determine the wave speed is presented in Appendix D.

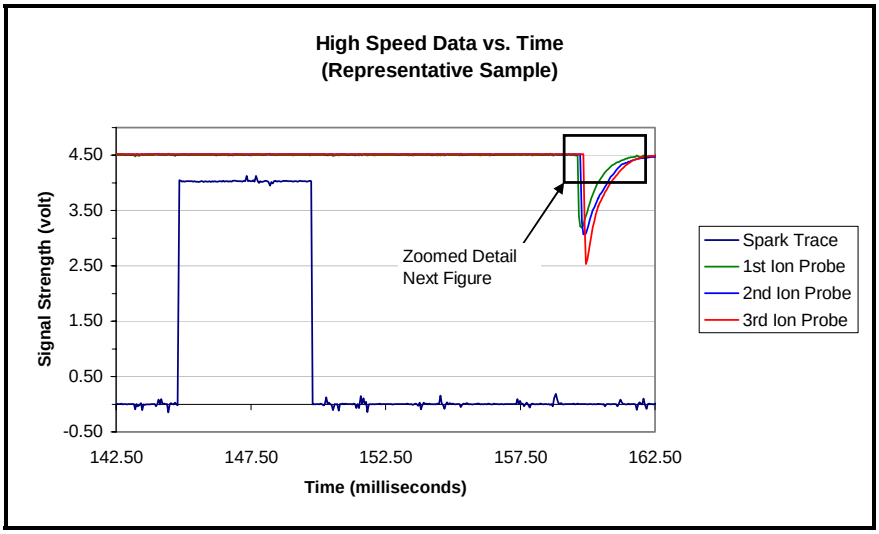

Figure 30. Sample high speed data with spark trace shown as the square wave and the ion probe drop due to the wave passing the sensors

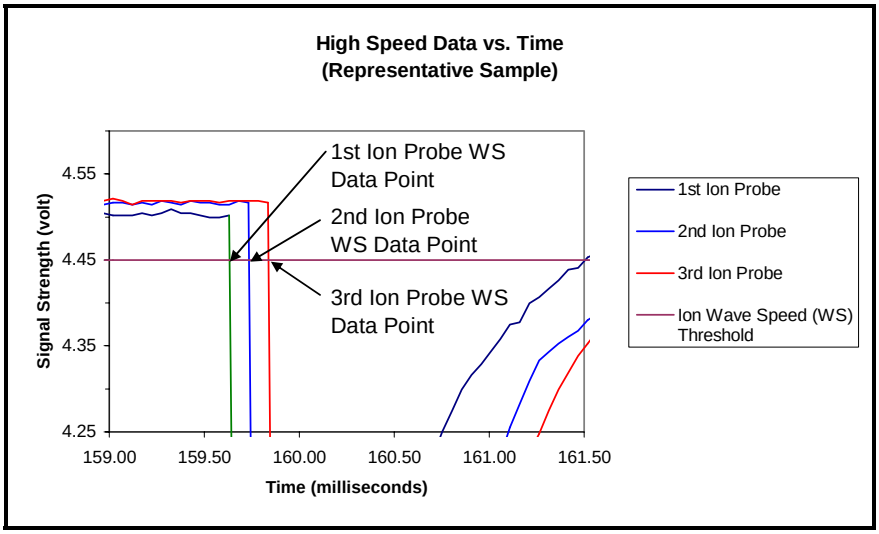

Figure 31. Detail of ion probe voltage as wave passes including the wave speed threshold about which the time is interpolated

PDE Tube Tests without Heat Exchanger

The steady-state surface temperature results for the plain tube avgas-air detonation test are shown in Figure 32. Maximum steady-state temperatures of 850 K to 875 K were seen at the end of the spiral in the 120 cm -160 cm axial positions. There is a linear temperature rise from the head of the PDE to the end of the spiral. The noticeable temperature drop at the end of the tube is due to the entrainment of cool air into the end of tube when an expansion wave is created after the wave and exhaust products have been ejected from the tube.

Equivalence ratios of near 1.1 provided the highest steady-state temperatures in the hot section. The richer mixtures showed over a 50 K drop at the hottest portion of the tube. Near stoichiometric mixtures provided highest temperatures forward of the hot section and temperatures near the maximum values in the hot section.

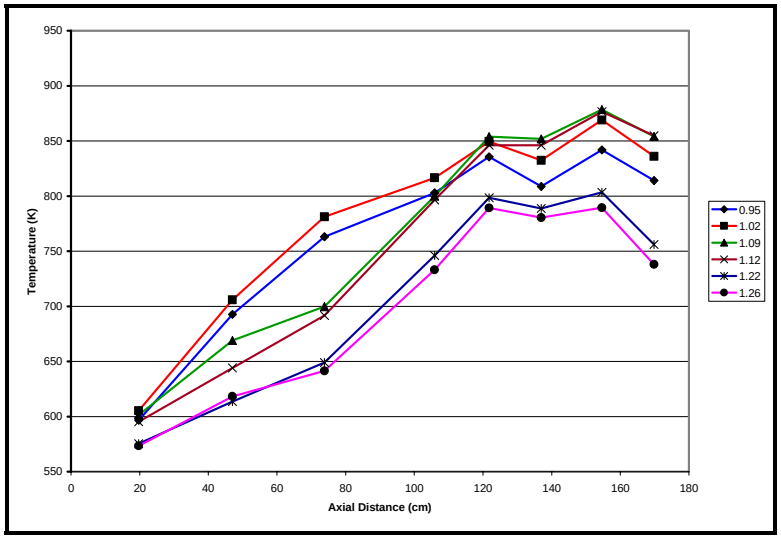

Figure 32. Plain tube surface temperature vs. axial distance w/ varying equivalence ratio avgas (298 K) – air (322 K), 15 Hz, 8 ms ignition delay, 1.829 m, 2" SS Sch 40 Tube w/ 1.219 m spiral

Wave speed profiles for the avgas test, shown in Figure 33, closely matched the temperature profile. The maximum wave speeds were obtained at the 110 cm – 130 cm region for equivalence ratios just above stoichiometric. It is at these locations that the wave speeds exceed the CJ detonation velocities. Both lean and rich mixtures experienced velocity increases with length but not to the magnitude of equivalence ratios near 1.1. The richest mixture shows an early velocity spike followed by a rapid decline to deflagration wave speeds. All other mixtures achieve CJ velocities by the end of the PDE tube.

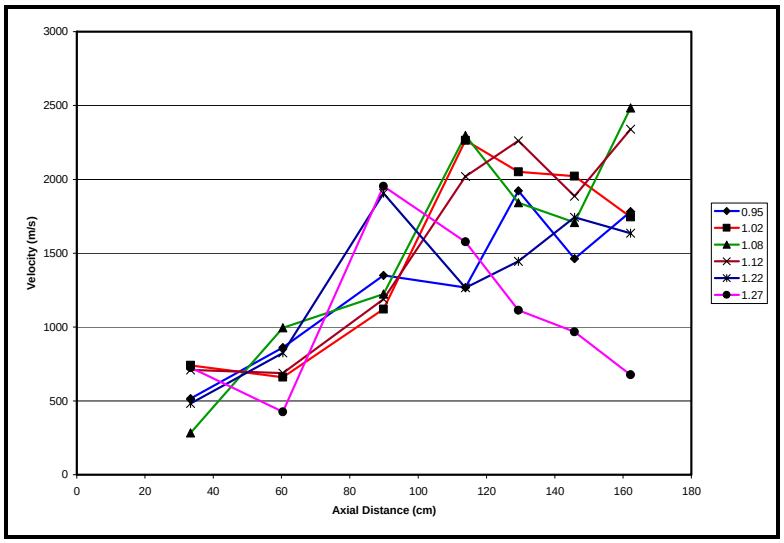

Figure 33. Plain tube wave speed vs. axial distance w/ varying equivalence ratio avgas (298 K) – air (322 K), 15 Hz, 8 ms ignition delay, 1.829 m, 2" SS Sch 40 Tube w/ 1.219 m spiral

The steady-state surface temperature results for the plain tube JP-8 - air detonation test are shown in Figure 34. JP-8 temperature and velocity profiles closely mimic those of the avgas tests for the equivalence ratios tested. The JP-8 did not provide reliable data for equivalence ratios that were lean or stoichiometric. JP-8 temperature profiles showed tighter grouping throughout the range of equivalence ratios. As was seen

in the avgas tests the maximum temperatures are seen in the 120 cm -160 cm. The JP-8 achieved from 25-50 K higher temperatures in the hot section compared to the avgas test.

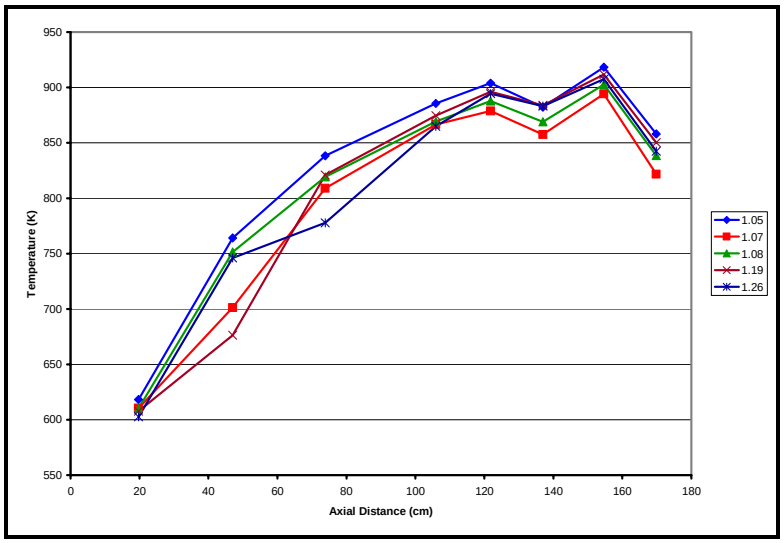

Figure 34. Plain tube surface temperature vs. axial distance w/ varying equivalence ratio JP-8 (298 K) - air (395 K), 15 Hz, 8 ms ignition delay, 1.829 m, 2" SS Sch 40 Tube w/ 1.219 m spiral

The JP-8 wave speed data, in Figure 35, showed a tighter wave speed grouping than avgas. Unlike avgas, JP-8 had maximum wave speeds at the richest equivalence ratios in the 1.2 range for unheated fuel. The transient overdriven wave speeds can be witnessed at the end of the spiral with a decrease to an equilibrium CJ point towards the end of the tube for all mixtures.

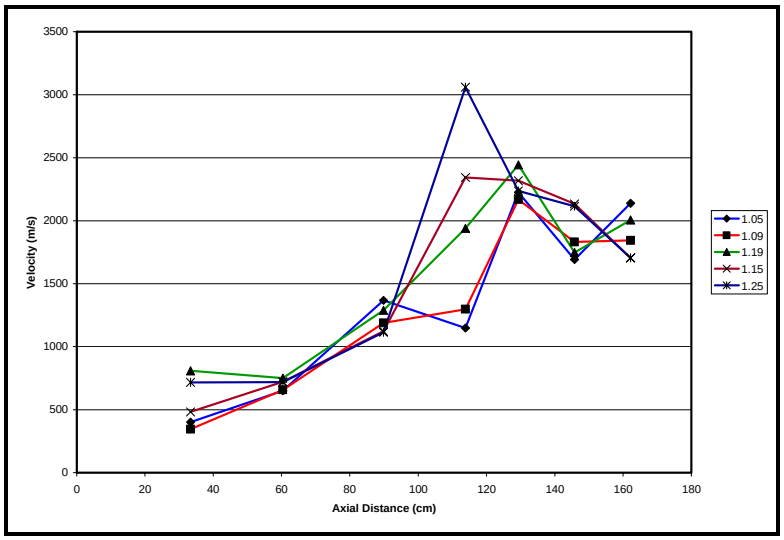

Figure 35. Plain tube wave speed vs. axial distance w/ varying equivalence ratio JP-8 (298 K) – air (395 K), 15 Hz, 8 ms ignition delay 1.829 m, 2" SS Sch 40 Tube w/ 1.219 m spiral

The heat transfer rate to the surroundings for the avgas test at the hot section was 1.8-2.5 kW/m; while JP-8 had values of 2.4-2.9 kW/m, shown in Figure 36 and Figure 37 respectively. The difference between the two tests is attributed to the higher maximum tube temperatures. The heat transfer rates are below the required heat transfer rate required for flash vaporization of JP-8 for mass flows at the same operating conditions. The high thermal resistance of free convection and radiation heat transfer limit the heat transfer possible. As will be shown, the heat exchanger tests show significantly lower thermal resistance and collect much higher heat loads required for flash vaporization.

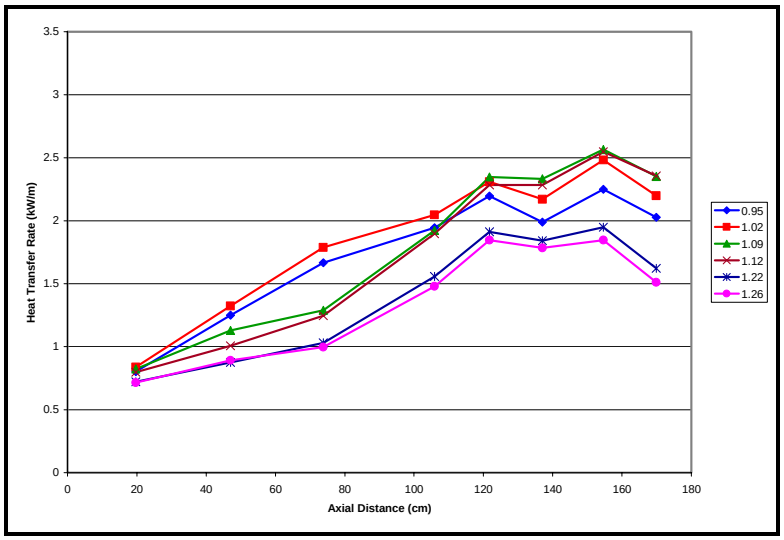

Figure 36. Plain tube heat transfer to surroundings vs. axial distance w/ varying equivalence ratio Avgas (298 K) –air (322 K), 15 Hz, 8 ms ignition delay 1.829 m, 2" SS Sch 40 Tube w/ 1.219 m spiral

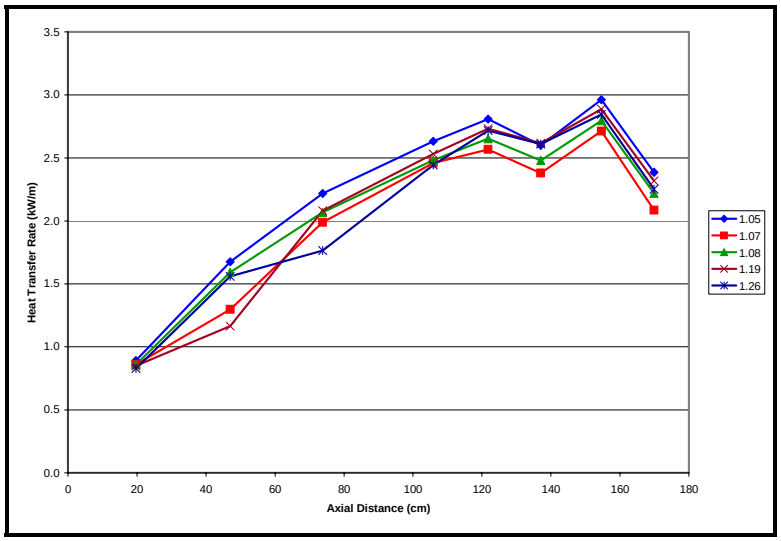

Figure 37. Plain tube heat transfer to surroundings vs. axial distance w/ varying equivalence ratio JP-8 (298 K) – air (395 K), 15 Hz, 8 ms ignition delay 1.829 m, 2" SS Sch 40 Tube w/ 1.219 m spiral

Water FVS with Hydrogen-Air Detonation

Hydrogen fueled tests with water FVS were required to prove the system design and determine initial heat transfer rates. For the first test, the long heat exchanger was used and spanned from 0.876-1.638 m measured from the head. Water pressure was maintained at 6.205-6.895 MPa. Water mass flow was varied by nozzle size until a

steady-state temperature was obtained in the 500 K-530 K range. At a water mass flow of 0.557 kg/min, the steady-state water outlet temperature of 512 K was achieved as shown in Figure 38.

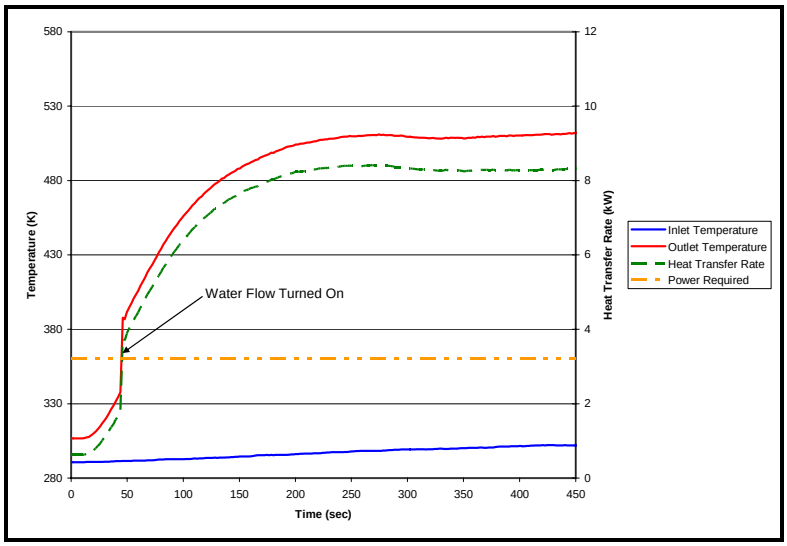

Figure 38. Temperature and heat transfer vs. time
Hydrogen - air detonation, phi 1.0, 10 Hz, ignition delay 6 ms
1.829 m, 2" SS Sch 40 Tube w/ 0.305 m spiral
Water mass flow 0.557 kg/min, heat exchanger location (0.876-1.638 m)

Steady-state heat transfer rates of over 8 kW calculated as shown in Figure 38. For a JP-8 fueled test at the same operating conditions and a two-tube configuration, using equations (17)-(21), the mass flow would have been 0.401 kg/min and the heat transfer required to obtain the same outlet temperatures would have been 3.211 kW. The high heat transfer results of this test indicated over twice the required heat transfer.

An additional hydrogen fueled test was completed at the same engine operating conditions with lower mass flow rates and lower water pressures. This test was originally intended to obtain a mass flow value closer to the JP-8 mass flow of 0.401 kg/min. The reduction in water pressure resulted in boiling within the heat exchanger. The results of

the boiling are presented so that the unique characteristics are known and can be avoided in JP-8 FVS testing.

For boiling test six thermocouples were compression clamped to the heat exchanger, three at the top and three at the bottom of the heat exchanger. The axial positions were determined by the helical coil geometry within the heat exchanger to ensure that the thermocouples were placed in the center of the flow channel. See Figure 39 for thermocouple locations and terminology. Measuring from the head, the heat exchanger spanned from 0.152-0.914 m. The water mass flow was reduced to 0.333 kg/min. The water pressure recorded at the outlet was 4.413 MPa during the test which correlates to boiling temperatures of 530 K.

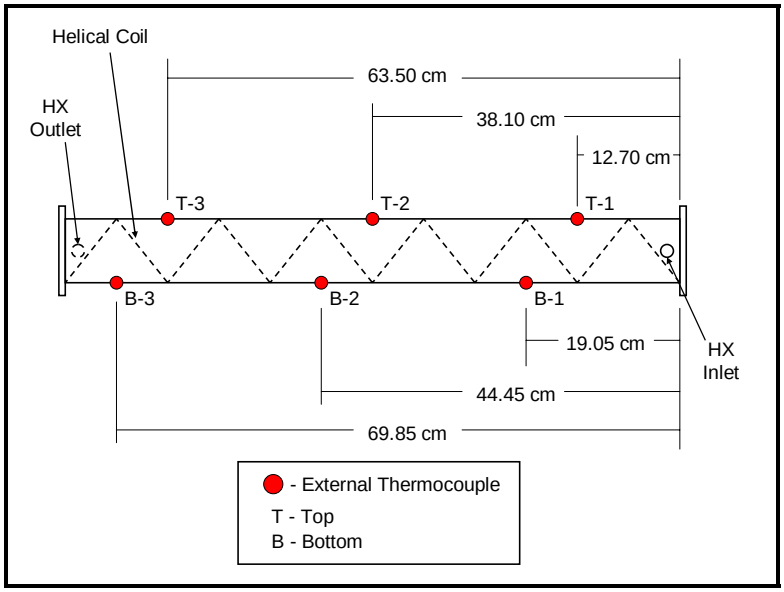

Figure 39. External thermocouple locations for hydrogen-air detonation with boiling

The data from the boiling test is shown in Figure 40 with temperatures plotted versus time. Approximately 160 seconds into the test there is a large fluctuation in the thermocouple readings. Boiling begins in this time frame and continues for the duration

of the test. The fluctuations in the various temperatures are due to the changing flow characteristics of caused by boiling. Looking at T-2 in the transient portion, the temperature plateaus momentarily at around 520 K then steadily rises to temperatures of 561 K. T-3 achieves steady-state temperatures near the boiling temperature of 534 K. When the drop through the wall which is approximately 10-15 K is accounted for the boiling may extend to this location. T-1 and all three lower thermocouples (not plotted) remained below the boiling temperature for the entire test.

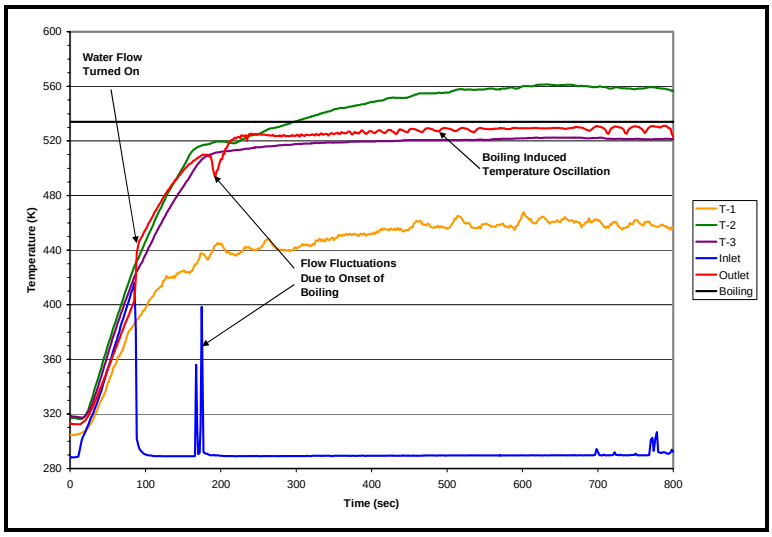

Figure 40. Temperature vs. time for boiling test
Hydrogen - air detonation, phi 1, 10 Hz, ignition delay 6 ms
1.829 m, 2" SS Sch 40 Tube w/ 0.305 m spiral
Water mass flow 0.333 kg/min, heat exchanger location (0.152-0.914 m)

The temperature readings corresponding to the time of the highest external thermocouple reading (632 seconds into the test) are shown versus axial location in Figure 41. The boiling temperature is also plotted. Note that the external temperatures do not account for the 10-15 K loss through the wall. Boiling occurs locally throughout the top portion of the heat exchanger from the middle to the outlet. The bottom of the

tube experiences a linear temperature increase throughout the length of the heat exchanger.

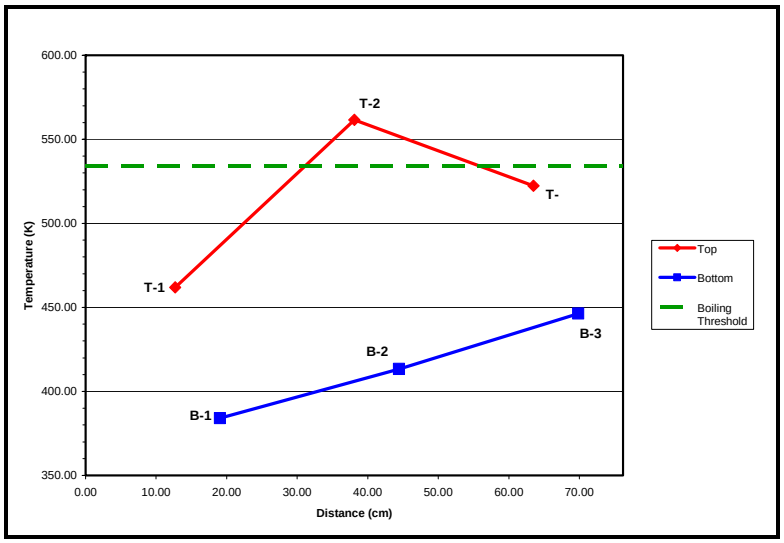

Figure 41. Steady-state external surface temperatures 632 seconds into the boiling test Hydrogen - air detonation, phi 1, 10 Hz, ignition delay 6 ms 1.829 m, 2" SS Sch 40 Tube w/ 0.305 m spiral Water mass flow 0.333 kg/min, heat exchanger location (0.152-0.914 m)

From the top and bottom temperature profile it can be concluded that the helical coil which was meant to direct flow in a helical path was not functioning as designed. If the coil had performed as designed the temperature profile would show a near linear temperature rise from inlet to the outlet on both the top and bottom as the flow travel in a helical path to the outlet.

This temperature data, which was not available for first test, provided an additional tool for monitoring boiling conditions. For the remainder of the tests either radial or spanwise temperature distributions were monitored.

Water FVS with Avgas-Air Detonation

The first hydrogen fueled water FVS test proved the FVS design and that there was more than enough heat transfer to the fluid. To determine the heat transfer of a liquid hydrocarbon fueled detonation, water FVS tests were completed with avgas as the detonation fuel.

One steady-state test was completed with the long heat exchanger using avgas-air detonations. The equivalence ratios varied from 1.04-1.10 throughout the duration of the test. The engine frequency was 15 Hz with a 4 ms ignition delay. Water mass flow was 0.837 kg/min. Water pressure was set to 6.619 MPa corresponding to a boiling temperature of 556 K. The temperature and heat transfer results are shown in Figure 42.

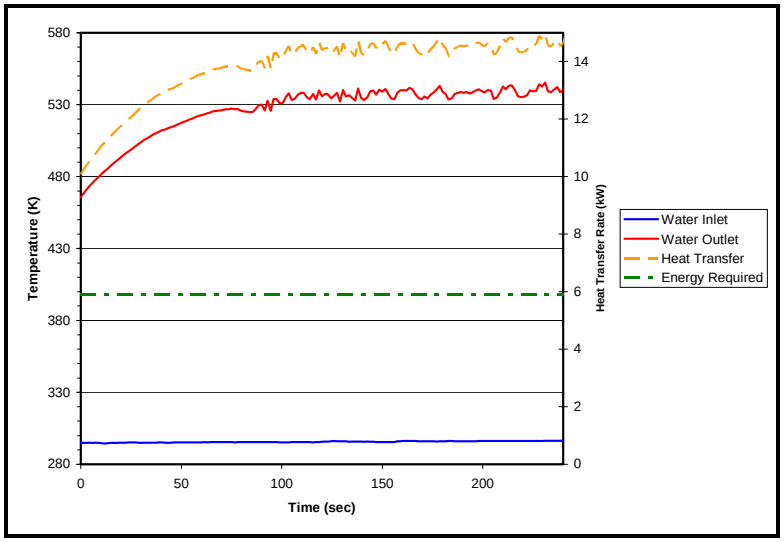

Figure 42. Temperature and heat transfer vs. time
Avgas (298 K) – air (322 K) detonation, phi 1.04-1.10, 15 Hz, ignition delay 4 ms
Water mass flow 0.837 kg/min, heat exchanger location (0.876-1.638 m)
1.829 m, 2" SS Sch 40 Tube w/ 1.219 m spiral

The steady-state temperature of 540 K was achieved with calculated heat transfer rates of over 14 kW. For a JP-8 fueled test at the same operating conditions and a two-

tube configuration, using equations (17)-(21), the mass flow would have been 0.582 kg/min and the heat transfer required to obtain the same outlet temperatures would have been 5.693 kW. Again the heat generated was over twice the required amount to flash vaporize the JP-8 mass flow for the operating conditions. Based on the results of this test and the previous water cooled tests a shorter heat exchanger was required to reduce the amount of heat transfer to the working fluid.

Noting the high thermal stratification in the previous water FVS tests, the radial temperature distribution was monitored by six thermocouples spaced at 36º increments from 0º to 180º as shown in Figure 43 for all short heat exchanger tests. The temperature profile was taken 12.7 cm prior to the heat exchanger outlet unless otherwise noted. An internal thermocouple at the same axial location recorded the internal flow temperature at the top of the heat exchanger.

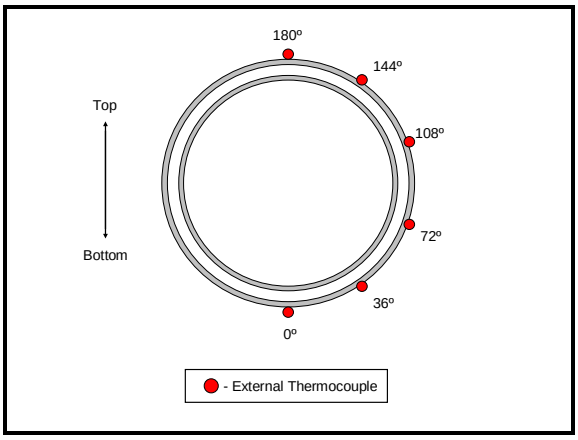

Figure 43. Thermocouple locations for radial temperature profile

For the first avgas-air test with the short heat exchanger, the engine frequency was 15 Hz with an ignition delay of 6 ms. Equivalence ratio varied from 1.05 to 1.11. The heat exchanger spanned from 1.130-1.511 m measured from the head.

With a water mass flow of 0.523 kg/min and steady-state temperature of 480 K the calculated heat transfer rate to the water was 7 kW. Using equations (17)-(21) and the same engine operating parameters and two-tube configuration the JP-8 mass flow and heat transfer would be 0.572 kg/min and 4.14 kW.

The final avgas-air test with the short heat exchanger had a measured water mass flow of 0.364 kg/min as compared to the JP-8 flow rate of 0.572 kg/min for the engine operating parameters and two-tube configuration, per equations (17)-(21). The steady-state water outlet temperature was 540 K; very closely matching the desired JP-8 flash vaporization temperature. The heat transfer rate of 6.4 kW was generated and is shown in Figure 44. For the JP-8 mass flow and the same inlet and outlet temperatures the JP-8 requires 5.48 kW of power. This test marked the first time that the heat transfer rate closely matched the heat transfer rate required for JP-8 with the same inlet and outlet temperatures.

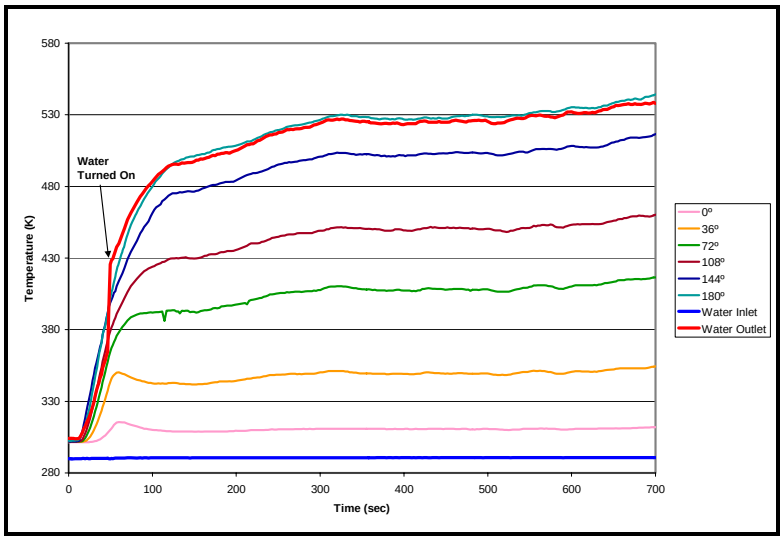

Figure 44. Inlet/Outlet and radial temperature vs. time
Avgas (298 K) – air (322 K) detonation, phi 1.06, 15 Hz, ignition delay 6 ms
Water mass flow 0.364 kg/min, heat exchanger location (1.130-1.511 m)
1.829 m, 2" SS Sch 40 Tube w/ 1.219 m spiral

From Figure 44 the radial temperature differential between consecutive radially spaced thermocouples appears to be nearly even. The radial temperature distribution also follows the same trends seen in the outlet temperature. The radial temperature profile at steady-state conditions is shown in Figure 45. The steady-state temperature profile had a 230 K thermal stratification ranging from 310 K at the bottom of the tube to the 540 K at the top of the tube. The temperature profile showed a near linear growth with radial position.

As will be shown later, the high thermal stratification is attributed to buoyancy forces. For the final outlet temperature to so closely reflect the temperature of the upper surface there must be an asymmetric velocity profile within the annular region with the hottest fluids at the top of the heat exchanger traveling at the highest velocities. This is an unexpected beneficial feature of the flow which reduces the residence time of the hottest fluids. The higher velocities in the hot fluid also contribute to higher local heat transfer coefficients which will increase heat transfer rates.

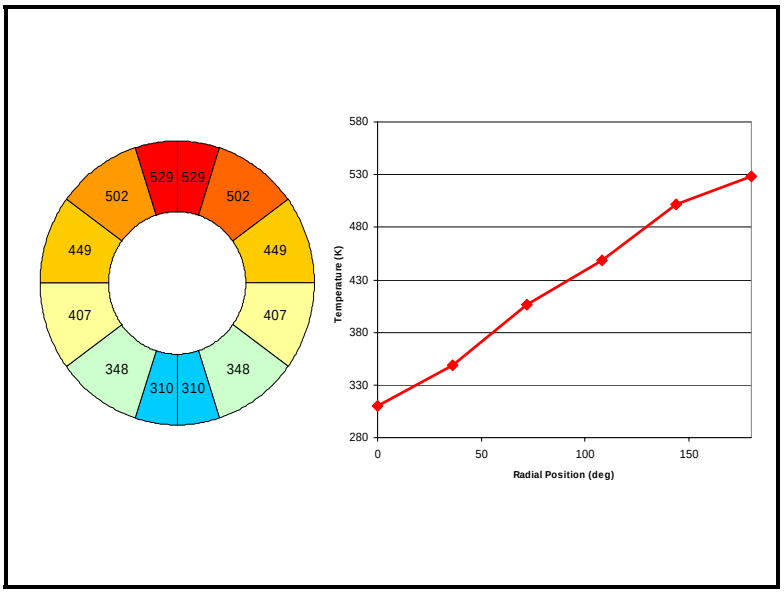

Figure 45. Radial Surface Temperature Profile (K) 25.4 cm Downstream of Inlet Avgas (298 K) – air (322 K) detonation, phi 1.06, 15 Hz, ignition delay 6 ms Water mass flow 0.364 kg/min, heat exchanger location (1.130-1.511 m) 1.829 m, 2" SS Sch 40 Tube w/ 1.219 m spiral

JP-8 Flash Vaporization System Tests

JP-8 FVS tests began with the short heat exchanger spanning from 0.470-0.851 m. The first test was completed with equivalence ratios from 1.0-1.1 with the air heated to 394 K. The engine frequency to maintain the desired equivalence ratio was 11.42 Hz and fuel mass flow of 0.355 kg/min. To prevent boiling of the JP-8 the fuel pressure was always a values above the critical pressure.

Steady-state outlet temperatures of 625 K were achieved, demonstrating the first successful flash vaporization of a JP-8-air mixture using PDE waste heat. Upon achieving steady-state heat exchanger outlet temperatures the air heater was shut off to determine if heated air is required after the fuel has been heated.

Temperature data and heat transfer rates are shown in Figure 46. Steady-state heat exchanger outlet temperatures of over 630 K were achieved after the air heater was

shut off with fuel injection temperatures of 607 K due to losses from the heat exchanger to the fuel inlet manifold. The rise in the steady-state temperature is attributed to a lower equivalence ratio which provided better engine performance as will be shown.

Steady-state heat transfer rates of 5 kW were observed. Note that steady-state conditions were maintained for over 10 minutes and the duration of the test was only limited by the fuel storage capacity.

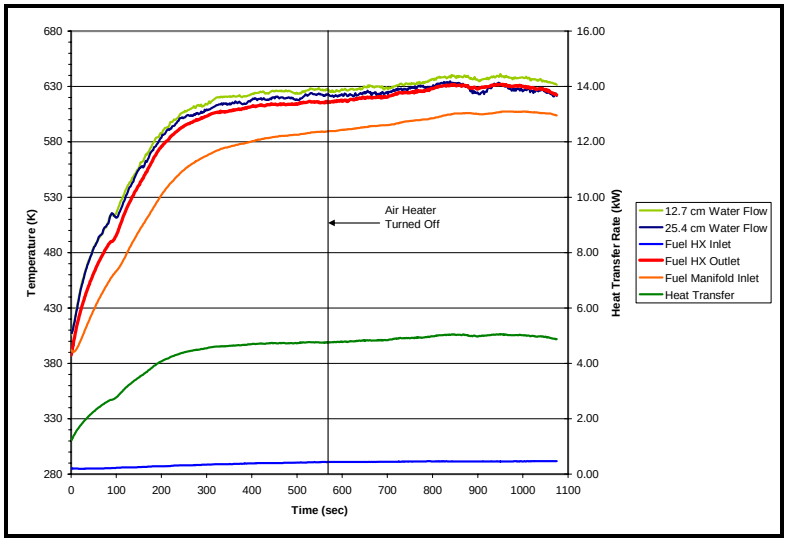

Figure 46. Temperature and heat transfer vs. time
JP-8 – air (394 K) detonation, 6 ms ignition delay
1.829 m, 2" SS Sch 40 Tube w/ 1.219 m spiral
Heat exchanger location (0.470-0.851 m)

It can be seen in Figure 47, that fuel-air mixture temperatures exceeded the 400 K threshold required for the fuel to remain in the vapor state after mixing (Tucker, 2005). In this test the mixture temperature did not achieve steady-state due to heating of the inlet manifold. Immediately prior to the air heater being shut off the mixture temperature was seven degrees Kelvin hotter than the upstream air temperature. After the air heater was shut off the transient temperature difference between mixture temperature and upstream

air temperature increased to 45 degree Kelvin. While flash vaporization was still occurring locally at the nozzles; the mixture was dual phase at temperatures below the mixture dew point. The fuel ran out prior to reaching steady-state mixture temperature for ambient upstream air temperatures.

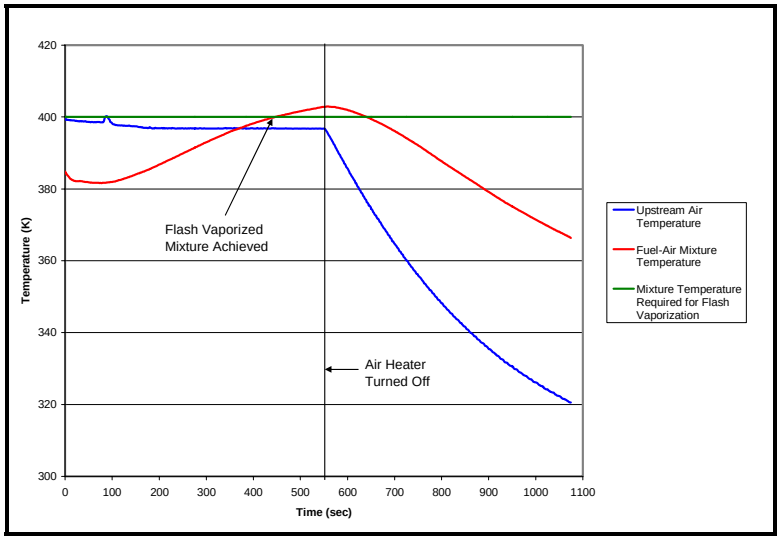

Figure 47. Mixture and Upstream Air Temperature
JP-8 – air (394 K) detonation, 6 ms ignition delay
1.829 m, 2" SS Sch 40 Tube w/ 1.219 m spiral
Heat exchanger location (0.470-0.851 m)

A twenty percent drop in mass flow occurred over the duration of the test as shown in Figure 48. For the fuel nozzles used, the mass flow is proportional to the square root of density and as a result of heating the fuel to near supercritical temperatures the reduction in density resulted in a large drop in the mass flow.

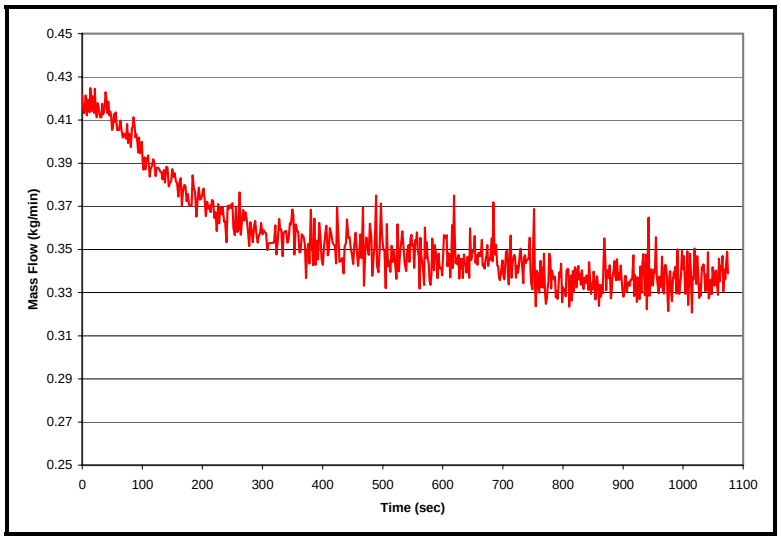

Figure 48. Fuel mass flow vs. time
JP-8 – air (394 K) detonation, 6 ms ignition delay
1.829 m, 2" SS Sch 40 Tube w/ 1.219 m spiral
Heat exchanger location (0.470-0.851 m)

Looking at normalized mass flow and the normalized square root of the AFRL SUPERTRAPP JP-8 surrogate density for the fuel outlet temperature, shown in Figure 49, it is clear the correlation between the two properties. A drawback of the fuel system used was that the fuel pressure could not be increased during the test to account for the change in density to maintain constant mass flow. To vary equivalence ratio the frequency was adjusted, effectively increased or decreased air mass flow to achieve the desired equivalence ratios.

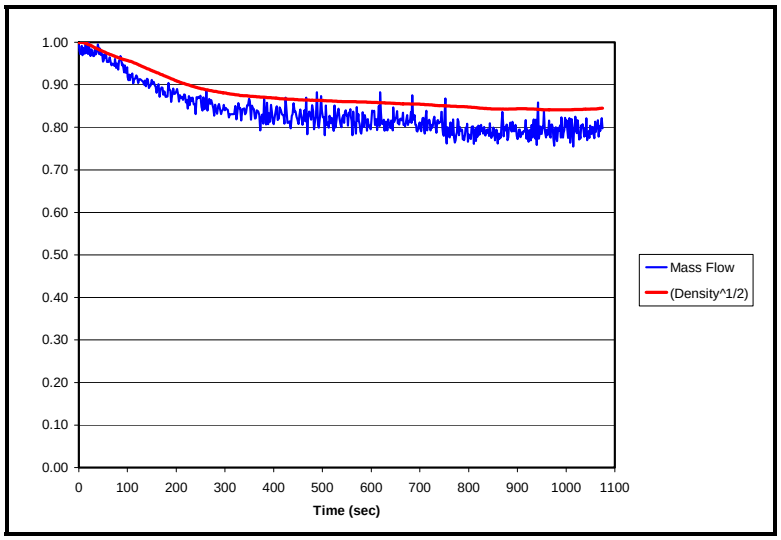

Figure 49. Normalized Mass Flow and Density$^{1/2}$
JP-8 – air (394 K) detonation, 6 ms ignition delay
1.829 m, 2" SS Sch 40 Tube w/ 1.219 m spiral
Heat exchanger location (0.470-0.851 m)

The radial temperature profile 12.7 cm from the outlet, shown Figure 50, reiterates the strong thermal gradients present in the heat exchanger. A 350 K difference between the top and bottom of the heat exchanger was present at steady-state conditions for this JP-8 FVS test.

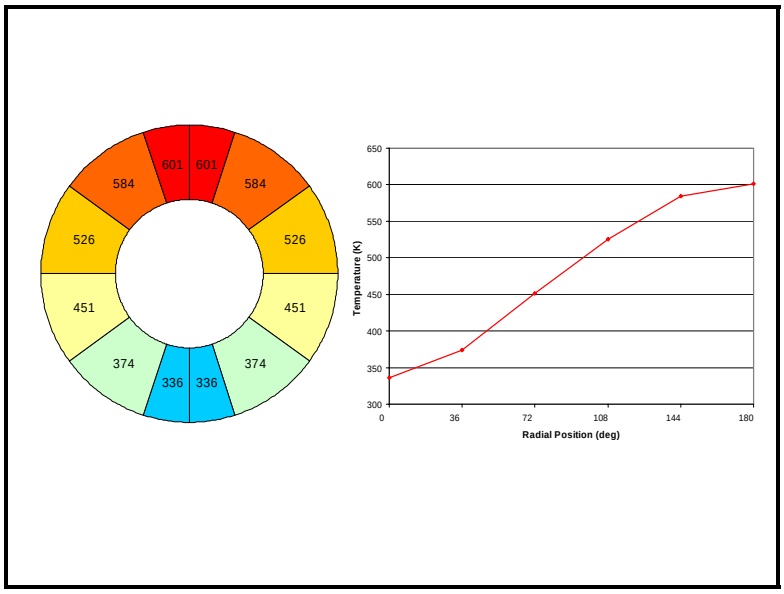

Figure 50. Surface Temperature Profile (K) 25.4 cm Downstream of Inlet
JP-8 – air (394 K) detonation, 6 ms ignition delay
1.829 m, 2" SS Sch 40 Tube w/ 1.219 m spiral
Heat exchanger location (0.470-0.851 m)

Wave speed data was developed for this test as a function of time and is presented in Figure 51. From the initial conditions to the flash vaporization state there were negligible changes in wave speed. When the air heater was shut off there was a drastic increase in wave speed. Also plotted with time is the equivalence ratio which decreases due to the decreased mass flow. The wave speed peaks at overdriven velocities at stoichiometric mixtures of flash vaporized JP-8 and then decreases but is still near the CJ velocity as equivalence ratios become lean. Remember from the plain tube tests it was not possible to obtain CJ velocities at stoichiometric and lean mixtures with unheated JP-8.

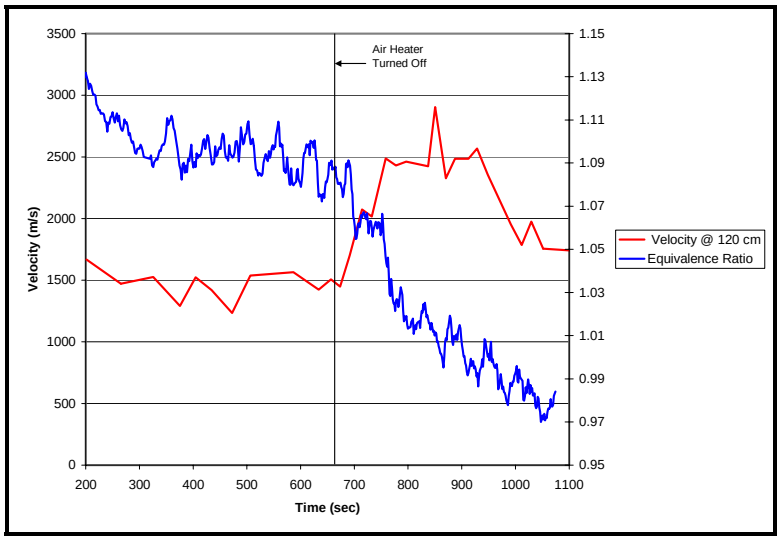

Figure 51. Wave speed and equivalence ratio vs. time
JP-8 – air (394 K) detonation, 6 ms ignition delay
1.829 m, 2" SS Sch 40 Tube w/ 1.219 m spiral
Heat exchanger location (0.470-0.851 m)

Supercritical JP-8 Tests

Having achieved flash vaporization temperatures, the scope of this work was expanded to see what JP-8 fluid temperatures could be achieved with the FVS and what complications or benefits arose from the elevated temperatures.

To obtain the highest heat transfer to the JP-8 the short heat exchanger tests moved to the hot section spanning from 1.130-1.511 m measured from the head. Engine frequency started at above 16 Hz but was adjusted throughout the test until thermal equilibrium was reached at which time the frequency was held constant at 13.88 Hz at an equivalence ratio of unity. The air was heated to 394K and ignition delay was constant at 6 ms.

Steady-state heat exchanger outlet temperatures of over 700 K, with fuel injection temperatures of 695 K and heat transfer rates of 8.85 kW were achieved as shown in

Figure 52. Note that the steady-state fuel injection temperature was well above the JP-8 critical temperature of 680 K. This was the first recorded use of supercritical JP-8 in a PDE engine.

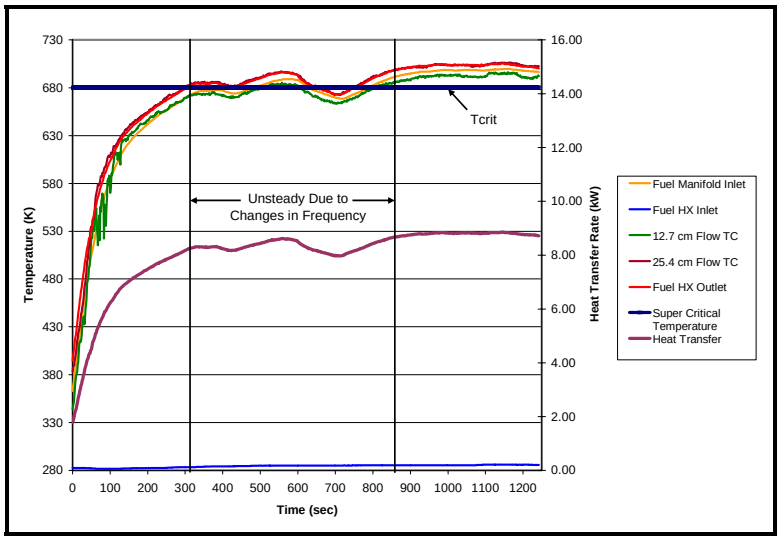

Figure 52. Fuel flow temperature vs. time
JP-8 – air (394 K) detonation, 6 ms ignition delay
1.829 m, 2" SS Sch 40 Tube w/ 1.219 m spiral
Heat exchanger location (1.130-1.511 m)

The fuel-air mixture temperature reached a steady-state temperature of 428 K. A radial temperature profile was obtained at the outlet with temperature stratification varying from 367 K at the bottom of the tube to 678 K at the top of the tube.

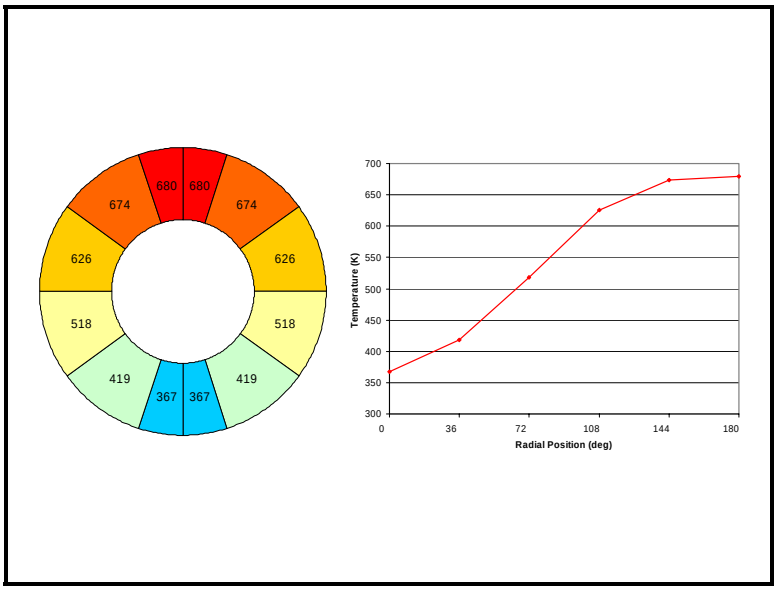

Figure 53. Radial temperature (K) profile
JP-8 – air (394 K) detonation, 6 ms ignition delay
1.829 m, 2" SS Sch 40 Tube w/ 1.219 m spiral
Heat exchanger location (1.130-1.511 m)

Mixture temperature and wave speed are plotted versus time in Figure 54. It can be seen that as the mixture temperature approaches the fully vaporized mixture temperature of 400 K that thrust tube wave speed at the end of the spiral increase to detonation wave speeds of greater than 1700 m/s (Glassman, 1996: 247).

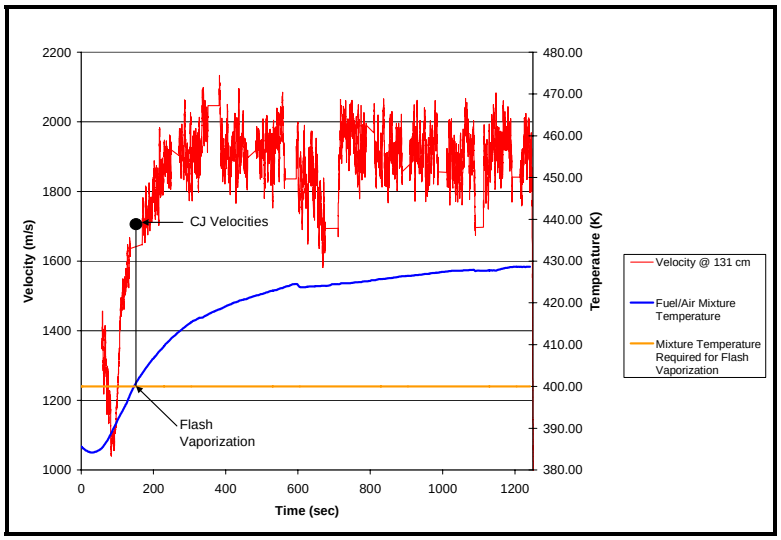

Figure 54. Wave speed and mixture temperature vs. time
JP-8 – air (394 K) detonation, 6 ms ignition delay
1.829 m, 2" SS Sch 40 Tube w/ 1.219 m spiral
Heat exchanger location (1.130-1.511 m)

The drop in superheated fuel density resulted in one third drop in fuel mass flow across the nozzles due to the mass flow proportionality to the square root of fuel density. Figure 55 shows normalized values of heat exchanger outlet temperature, the square root of AFRL SUPERTRAPP JP-8 surrogate density for the outlet temperature, and mass flow. Again the square root of the density tracks very well mass flow as a function of time.

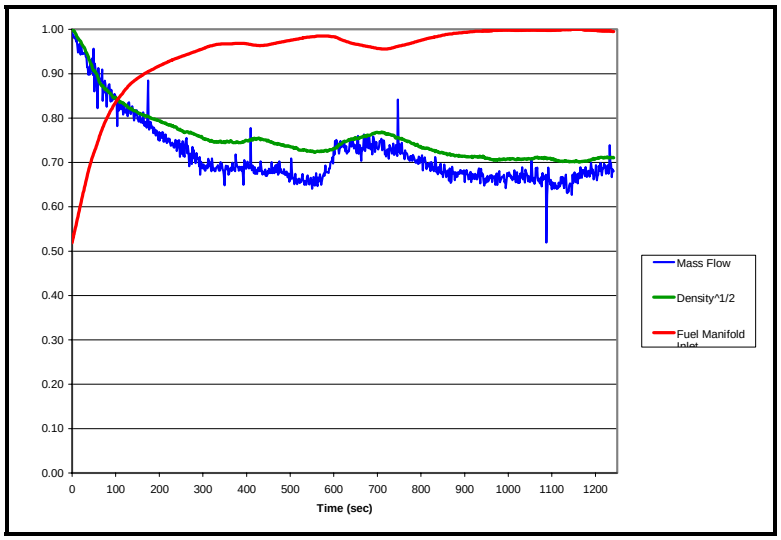

Figure 55. Normalized fuel manifold inlet temperature, mass flow, and square root of density JP-8 – air (394 K) detonation, 6 ms ignition delay 1.829 m, 2" SS Sch 40 Tube w/ 1.219 m spiral Heat exchanger location (1.130-1.511 m)

The final JP-8 FVS test was completed with the long heat exchanger installed at the hot section spanning from 0.797-1.559 m measure from the head. Engine frequency began at 20 Hz but was adjusted throughout the test until thermal equilibrium was reached at which time the frequency was held constant at 12 Hz. The air was heated to 394K and ignition delay was constant at 6 ms. Equivalence ratios varied through the test with frequency and temperature changes with steady-state equivalence ratios of approximately 1.0.

Supercritical steady-state temperatures of 760 K were achieved with a calculated heat transfer rate of 7.9 kW. The fuel-air mixture reached temperatures of 448 K which is near the auto-ignition temperature of 483 K.

The supercritical mass flow dropped significantly throughout the duration of the test with final steady-state mass flows approximately 40% of the starting value. The

square root of the AFRL SUPERTRAPP JP-8 surrogate density interpolated for the fuel manifold inlet temperate exhibits the same trends as the mass flow, but a divergence between the two data sets is apparent in the data sets shown in Figure 56.

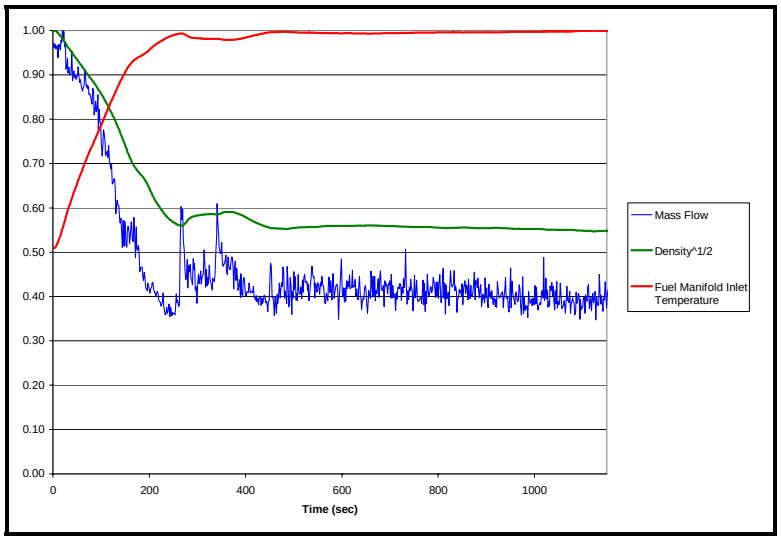

Figure 56. Normalized fuel manifold inlet temperature, mass flow, and square root of density JP-8 – air (394 K) detonation, 6 ms ignition delay 1.829 m, 2" SS Sch 40 Tube w/ 1.219 m spiral Heat exchanger location (0.797-1.559 m)

Experimental Supercritical Density Calculation

For the flow nozzles used, the mass flow is proportional to the square root of the pressure differential and the square root of the fluid density. The proportionality is multiplied by a constant to obtain the mass flow. This constant is termed the flow number (FN). The FN varies with the nozzle flow area and fluid but may be determined experimentally with known mass flows, pressures, and densities. The three forms of the nozzle mass flow equation (Bartok and Sarofim, 1991:553) are

$$FN = \frac{m_{dot}}{\sqrt{\Delta P}\cdot\sqrt{\rho}} \tag{45}$$

$$m_{dot} = FN\cdot\sqrt{\Delta P}\cdot\sqrt{\rho} \tag{46}$$

$$\rho = \frac{m_{dot}^{2}}{\Delta P\cdot FN^{2}} \tag{47}$$

For low temperature JP-8 testing the mass flow, pressure differential, and density are known allowing for the calculation of FN for a set of fuel nozzles. This is termed calibration FN which is assumed to remain constant. For all JP-8 tests, the fuel pressure was constant and the mass flow was obtained upstream of the heat exchanger allowing for the density to be calculated.

For the above method to be valid during the transient portion of the test it must be proven that the change in mass flow due to the density change may be neglected. This analysis was not completed under this work. Therefore, this method is presented as an experimental supercritical density calculation only at steady-state conditions with the assumption that the above equations are remain valid in the supercritical temperature regime tested.

Free Convection versus Forced Convection

The initial heat exchanger design analysis assumed heat transfer due to uniform flow. After the first water-cooled tests it was apparent from the thermal gradients that uniform flow could not be assumed. An analysis was completed to determine whether the buoyant or inertial forces dominated flow characteristics. A temperature range from 290 K and 650 K was used for the analysis. The mass flow rate varied from 0.3 kg/min

to 0.6 kg/min. The property data used for the analysis was the SUPERTRAPP JP-8 surrogate data presented in Appendix A.

For the analysis the Reynolds (Re) number and Grashof (Gr) number were required. The Reynolds number is the ratio of inertia forces to the viscous forces, while the Grashof number is the ratio of buoyant to inertia forces.

It can be shown that the Reynolds number for the heat exchanger is

$$Re = \frac{4 \cdot m_{dot}}{\pi \cdot (d_{oi} + d_{io}) \cdot \mu} \tag{48}$$

Where

$d_{io} = 60.325\,mm$ Inner tube outer diameter

$d_{oi} = 66.929\,mm$ Outer tube inner diameter

μ = Dynamic viscosity (N-s/m^2)

The Grashof number is

$$Gr = \frac{g \cdot \beta \cdot (T_{oi} - T_{fuel}) \cdot (d_{oi} - d_{io})^3}{\nu} \tag{49}$$

Where

T_{oi} = Inner tube outer diameter surface temperature (K)

T_{fuel} = Fuel temperature at ½ thickness of annular region (K)

$\beta = \frac{-1}{\rho} \cdot \left(\frac{d\rho}{dT} \right)$ Expansion coefficient (1/ K)

$g = 9.807 \frac{m}{s^2}$ Acceleration due to gravity

ν = Kinematic viscosity ($m^2/2$)

The temperature data for the inner tube outer diameter surface temperature was estimated to be 5 K hotter than the fuel temperature.

The ratio of Grashof number to Reynolds number squared provides insight as to whether free convection due to buoyancy or forced convection dominate. For ratios of much less than 1 the flow is dominated by forced convection. For ratios much greater than 1 the flow is dominated by free convection. For ratios of approximately one the combined effects of free and force convection must be considered (Incropera, 1996:451). The ratio of Grashof number to Reynolds number squared is presented for the temperature range in Figure 57.

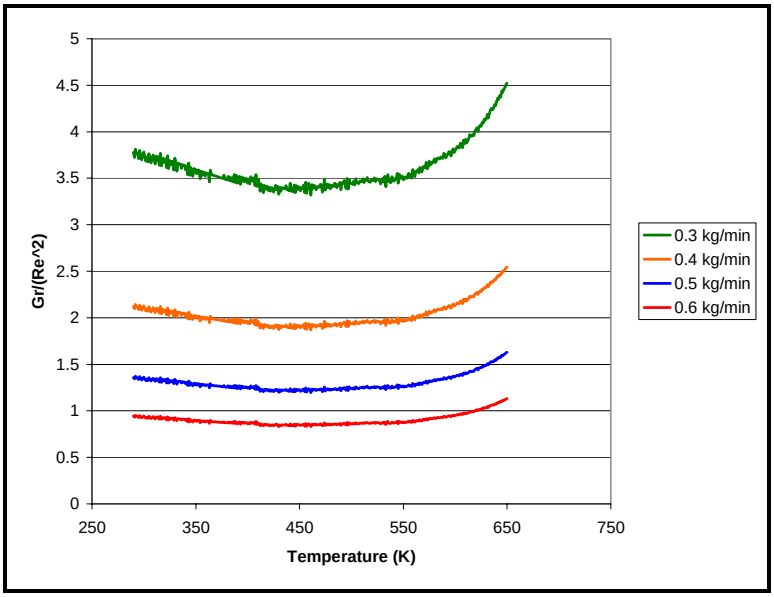

Figure 57. Ratio of Grashof number to Reynolds number squared for simulated mass flows and temperature

For the simulated mass flows, which span the range for all tests completed, the ratio indicates that buoyant forces must be considered. This analysis explains the high thermal gradients witnessed.

Coking/Deposits

Clean fuel nozzles were photographed prior to installation of J-8 FVS testing. Two supercritical JP-8 tests for a total test time of less than thirty minutes were completed. The nozzles were then removed and photographed. The photographs are presented in Figures 58 and 59. It is apparent from the blackening of the nozzles in the post test condition that some deposits have been collected on the fuel nozzles.

Figure 58. JP-8 fuel nozzles pretest condition

Figure 59. JP-8 fuel nozzles posttest condition

The deposits visible on the nozzles prompted interest into what was occurring in the heat exchanger. The long heat exchanger was no longer required after the completion of testing and was disassembled to visually determine if fuel deposits were a significant issue. The disassembled heat exchanger is pictured in Figure 60. It can be seen that surface deposits occurred throughout the heat exchanger with the exception of the local inlet area which was being cooled by the inlet flow. It can also be seen that the helical coil did not restrict the flow to the helical path as was hypothesized due to the high thermal stratification.

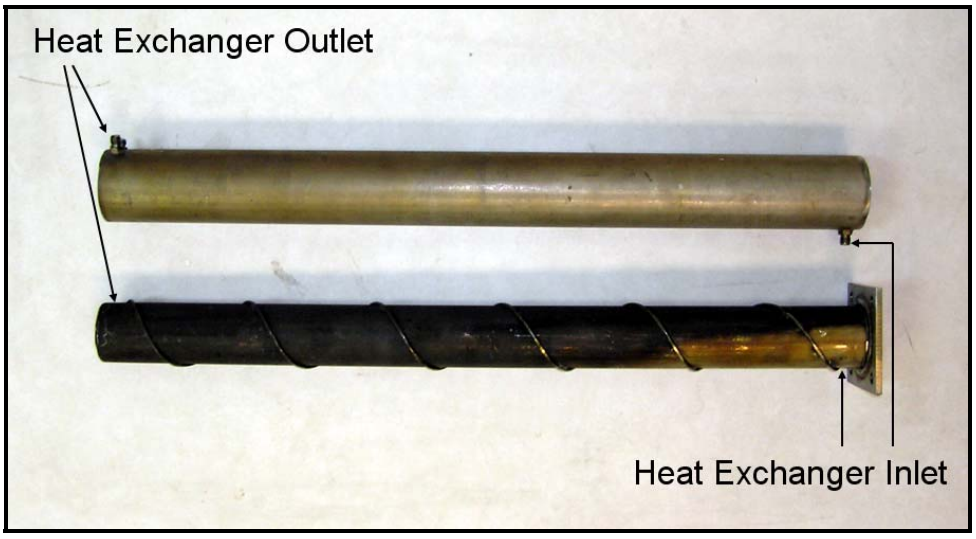

Figure 60. Disassembled long heat exchanger with carbon deposits

Fuel coking and deposits did not appear to affect any of the experimental data, but it could be seen in the fuel nozzles and long heat exchanger that deposits did occur during JP-8 FVS testing.

V. Conclusions and Recommendations

This work demonstrated the first successful use of the waste heat generated by a PDE engine for the self-sustained operation and flash vaporization of a JP-8-air mixture. The duration of the steady-state tests exceeded the operating time of any previous JP-8 fueled PDE's with run times in excess of twenty minutes and limited only by fuel storage capacity.

The flash vaporization system used permits research to be completed using liquid hydrocarbon fuels-air mixtures at steady-state conditions. The practicality of the flash vaporization system used also serves as a proof-of-concept for future PDE aerial vehicles as an efficient, simple method for the use of liquid hydrocarbon fuels.

This work also demonstrated the first successful use of supercritical JP-8 in a PDE engine. The ability to heat the fuel to supercritical temperatures without prohibitive amounts of fuel deposits or fuel thermal stability issues are attributed to the steady-state flow and the low residence time of the fuel in the heat exchanger and feed lines. Heating the fuel to supercritical temperatures and detonating the superheated fuel provides an important step to using endothermic fuels and/or experiencing endothermic reactions.

For JP-8 FVS tests fuel injection temperatures of 630 -760 K were achieved with heat transfer rates from the heat exchanger ranging from 5.0-7.9 kW. The time to achieve steady-state conditions for either heat exchanger was less than five minutes.

The heat exchanger design did not account for buoyancy effects which were shown to be a contributing factor in the test configuration. The asymmetric temperature and velocity profile of the fuel in the heat exchanger, due to the contributions on forced

and free convection, led to significantly higher heat transfer rates allowing for supercritical temperatures to be reached.

Another milestone of this work was the development of a method to experimentally determine the density of supercritical fuels by the use of mass flow rate data, temperature data, and pressure data. The method presented is only valid in during steady-state operation and assumes the governing equations are valid in the supercritical temperature range.

Using the AFRL SUPERTRAPP JP-8 surrogate, a complete set of thermodynamic property data including density, viscosity, specific heat, enthalpy, and thermal conductivity were generated for temperatures ranging from 273 - 998 K and pressures from 1 – 85 atmospheres. The tables provide a valuable tool in analysis and compare well with existing thermodynamic properties for JP-8 at low temperatures and with existing thermodynamic property prediction models at elevated temperatures.

To the author's knowledge the AFRL SUPERTRAPP JP-8 surrogate tables developed and presented in Appendix A encompass the largest surrogate data set available for JP-8. In lieu of actual JP-8 thermodynamic data this data provides reasonable approximation for analytical research and experimental predictions.

Recommendations

The fuel pressurization system used for this work was limited to a constant pressure during testing. For all of the JP-8 tests the reduction in the density due to the temperature dependence prevented the mass flow from remaining constant until steady-state conditions were reached. With this restriction the PDE frequency was varied to

obtain the desired equivalence ratio. The change in engine frequency and equivalence ratios throughout the transient portion of the test was prohibitive in determining the transient PDE characteristics. It is recommended that a variable fuel pressure system be incorporated into the existing PDE configuration to allow for constant mass flow and equivalence ratios in further high temperature liquid hydrocarbon testing.

Supercritcal temperatures were achieved in this work with the use of only one tube mounted heat exchanger feeding mass flow for a two-tube PDE configuration. Significantly higher temperatures are possible by the use of one heat exchanger per tube running the mass flow only for that tube. It may be possible with such a configuration to achieve the temperatures required for endothermic reactions. Just as performance benefits were shown by Tucker (Tucker, 2005) to occur when using a flash vaporized mixture the same may be shown by achieving endothermic reactions in the fuel.

The heat transfer to the fuel was significantly higher than the finite difference method model predicted. The model was based on a uniform flow force convection flow calculation when in actuality the flow had over a 300 K circumferential temperature gradient indicating a strong asymmetric flow profile within the heat exchanger. The strong thermal gradient and Grashof number calculations also indicated that internal heat transfer was dominated by free convection rather than forced convection. It is recommended that the fluid velocity profile and free convective heat transfer be modeled to determine if a more efficient heat exchanger design is possible. With a more efficient heat exchanger, higher temperatures and smaller lighter designs are possible.

It is recommended that further research be completed to validate the method and assumptions used to experimentally determine the liquid hydrocarbon density at supercritical temperatures. If the method is validated, it is recommended that a complete set of supercritical density tables with functions of temperature and pressure be experimentally generated. This method is not limited to JP-8 and may be incorporated in determining the supercritical density properties of any number of liquids that abide by the flow nozzle characteristics presented.

Appendix A. AFRL SUPERTRAPP JP-8 Surrogate Thermodynamic Data

AFRL SUPERTRAPP JP-8 Surrogate
Specific Heat [kJ/(kg-K)]

Temp. (K)	Pressure (atm)																	
	1	5	10	15	20	25	30	35	40	45	50	55	60	65	70	75	80	85
273	1.775	1.775	1.774	1.774	1.773	1.773	1.773	1.772	1.772	1.771	1.771	1.771	1.770	1.770	1.769	1.769	1.769	1.768
280	1.801	1.800	1.800	1.799	1.799	1.798	1.798	1.798	1.797	1.797	1.796	1.796	1.796	1.795	1.795	1.794	1.794	1.794
290	1.840	1.840	1.839	1.839	1.838	1.838	1.837	1.837	1.836	1.836	1.835	1.835	1.835	1.834	1.834	1.833	1.833	1.833
300	1.880	1.879	1.879	1.879	1.878	1.877	1.877	1.877	1.876	1.875	1.875	1.875	1.874	1.874	1.873	1.873	1.872	1.872
310	1.920	1.920	1.919	1.918	1.918	1.917	1.917	1.916	1.916	1.915	1.915	1.914	1.914	1.913	1.913	1.912	1.912	1.911
320	1.960	1.959	1.959	1.958	1.958	1.957	1.956	1.956	1.955	1.955	1.954	1.954	1.953	1.952	1.952	1.952	1.951	1.950
330	2.000	1.999	1.998	1.998	1.997	1.996	1.996	1.995	1.995	1.994	1.994	1.993	1.992	1.992	1.991	1.991	1.990	1.990
340	2.039	2.039	2.038	2.038	2.037	2.036	2.035	2.035	2.034	2.034	2.033	2.032	2.032	2.031	2.031	2.030	2.029	2.029
350	2.079	2.079	2.078	2.077	2.077	2.076	2.075	2.075	2.074	2.073	2.072	2.072	2.071	2.071	2.070	2.069	2.069	2.068
360	2.119	2.119	2.118	2.117	2.116	2.116	2.115	2.114	2.113	2.113	2.112	2.111	2.111	2.110	2.109	2.108	2.108	2.107
370	2.159	2.159	2.158	2.157	2.156	2.155	2.154	2.154	2.153	2.152	2.151	2.151	2.150	2.149	2.148	2.147	2.147	2.146
380	2.199	2.198	2.197	2.196	2.195	2.194	2.193	2.192	2.192	2.191	2.190	2.189	2.188	2.187	2.187	2.186	2.185	2.184
390	2.237	2.236	2.236	2.234	2.233	2.232	2.231	2.231	2.229	2.229	2.228	2.227	2.226	2.225	2.224	2.223	2.223	2.222
400	2.276	2.275	2.274	2.273	2.272	2.271	2.269	2.268	2.267	2.266	2.265	2.264	2.263	2.263	2.262	2.261	2.260	2.259
410	2.314	2.313	2.312	2.311	2.309	2.308	2.307	2.306	2.305	2.304	2.303	2.302	2.301	2.300	2.299	2.298	2.297	2.296
420	2.354	2.353	2.351	2.350	2.349	2.347	2.346	2.345	2.344	2.343	2.341	2.340	2.339	2.338	2.337	2.336	2.335	2.334
430	2.394	2.393	2.391	2.390	2.388	2.387	2.386	2.384	2.383	2.382	2.380	2.379	2.378	2.377	2.376	2.374	2.373	2.372
440	2.460	2.433	2.432	2.430	2.428	2.427	2.425	2.424	2.422	2.421	2.419	2.418	2.417	2.415	2.414	2.413	2.412	2.410
450	2.583	2.474	2.472	2.470	2.468	2.466	2.465	2.463	2.461	2.460	2.458	2.457	2.455	2.454	2.452	2.451	2.450	2.448
460	2.720	2.514	2.512	2.510	2.508	2.506	2.504	2.502	2.500	2.499	2.497	2.495	2.494	2.492	2.491	2.489	2.488	2.486
470	2.876	2.555	2.553	2.550	2.548	2.546	2.544	2.542	2.539	2.538	2.536	2.534	2.532	2.530	2.529	2.527	2.526	2.524
480	3.056	2.596	2.594	2.591	2.588	2.586	2.583	2.581	2.579	2.577	2.575	2.572	2.571	2.569	2.567	2.565	2.563	2.561
490	3.258	2.638	2.635	2.632	2.629	2.626	2.623	2.621	2.618	2.616	2.613	2.611	2.609	2.607	2.605	2.603	2.601	2.599
500	2.291	2.680	2.677	2.673	2.670	2.666	2.663	2.660	2.658	2.655	2.652	2.650	2.647	2.645	2.643	2.640	2.638	2.636
510	2.323	2.723	2.719	2.715	2.711	2.707	2.704	2.700	2.697	2.694	2.691	2.688	2.686	2.683	2.680	2.678	2.676	2.673
520	2.354	2.767	2.762	2.758	2.753	2.749	2.745	2.741	2.737	2.734	2.730	2.727	2.724	2.721	2.718	2.715	2.713	2.710
530	2.385	2.870	2.806	2.800	2.795	2.790	2.785	2.781	2.777	2.773	2.769	2.765	2.762	2.758	2.755	2.752	2.749	2.746
540	2.416	3.006	2.850	2.843	2.837	2.831	2.826	2.821	2.816	2.811	2.807	2.803	2.799	2.795	2.791	2.788	2.785	2.782
550	2.447	3.158	2.894	2.886	2.879	2.872	2.866	2.860	2.854	2.849	2.844	2.839	2.835	2.831	2.827	2.823	2.819	2.816
560	2.478	3.328	2.940	2.930	2.922	2.913	2.906	2.899	2.892	2.886	2.881	2.876	2.870	2.866	2.861	2.857	2.853	2.849
570	2.508	2.590	2.989	2.977	2.966	2.956	2.947	2.939	2.932	2.925	2.918	2.912	2.906	2.901	2.896	2.891	2.887	2.883
580	2.537	2.611	3.104	3.027	3.014	3.001	2.991	2.981	2.972	2.964	2.956	2.949	2.943	2.937	2.931	2.926	2.921	2.916
590	2.567	2.632	3.246	3.082	3.065	3.050	3.036	3.024	3.014	3.004	2.995	2.987	2.980	2.973	2.966	2.960	2.955	2.950
600	2.595	2.654	3.403	3.145	3.122	3.102	3.086	3.071	3.058	3.046	3.036	3.026	3.018	3.010	3.002	2.996	2.989	2.984
610	2.624	2.677	2.821	3.244	3.187	3.161	3.140	3.121	3.105	3.091	3.078	3.067	3.057	3.048	3.039	3.032	3.025	3.018
620	2.652	2.700	2.820	3.388	3.265	3.229	3.199	3.175	3.155	3.138	3.123	3.109	3.097	3.087	3.077	3.068	3.060	3.053
630	2.680	2.724	2.826	3.546	3.365	3.309	3.268	3.236	3.209	3.187	3.169	3.153	3.139	3.126	3.115	3.105	3.096	3.088
640	2.707	2.747	2.836	3.076	3.505	3.414	3.350	3.304	3.269	3.241	3.218	3.198	3.181	3.166	3.154	3.142	3.132	3.122
650	2.734	2.771	2.848	3.028	3.664	3.566	3.456	3.386	3.337	3.299	3.269	3.245	3.225	3.208	3.192	3.179	3.167	3.157
660	2.761	2.795	2.863	3.004	3.568	3.952	3.609	3.490	3.416	3.365	3.326	3.295	3.271	3.250	3.232	3.217	3.203	3.191
670	2.787	2.818	2.879	2.994	3.319	5.028	3.883	3.636	3.515	3.440	3.388	3.349	3.318	3.293	3.272	3.254	3.239	3.226
680	2.813	2.842	2.896	2.992	3.213	4.501	4.660	3.871	3.645	3.530	3.457	3.406	3.368	3.337	3.313	3.292	3.275	3.260
690	2.838	2.865	2.914	2.995	3.160	3.672	7.388	4.326	3.829	3.640	3.536	3.468	3.420	3.383	3.354	3.330	3.310	3.293
700	2.863	2.888	2.932	3.003	3.131	3.433	4.707	5.027	4.092	3.777	3.626	3.535	3.474	3.430	3.396	3.368	3.345	3.326
710	2.887	2.911	2.951	3.013	3.117	3.323	3.869	4.899	4.358	3.931	3.724	3.606	3.531	3.477	3.437	3.405	3.380	3.359
720	2.912	2.933	2.970	3.025	3.111	3.263	3.580	4.247	4.402	4.057	3.818	3.677	3.586	3.523	3.477	3.442	3.413	3.390
730	2.935	2.956	2.990	3.038	3.111	3.230	3.442	3.837	4.204	4.092	3.887	3.738	3.637	3.567	3.515	3.476	3.445	3.420
740	2.959	2.978	3.009	3.052	3.115	3.211	3.366	3.622	3.942	4.027	3.909	3.779	3.679	3.605	3.550	3.508	3.475	3.447
750	2.982	2.999	3.028	3.068	3.122	3.202	3.321	3.501	3.740	3.901	3.883	3.794	3.706	3.635	3.579	3.536	3.501	3.473
760	3.004	3.021	3.048	3.083	3.132	3.199	3.294	3.429	3.606	3.768	3.821	3.782	3.716	3.654	3.602	3.559	3.525	3.496
770	3.026	3.042	3.067	3.100	3.143	3.200	3.278	3.384	3.518	3.658	3.744	3.749	3.711	3.663	3.617	3.577	3.544	3.516
780	3.048	3.063	3.086	3.116	3.155	3.205	3.270	3.355	3.461	3.577	3.668	3.704	3.693	3.661	3.624	3.590	3.559	3.533
790	3.070	3.084	3.106	3.133	3.168	3.212	3.268	3.338	3.424	3.518	3.603	3.655	3.666	3.651	3.625	3.597	3.570	3.546
800	3.091	3.104	3.125	3.150	3.181	3.221	3.269	3.328	3.399	3.477	3.553	3.609	3.634	3.634	3.620	3.599	3.577	3.556
810	3.111	3.124	3.143	3.167	3.196	3.231	3.273	3.324	3.383	3.449	3.515	3.570	3.603	3.615	3.610	3.597	3.580	3.563
820	3.132	3.144	3.162	3.184	3.210	3.242	3.280	3.324	3.374	3.430	3.487	3.538	3.575	3.594	3.598	3.592	3.581	3.567
830	3.152	3.163	3.180	3.201	3.225	3.254	3.288	3.326	3.370	3.418	3.468	3.514	3.551	3.574	3.585	3.585	3.579	3.570
840	3.172	3.183	3.199	3.218	3.240	3.266	3.297	3.331	3.370	3.411	3.455	3.496	3.531	3.557	3.572	3.577	3.576	3.570
850	3.191	3.201	3.217	3.235	3.256	3.280	3.307	3.338	3.372	3.408	3.446	3.484	3.517	3.543	3.560	3.570	3.572	3.570
860	3.210	3.220	3.235	3.251	3.271	3.293	3.318	3.346	3.376	3.409	3.442	3.475	3.506	3.532	3.550	3.562	3.568	3.569
870	3.229	3.238	3.252	3.268	3.286	3.307	3.329	3.355	3.382	3.411	3.441	3.471	3.499	3.523	3.543	3.556	3.564	3.567
880	3.247	3.257	3.270	3.285	3.301	3.321	3.341	3.365	3.389	3.415	3.442	3.469	3.495	3.518	3.537	3.551	3.561	3.566
890	3.265	3.274	3.287	3.301	3.317	3.334	3.354	3.375	3.397	3.421	3.446	3.470	3.493	3.515	3.533	3.548	3.559	3.566
900	3.283	3.292	3.304	3.317	3.332	3.349	3.367	3.386	3.407	3.428	3.450	3.472	3.494	3.514	3.532	3.546	3.558	3.565
910	3.301	3.309	3.321	3.333	3.347	3.363	3.380	3.398	3.416	3.436	3.456	3.477	3.496	3.515	3.532	3.546	3.558	3.566
920	3.318	3.326	3.337	3.349	3.363	3.377	3.393	3.409	3.427	3.445	3.463	3.482	3.500	3.517	3.533	3.547	3.559	3.568
930	3.336	3.343	3.354	3.365	3.378	3.391	3.406	3.422	3.438	3.454	3.471	3.489	3.505	3.521	3.536	3.550	3.561	3.570
940	3.352	3.360	3.370	3.381	3.393	3.406	3.419	3.434	3.449	3.464	3.480	3.496	3.511	3.526	3.540	3.553	3.564	3.573
950	3.369	3.376	3.386	3.396	3.408	3.420	3.433	3.446	3.460	3.475	3.489	3.504	3.519	3.532	3.546	3.558	3.568	3.577
960	3.386	3.392	3.402	3.412	3.423	3.434	3.446	3.459	3.472	3.486	3.499	3.513	3.526	3.539	3.552	3.563	3.573	3.582
970	3.402	3.409	3.417	3.427	3.437	3.448	3.460	3.472	3.484	3.497	3.510	3.522	3.535	3.547	3.559	3.569	3.579	3.588
980	3.418	3.425	3.433	3.442	3.452	3.463	3.474	3.485	3.496	3.508	3.520	3.532	3.544	3.555	3.566	3.576	3.586	3.594
990	3.434	3.440	3.449	3.457	3.467	3.477	3.487	3.498	3.509	3.520	3.531	3.542	3.553	3.564	3.574	3.584	3.593	3.601

AFRL SUPERTRAPP JP-8 Surrogate
Enthalpy [kJ/kg]

Temp. (K)	Pressure (atm)																	
	1	5	10	15	20	25	30	35	40	45	50	55	60	65	70	75	80	85
273	485	484	484	484	484	484	484	484	484	484	483	483	483	483	483	483	483	483
280	504	504	504	504	504	504	503	503	503	503	503	503	503	503	503	502	502	502
290	534	534	533	533	533	533	533	533	533	532	532	532	532	532	532	532	532	531
300	564	564	564	564	563	563	563	563	563	563	563	562	562	562	562	562	562	562
310	595	595	595	595	595	594	594	594	594	594	594	593	593	593	593	593	593	592
320	627	627	627	627	626	626	626	626	626	626	625	625	625	625	625	624	624	624
330	660	660	659	659	659	659	659	658	658	658	658	658	657	657	657	657	657	657
340	693	693	693	693	693	692	692	692	692	691	691	691	691	691	690	690	690	690
350	728	728	727	727	727	727	726	726	726	726	725	725	725	725	724	724	724	724
360	763	763	762	762	762	762	761	761	761	761	760	760	760	759	759	759	759	759
370	799	799	798	798	798	797	797	797	797	796	796	796	795	795	795	795	794	794
380	836	835	835	835	834	834	833	833	833	832	832	832	832	831	831	831	830	830
390	873	872	872	871	871	871	870	870	870	869	869	868	868	868	867	867	867	867
400	910	910	910	909	909	908	908	907	907	907	906	906	905	905	905	904	904	904
410	949	948	948	947	947	946	946	946	945	945	944	944	943	943	943	942	942	941
420	989	988	988	987	986	986	985	985	984	984	983	983	982	982	982	981	981	980
430	1030	1029	1028	1028	1027	1026	1026	1025	1025	1024	1024	1023	1023	1022	1022	1021	1021	1020
440	1082	1071	1070	1069	1068	1068	1067	1066	1066	1065	1064	1064	1063	1063	1062	1062	1061	1061
450	1162	1113	1112	1111	1111	1110	1109	1108	1108	1107	1106	1105	1105	1104	1104	1103	1102	1102
460	1251	1157	1156	1155	1154	1153	1152	1151	1150	1149	1149	1148	1147	1146	1146	1145	1144	1144
470	1352	1201	1200	1199	1198	1197	1195	1195	1194	1193	1192	1191	1190	1189	1188	1188	1187	1186
480	1467	1246	1245	1244	1242	1241	1240	1239	1238	1237	1236	1235	1234	1233	1232	1231	1230	1229
490	1596	1293	1291	1290	1288	1287	1285	1284	1283	1282	1281	1279	1278	1277	1276	1275	1274	1273
500	1145	1340	1338	1337	1335	1333	1332	1330	1329	1327	1326	1325	1324	1322	1321	1320	1319	1318
510	1185	1389	1387	1385	1383	1381	1379	1377	1376	1374	1373	1371	1370	1368	1367	1366	1365	1363
520	1224	1439	1436	1434	1432	1429	1427	1425	1423	1421	1420	1418	1416	1415	1413	1412	1411	1409
530	1264	1521	1487	1484	1481	1479	1476	1474	1472	1469	1467	1466	1464	1462	1460	1459	1457	1456
540	1305	1623	1539	1535	1532	1529	1526	1523	1520	1518	1516	1513	1511	1509	1507	1506	1504	1502
550	1346	1737	1592	1588	1583	1580	1576	1573	1570	1567	1564	1562	1559	1557	1555	1553	1551	1549
560	1387	1864	1646	1641	1636	1632	1627	1623	1620	1616	1613	1610	1607	1605	1602	1600	1598	1596
570	1429	1476	1704	1697	1691	1685	1680	1675	1671	1667	1663	1660	1657	1654	1651	1648	1646	1643
580	1472	1514	1800	1756	1748	1741	1735	1729	1724	1719	1715	1710	1707	1703	1700	1697	1694	1691
590	1514	1553	1915	1818	1808	1799	1791	1784	1778	1772	1767	1762	1758	1754	1750	1747	1743	1740
600	1557	1593	2042	1887	1873	1861	1851	1842	1835	1828	1821	1816	1811	1806	1801	1797	1794	1790
610	1601	1633	1721	1979	1944	1928	1915	1904	1894	1885	1878	1871	1865	1859	1854	1849	1845	1841
620	1644	1674	1749	2100	2025	2002	1984	1969	1956	1945	1936	1928	1920	1914	1908	1902	1897	1893
630	1688	1716	1780	2234	2120	2085	2059	2038	2022	2008	1996	1986	1977	1970	1962	1956	1950	1945
640	1733	1758	1815	1969	2243	2185	2144	2115	2092	2074	2059	2047	2036	2026	2018	2011	2004	1998
650	1777	1801	1851	1968	2381	2318	2246	2201	2169	2144	2125	2109	2096	2085	2075	2066	2059	2052
660	1822	1845	1889	1983	2355	2608	2382	2303	2255	2221	2195	2175	2159	2145	2133	2123	2114	2106
670	1867	1888	1929	2006	2224	3369	2602	2436	2355	2305	2270	2244	2223	2206	2192	2180	2170	2161
680	1913	1932	1969	2034	2185	3061	3169	2632	2479	2400	2351	2316	2290	2270	2253	2239	2227	2217
690	1958	1977	2010	2067	2180	2533	5098	2985	2642	2512	2440	2393	2360	2334	2314	2298	2284	2272
700	2004	2021	2052	2102	2192	2403	3295	3519	2864	2644	2538	2475	2432	2401	2377	2358	2342	2328
710	2050	2067	2095	2139	2213	2359	2747	3479	3094	2791	2644	2561	2507	2469	2440	2418	2400	2385
720	2096	2112	2139	2178	2240	2350	2578	3058	3169	2921	2749	2647	2582	2537	2504	2478	2458	2441
730	2143	2158	2182	2218	2271	2358	2513	2801	3069	2987	2838	2729	2655	2604	2566	2538	2515	2496
740	2189	2203	2227	2259	2305	2376	2491	2680	2917	2980	2893	2796	2722	2668	2627	2596	2571	2551
750	2236	2250	2271	2301	2342	2401	2491	2626	2805	2926	2913	2845	2779	2726	2684	2652	2626	2605
760	2283	2296	2316	2343	2380	2431	2503	2606	2740	2864	2904	2874	2824	2777	2737	2705	2679	2657
770	2330	2342	2362	2387	2420	2464	2524	2605	2709	2817	2883	2887	2858	2820	2785	2754	2729	2707
780	2378	2389	2407	2431	2461	2500	2551	2617	2700	2790	2861	2889	2880	2856	2827	2800	2776	2755
790	2425	2436	2453	2475	2503	2537	2582	2637	2705	2779	2847	2887	2896	2884	2864	2841	2820	2801
800	2472	2483	2500	2520	2545	2576	2615	2663	2719	2782	2842	2887	2908	2908	2896	2879	2861	2845
810	2520	2531	2546	2565	2589	2617	2651	2693	2741	2794	2847	2891	2919	2928	2924	2914	2900	2886
820	2568	2578	2593	2611	2632	2658	2689	2726	2767	2813	2860	2901	2931	2947	2950	2946	2936	2925
830	2616	2626	2640	2657	2677	2701	2729	2761	2797	2837	2878	2917	2947	2967	2975	2976	2971	2963
840	2664	2673	2687	2703	2722	2744	2769	2798	2830	2866	2902	2937	2966	2988	3000	3005	3004	2999
850	2712	2721	2734	2749	2767	2788	2811	2837	2866	2897	2930	2961	2989	3011	3026	3034	3036	3034
860	2761	2769	2782	2796	2813	2832	2853	2877	2903	2931	2960	2989	3015	3037	3053	3063	3068	3069
870	2809	2817	2829	2843	2859	2877	2897	2919	2942	2968	2994	3020	3044	3065	3082	3094	3101	3104
880	2858	2866	2877	2890	2905	2922	2941	2961	2982	3005	3029	3053	3076	3096	3112	3125	3134	3138
890	2906	2914	2925	2938	2952	2968	2985	3004	3024	3045	3066	3088	3109	3128	3145	3158	3167	3173
900	2955	2963	2973	2985	2999	3014	3030	3047	3066	3085	3105	3125	3145	3163	3178	3192	3202	3209
910	3004	3011	3022	3033	3046	3060	3075	3092	3109	3127	3145	3164	3182	3199	3214	3227	3237	3245
920	3053	3060	3070	3081	3094	3107	3121	3137	3153	3169	3186	3203	3220	3236	3251	3263	3274	3282
930	3102	3109	3119	3130	3141	3154	3168	3182	3197	3213	3228	3244	3260	3275	3289	3301	3312	3320
940	3151	3158	3168	3178	3189	3201	3214	3228	3242	3257	3271	3286	3301	3315	3328	3340	3350	3359
950	3201	3207	3217	3226	3237	3249	3261	3274	3287	3301	3315	3329	3343	3356	3368	3380	3390	3399
960	3250	3257	3266	3275	3286	3297	3309	3321	3333	3346	3359	3372	3385	3398	3410	3420	3430	3439
970	3300	3306	3315	3324	3334	3345	3356	3368	3380	3392	3404	3417	3429	3440	3452	3462	3472	3480
980	3350	3356	3364	3373	3383	3393	3404	3415	3426	3438	3450	3461	3473	3484	3495	3505	3514	3522
990	3400	3406	3414	3423	3432	3442	3452	3463	3474	3485	3496	3507	3518	3528	3538	3548	3557	3565

AFRL SUPERTRAPP JP-8 Surrogate
Thermal Conductivity [W/(m-K)]

Temp. (K)	Pressure (atm)																	
	1	5	10	15	20	25	30	35	40	45	50	55	60	65	70	75	80	85
273	0.137	0.138	0.138	0.138	0.138	0.138	0.139	0.139	0.139	0.139	0.139	0.139	0.140	0.140	0.140	0.140	0.140	0.141
280	0.137	0.137	0.137	0.137	0.137	0.138	0.138	0.138	0.138	0.138	0.139	0.139	0.139	0.139	0.139	0.140	0.140	0.140
290	0.136	0.136	0.136	0.136	0.136	0.137	0.137	0.137	0.137	0.137	0.138	0.138	0.138	0.138	0.138	0.139	0.139	0.139
300	0.134	0.135	0.135	0.135	0.135	0.135	0.136	0.136	0.136	0.136	0.136	0.137	0.137	0.137	0.137	0.137	0.138	0.138
310	0.133	0.133	0.134	0.134	0.134	0.134	0.134	0.135	0.135	0.135	0.135	0.135	0.136	0.136	0.136	0.136	0.136	0.137
320	0.132	0.132	0.132	0.132	0.133	0.133	0.133	0.133	0.134	0.134	0.134	0.134	0.134	0.135	0.135	0.135	0.135	0.135
330	0.130	0.131	0.131	0.131	0.131	0.132	0.132	0.132	0.132	0.132	0.133	0.133	0.133	0.133	0.134	0.134	0.134	0.134
340	0.129	0.129	0.129	0.130	0.130	0.130	0.130	0.131	0.131	0.131	0.131	0.132	0.132	0.132	0.132	0.132	0.133	0.133
350	0.127	0.128	0.128	0.128	0.128	0.129	0.129	0.129	0.129	0.130	0.130	0.130	0.130	0.131	0.131	0.131	0.131	0.132
360	0.126	0.126	0.126	0.127	0.127	0.127	0.127	0.128	0.128	0.128	0.128	0.129	0.129	0.129	0.129	0.130	0.130	0.130
370	0.124	0.125	0.125	0.125	0.125	0.126	0.126	0.126	0.126	0.127	0.127	0.127	0.127	0.128	0.128	0.128	0.129	0.129
380	0.123	0.123	0.123	0.123	0.124	0.124	0.124	0.125	0.125	0.125	0.125	0.126	0.126	0.126	0.126	0.127	0.127	0.127
390	0.121	0.121	0.122	0.122	0.122	0.122	0.123	0.123	0.123	0.124	0.124	0.124	0.124	0.125	0.125	0.125	0.125	0.126
400	0.119	0.119	0.120	0.120	0.120	0.121	0.121	0.121	0.122	0.122	0.122	0.122	0.123	0.123	0.123	0.124	0.124	0.124
410	0.118	0.118	0.118	0.118	0.119	0.119	0.119	0.120	0.120	0.120	0.121	0.121	0.121	0.122	0.122	0.122	0.122	0.123
420	0.116	0.116	0.116	0.117	0.117	0.117	0.118	0.118	0.118	0.119	0.119	0.119	0.120	0.120	0.120	0.120	0.121	0.121
430	0.114	0.114	0.114	0.115	0.115	0.115	0.116	0.116	0.116	0.117	0.117	0.117	0.118	0.118	0.118	0.119	0.119	0.119
440	0.112	0.112	0.113	0.113	0.113	0.114	0.114	0.114	0.115	0.115	0.115	0.116	0.116	0.116	0.117	0.117	0.117	0.118
450	0.112	0.110	0.110	0.111	0.111	0.112	0.112	0.112	0.113	0.113	0.113	0.114	0.114	0.114	0.115	0.115	0.115	0.116
460	0.111	0.108	0.108	0.108	0.109	0.109	0.110	0.110	0.110	0.111	0.111	0.111	0.112	0.112	0.112	0.113	0.113	0.114
470	0.111	0.105	0.106	0.106	0.106	0.107	0.107	0.108	0.108	0.108	0.109	0.109	0.110	0.110	0.110	0.111	0.111	0.111
480	0.110	0.103	0.103	0.103	0.104	0.104	0.105	0.105	0.105	0.106	0.106	0.107	0.107	0.107	0.108	0.108	0.109	0.109
490	0.108	0.100	0.100	0.101	0.101	0.102	0.102	0.103	0.103	0.103	0.104	0.104	0.105	0.105	0.105	0.106	0.106	0.107
500	0.025	0.097	0.098	0.098	0.099	0.099	0.100	0.100	0.101	0.101	0.101	0.102	0.102	0.103	0.103	0.103	0.104	0.104
510	0.026	0.095	0.095	0.096	0.096	0.097	0.097	0.098	0.098	0.099	0.099	0.100	0.100	0.100	0.101	0.101	0.102	0.102
520	0.027	0.093	0.093	0.094	0.094	0.095	0.095	0.095	0.096	0.096	0.097	0.097	0.098	0.098	0.099	0.099	0.099	0.100
530	0.028	0.091	0.091	0.091	0.092	0.092	0.093	0.093	0.094	0.094	0.095	0.095	0.095	0.096	0.096	0.097	0.097	0.098
540	0.029	0.091	0.088	0.089	0.089	0.090	0.090	0.091	0.091	0.092	0.092	0.093	0.093	0.094	0.094	0.095	0.095	0.096
550	0.030	0.090	0.086	0.087	0.087	0.088	0.088	0.089	0.089	0.090	0.090	0.091	0.091	0.092	0.092	0.093	0.093	0.094
560	0.031	0.089	0.084	0.084	0.085	0.086	0.086	0.087	0.087	0.088	0.088	0.089	0.089	0.090	0.090	0.091	0.091	0.092
570	0.032	0.033	0.081	0.082	0.083	0.083	0.084	0.085	0.085	0.086	0.086	0.087	0.087	0.088	0.088	0.089	0.089	0.090
580	0.033	0.034	0.081	0.080	0.081	0.081	0.082	0.083	0.083	0.084	0.084	0.085	0.085	0.086	0.086	0.087	0.087	0.088
590	0.034	0.035	0.080	0.078	0.078	0.079	0.080	0.080	0.081	0.082	0.082	0.083	0.084	0.084	0.085	0.085	0.086	0.086
600	0.035	0.036	0.079	0.075	0.076	0.077	0.078	0.078	0.079	0.080	0.080	0.081	0.082	0.082	0.083	0.083	0.084	0.084
610	0.036	0.037	0.038	0.074	0.074	0.075	0.076	0.077	0.077	0.078	0.079	0.079	0.080	0.080	0.081	0.082	0.082	0.083
620	0.037	0.038	0.039	0.073	0.072	0.073	0.074	0.075	0.075	0.076	0.077	0.077	0.078	0.079	0.079	0.080	0.081	0.081
630	0.038	0.039	0.040	0.073	0.070	0.071	0.072	0.073	0.073	0.074	0.075	0.076	0.076	0.077	0.078	0.078	0.079	0.079
640	0.039	0.040	0.041	0.042	0.069	0.068	0.070	0.071	0.072	0.072	0.073	0.074	0.075	0.075	0.076	0.077	0.077	0.078
650	0.040	0.041	0.042	0.043	0.068	0.066	0.067	0.068	0.069	0.070	0.071	0.072	0.073	0.073	0.074	0.075	0.075	0.076
660	0.041	0.042	0.043	0.043	0.045	0.061	0.064	0.065	0.066	0.067	0.068	0.069	0.070	0.071	0.071	0.072	0.072	0.073
670	0.042	0.043	0.044	0.044	0.046	0.058	0.061	0.062	0.064	0.065	0.066	0.066	0.067	0.068	0.069	0.069	0.070	0.070
680	0.044	0.044	0.045	0.045	0.046	0.049	0.059	0.061	0.063	0.064	0.065	0.066	0.067	0.067	0.068	0.069	0.069	0.070
690	0.045	0.045	0.046	0.046	0.047	0.049	0.054	0.059	0.062	0.063	0.064	0.065	0.066	0.067	0.068	0.068	0.069	0.070
700	0.046	0.046	0.047	0.047	0.048	0.050	0.052	0.057	0.060	0.062	0.063	0.065	0.066	0.066	0.067	0.068	0.069	0.069
710	0.047	0.047	0.048	0.048	0.049	0.050	0.052	0.055	0.059	0.061	0.063	0.064	0.065	0.066	0.067	0.068	0.068	0.069
720	0.048	0.048	0.049	0.049	0.050	0.051	0.052	0.055	0.058	0.060	0.062	0.063	0.065	0.066	0.066	0.067	0.068	0.069
730	0.049	0.049	0.050	0.050	0.051	0.052	0.053	0.055	0.057	0.059	0.061	0.063	0.064	0.065	0.066	0.067	0.068	0.069
740	0.050	0.050	0.051	0.051	0.052	0.053	0.054	0.055	0.057	0.059	0.061	0.063	0.064	0.065	0.066	0.067	0.068	0.068
750	0.051	0.051	0.052	0.052	0.053	0.054	0.055	0.056	0.057	0.059	0.061	0.062	0.064	0.065	0.066	0.067	0.068	0.068
760	0.052	0.052	0.053	0.053	0.054	0.055	0.056	0.057	0.058	0.059	0.061	0.062	0.064	0.065	0.066	0.067	0.068	0.068
770	0.053	0.053	0.054	0.054	0.055	0.056	0.057	0.057	0.059	0.060	0.061	0.062	0.064	0.065	0.066	0.067	0.068	0.069
780	0.054	0.054	0.055	0.055	0.056	0.057	0.057	0.058	0.059	0.060	0.062	0.063	0.064	0.065	0.066	0.067	0.068	0.069
790	0.055	0.055	0.056	0.057	0.057	0.058	0.058	0.059	0.060	0.061	0.062	0.063	0.064	0.065	0.066	0.067	0.068	0.069
800	0.056	0.057	0.057	0.058	0.058	0.059	0.059	0.060	0.061	0.062	0.063	0.064	0.065	0.066	0.067	0.068	0.068	0.069
810	0.057	0.058	0.058	0.059	0.059	0.060	0.060	0.061	0.062	0.063	0.063	0.064	0.065	0.066	0.067	0.068	0.069	0.069
820	0.058	0.059	0.059	0.060	0.060	0.061	0.061	0.062	0.063	0.063	0.064	0.065	0.066	0.067	0.068	0.068	0.069	0.070
830	0.059	0.060	0.060	0.061	0.061	0.062	0.062	0.063	0.063	0.064	0.065	0.066	0.067	0.067	0.068	0.069	0.070	0.070
840	0.060	0.061	0.061	0.062	0.062	0.063	0.063	0.064	0.064	0.065	0.066	0.066	0.067	0.068	0.069	0.069	0.070	0.071
850	0.061	0.062	0.062	0.063	0.063	0.064	0.064	0.065	0.065	0.066	0.067	0.067	0.068	0.069	0.069	0.070	0.071	0.071
860	0.062	0.063	0.063	0.064	0.064	0.065	0.065	0.066	0.066	0.067	0.067	0.068	0.069	0.069	0.070	0.071	0.071	0.072
870	0.063	0.064	0.064	0.065	0.065	0.066	0.066	0.067	0.067	0.068	0.068	0.069	0.070	0.070	0.071	0.071	0.072	0.073
880	0.065	0.065	0.065	0.066	0.066	0.067	0.067	0.068	0.068	0.069	0.069	0.070	0.070	0.071	0.072	0.072	0.073	0.073
890	0.066	0.066	0.066	0.067	0.067	0.068	0.068	0.069	0.069	0.070	0.070	0.071	0.071	0.072	0.072	0.073	0.073	0.074
900	0.067	0.067	0.067	0.068	0.068	0.069	0.069	0.070	0.070	0.070	0.071	0.072	0.072	0.073	0.073	0.074	0.074	0.075
910	0.068	0.068	0.068	0.069	0.069	0.070	0.070	0.070	0.071	0.071	0.072	0.072	0.073	0.073	0.074	0.075	0.075	0.076
920	0.069	0.069	0.069	0.070	0.070	0.071	0.071	0.071	0.072	0.072	0.073	0.073	0.074	0.074	0.075	0.075	0.076	0.076
930	0.070	0.070	0.070	0.071	0.071	0.072	0.072	0.072	0.073	0.073	0.074	0.074	0.075	0.075	0.076	0.076	0.077	0.077
940	0.071	0.071	0.071	0.072	0.072	0.073	0.073	0.073	0.074	0.074	0.075	0.075	0.076	0.076	0.077	0.077	0.077	0.078
950	0.072	0.072	0.072	0.073	0.073	0.074	0.074	0.074	0.075	0.075	0.076	0.076	0.077	0.077	0.077	0.078	0.078	0.079
960	0.073	0.073	0.073	0.074	0.074	0.075	0.075	0.075	0.076	0.076	0.077	0.077	0.077	0.078	0.078	0.079	0.079	0.080
970	0.074	0.074	0.074	0.075	0.075	0.076	0.076	0.076	0.077	0.077	0.078	0.078	0.078	0.079	0.079	0.080	0.080	0.080
980	0.075	0.075	0.075	0.076	0.076	0.077	0.077	0.077	0.078	0.078	0.078	0.079	0.079	0.080	0.080	0.080	0.081	0.081
990	0.076	0.076	0.076	0.077	0.077	0.078	0.078	0.078	0.079	0.079	0.079	0.080	0.080	0.081	0.081	0.081	0.082	0.082

AFRL SUPERTRAPP JP-8 Surrogate
Density [kg/m^3]

Temp. (K)	Pressure (atm)																	
	1	5	10	15	20	25	30	35	40	45	50	55	60	65	70	75	80	85
273	838	838	839	839	839	840	840	840	841	841	841	842	842	842	843	843	843	844
280	831	832	832	832	833	833	833	834	834	834	835	835	835	836	836	836	837	837
290	823	823	824	824	824	825	825	825	826	826	827	827	827	828	828	828	829	829
300	815	815	815	816	816	817	817	817	818	818	818	819	819	820	820	820	821	821
310	807	807	807	808	808	808	809	809	810	810	810	811	811	812	812	812	813	813
320	798	799	799	799	800	800	801	801	802	802	802	803	803	804	804	804	805	805
330	790	790	791	791	792	792	793	793	793	794	794	795	795	796	796	796	797	797
340	782	782	782	783	783	784	784	785	785	786	786	787	787	787	788	788	789	789
350	773	774	774	775	775	776	776	777	777	778	778	778	779	779	780	780	781	781
360	765	765	766	766	767	767	768	768	769	769	770	770	771	771	772	772	773	773
370	756	757	757	758	759	759	760	760	761	761	762	762	763	763	764	764	765	765
380	748	748	749	750	750	751	751	752	752	753	754	754	755	755	756	756	757	757
390	739	740	741	741	742	742	743	744	744	745	745	746	747	747	748	748	749	749
400	731	731	732	733	733	734	735	735	736	737	737	738	738	739	740	740	741	741
410	722	723	723	724	725	725	726	727	727	728	729	729	730	731	731	732	733	733
420	713	714	715	715	716	717	718	718	719	720	721	721	722	723	723	724	725	725
430	705	705	706	707	708	708	709	710	711	711	712	713	714	714	715	716	717	717
440	689	696	697	698	699	700	701	701	702	703	704	705	705	706	707	708	708	709
450	661	687	688	689	690	691	692	693	694	694	695	696	697	698	699	699	700	701
460	632	678	679	680	681	682	683	684	685	686	687	688	688	689	690	691	692	693
470	602	669	670	671	672	673	674	675	676	677	678	679	680	681	682	683	683	684
480	569	659	660	662	663	664	665	666	667	668	669	670	671	672	673	674	675	676
490	536	650	651	652	653	654	656	657	658	659	660	661	662	663	664	665	666	667
500	4	640	641	642	644	645	646	647	649	650	651	652	653	654	655	656	658	659
510	4	629	631	632	634	635	636	638	639	640	642	643	644	645	646	648	649	650
520	4	619	620	622	623	625	626	628	629	631	632	633	635	636	637	639	640	641
530	4	598	609	611	613	615	616	618	619	621	622	624	625	627	628	629	631	632
540	3	572	598	600	602	604	606	608	609	611	613	614	616	617	619	620	622	623
550	3	546	587	589	591	593	595	597	599	601	603	604	606	608	609	611	612	614
560	3	519	575	577	580	582	584	586	589	591	592	594	596	598	600	601	603	605
570	3	19	562	565	568	570	573	575	578	580	582	584	586	588	590	592	593	595
580	3	18	541	552	555	558	561	564	566	569	571	573	576	578	580	582	584	586
590	3	18	518	538	542	545	549	552	555	557	560	562	565	567	569	572	574	576
600	3	17	493	524	528	532	536	539	542	545	548	551	554	556	559	561	564	566
610	3	17	39	505	513	517	522	526	530	533	536	539	542	545	548	551	553	556
620	3	16	38	483	496	502	507	512	516	520	524	527	531	534	537	540	543	545
630	3	16	36	461	477	485	491	497	502	506	511	515	519	522	526	529	532	535
640	3	16	35	64	457	465	473	480	487	492	497	502	506	510	514	517	521	524
650	3	15	34	60	436	443	454	462	470	477	483	488	493	497	502	505	509	513
660	3	15	33	57	97	409	430	442	452	460	467	473	479	484	489	493	497	501
670	3	15	32	55	88	367	401	419	432	442	450	458	464	470	476	481	485	490
680	3	14	31	53	82	139	357	390	409	422	433	441	449	456	462	468	473	478
690	3	14	31	51	77	119	254	351	381	399	413	424	433	441	448	454	460	465
700	3	14	30	49	74	108	173	293	347	374	391	405	416	425	433	440	447	453
710	3	14	29	48	70	100	147	230	305	344	368	385	398	409	418	426	433	440
720	3	13	29	46	68	95	132	189	261	311	342	363	379	391	402	411	420	427
730	3	13	28	45	65	90	122	166	224	277	314	340	359	374	386	396	405	413
740	2	13	27	44	63	86	114	150	197	247	287	316	338	355	369	381	391	400
750	2	13	27	43	61	83	108	139	178	222	261	293	318	337	352	365	377	386
760	2	13	26	42	59	80	103	131	164	202	239	271	298	319	336	350	362	373
770	2	12	26	41	58	77	99	124	153	186	220	252	279	301	319	335	348	359
780	2	12	26	40	56	75	95	118	144	174	204	234	261	284	303	319	334	346
790	2	12	25	39	55	72	92	113	137	164	191	219	245	268	288	305	320	333
800	2	12	25	39	54	70	89	109	131	155	181	206	231	254	274	291	307	320
810	2	12	24	38	53	69	86	105	126	148	171	195	219	241	261	278	294	308
820	2	12	24	37	51	67	84	102	121	142	164	186	208	229	248	266	282	296
830	2	11	24	36	50	65	81	99	117	136	157	178	198	218	237	255	271	285
840	2	11	23	36	49	64	79	96	113	132	151	170	190	209	227	244	260	275
850	2	11	23	35	49	63	78	93	110	127	145	164	182	201	218	235	250	265
860	2	11	22	35	48	61	76	91	107	123	141	158	176	193	210	226	241	255
870	2	11	22	34	47	60	74	89	104	120	136	153	170	186	203	218	233	247
880	2	11	22	34	46	59	73	87	101	117	132	148	164	180	196	211	225	239
890	2	11	22	33	45	58	71	85	99	114	129	144	159	174	189	204	218	231
900	2	10	21	33	44	57	70	83	97	111	125	140	155	169	184	198	212	225
910	2	10	21	32	44	56	68	81	95	108	122	136	150	165	179	192	205	218
920	2	10	21	32	43	55	67	80	93	106	119	133	147	160	174	187	200	212
930	2	10	20	31	42	54	66	78	91	104	117	130	143	156	169	182	194	206
940	2	10	20	31	42	53	65	77	89	102	114	127	140	152	165	177	189	201
950	2	10	20	30	41	52	64	75	87	100	112	124	137	149	161	173	185	196
960	2	10	20	30	41	52	63	74	86	98	110	122	134	146	157	169	181	192
970	2	10	19	30	40	51	62	73	84	96	107	119	131	142	154	165	177	187
980	2	9	19	29	40	50	61	72	83	94	105	117	128	140	151	162	173	183
990	2	9	19	29	39	49	60	71	82	93	104	115	126	137	148	158	169	180

AFRL SUPERTRAPP JP-8 Surrogate
Dynamic Viscosity [(N-s)/(m^2)]*10^6

Temp. (K)	Pressure (atm)																	
	1	5	10	15	20	25	30	35	40	45	50	55	60	65	70	75	80	85
273	2079	2089	2102	2115	2128	2140	2153	2166	2179	2192	2206	2219	2232	2245	2259	2272	2285	2299
280	1820	1829	1840	1851	1862	1873	1884	1895	1906	1918	1929	1940	1952	1963	1975	1986	1998	2009
290	1522	1530	1539	1548	1557	1566	1575	1584	1593	1602	1612	1621	1630	1640	1649	1659	1668	1678
300	1290	1296	1304	1311	1319	1326	1334	1342	1349	1357	1365	1372	1380	1388	1396	1404	1412	1420
310	1106	1111	1117	1124	1130	1137	1143	1149	1156	1162	1169	1175	1182	1189	1195	1202	1209	1215
320	958	963	968	974	979	985	990	996	1001	1007	1012	1018	1024	1029	1035	1041	1046	1052
330	838	842	847	852	856	861	866	871	876	881	885	890	895	900	905	910	915	920
340	741	744	748	752	757	761	765	769	774	778	782	786	791	795	799	804	808	812
350	661	664	668	671	675	679	683	686	690	694	698	702	706	709	713	717	721	725
360	594	597	600	604	607	610	614	617	621	624	628	631	635	638	641	645	648	652
370	538	540	543	546	550	553	556	559	562	565	568	572	575	578	581	584	587	591
380	490	492	495	498	501	503	506	509	512	515	518	521	524	527	530	533	536	538
390	448	450	453	456	459	461	464	467	469	472	475	477	480	483	486	488	491	494
400	413	415	417	420	422	425	427	430	432	435	437	440	443	445	448	450	453	455
410	380	382	385	387	390	392	394	397	399	402	404	406	409	411	414	416	419	421
420	352	354	356	358	361	363	365	368	370	372	374	377	379	381	384	386	388	391
430	327	329	331	333	335	337	340	342	344	346	348	351	353	355	357	359	362	364
440	309	306	308	310	312	315	317	319	321	323	325	327	329	332	334	336	338	340
450	302	286	288	290	292	294	296	298	300	302	304	306	309	311	313	315	317	319
460	296	268	270	272	274	276	278	280	282	284	286	288	290	292	294	296	298	300
470	291	251	253	255	257	259	261	263	265	267	269	271	273	275	276	278	280	282
480	285	235	237	239	241	243	245	247	249	251	252	254	256	258	260	262	264	266
490	277	218	220	222	224	226	228	230	232	234	236	237	239	241	243	245	247	249
500	9	203	205	207	208	210	212	214	216	218	220	222	223	225	227	229	231	232
510	9	189	191	192	194	196	198	200	202	204	205	207	209	211	213	214	216	218
520	9	176	177	179	181	183	185	187	189	190	192	194	196	198	199	201	203	205
530	9	170	165	167	169	171	173	175	177	178	180	182	184	185	187	189	191	192
540	10	166	154	156	158	160	162	163	165	167	169	171	172	174	176	177	179	181
550	10	163	143	145	147	149	151	153	155	157	158	160	162	164	165	167	169	170
560	10	158	133	135	137	139	141	143	145	147	149	150	152	154	155	157	159	161
570	10	10	124	126	128	130	132	134	136	138	139	141	143	145	146	148	150	151
580	10	10	120	116	119	121	123	125	127	128	130	132	134	136	137	139	141	142
590	11	11	118	108	110	112	114	116	118	120	122	124	125	127	129	131	132	134
600	11	11	115	99	101	104	106	108	110	112	114	116	118	119	121	123	124	126
610	11	11	11	93	93	96	98	100	102	104	106	108	110	112	114	115	117	119
620	11	11	12	92	85	88	90	93	95	97	99	101	103	105	107	109	110	112
630	11	11	12	89	77	80	83	86	88	90	92	94	96	98	100	102	104	106
640	11	11	12	13	74	73	76	79	81	84	86	88	90	92	94	96	98	99
650	12	12	12	13	72	65	69	72	75	77	80	82	84	86	88	90	92	94
660	12	12	12	13	15	54	61	65	68	71	74	76	79	81	83	85	87	89
670	12	12	12	13	15	46	54	58	62	65	68	71	73	76	78	80	82	83
680	12	12	13	13	14	18	44	51	56	59	63	65	68	70	73	75	77	79
690	12	12	13	13	14	17	28	43	49	54	57	60	63	66	68	70	72	74
700	12	13	13	13	14	16	21	34	42	48	52	55	58	61	63	66	68	70
710	13	13	13	14	14	16	19	26	36	42	47	50	54	56	59	61	64	66
720	13	13	13	14	15	16	18	22	30	37	42	46	49	52	55	57	60	62
730	13	13	13	14	15	16	18	21	26	32	37	42	45	48	51	54	56	58
740	13	13	14	14	15	16	17	20	23	28	33	38	42	45	48	50	52	55
750	13	13	14	14	15	16	17	19	22	26	30	34	38	41	44	47	49	52
760	13	14	14	14	15	16	17	19	21	24	28	32	35	38	41	44	46	49
770	14	14	14	15	15	16	17	19	21	23	26	30	33	36	39	41	44	46
780	14	14	14	15	15	16	17	18	20	22	25	28	31	34	36	39	41	43
790	14	14	14	15	15	16	17	18	20	22	24	26	29	32	34	37	39	41
800	14	14	15	15	16	16	17	18	20	21	23	25	28	30	33	35	37	39
810	14	14	15	15	16	16	17	18	19	21	23	25	27	29	31	33	35	38
820	14	15	15	15	16	17	17	18	19	21	22	24	26	28	30	32	34	36
830	15	15	15	16	16	17	17	18	19	21	22	24	25	27	29	31	33	35
840	15	15	15	16	16	17	17	18	19	20	22	23	25	26	28	30	32	33
850	15	15	15	16	16	17	18	18	19	20	22	23	24	26	27	29	31	32
860	15	15	16	16	16	17	18	18	19	20	21	23	24	25	27	28	30	31
870	15	15	16	16	17	17	18	19	19	20	21	22	24	25	26	28	29	31
880	15	16	16	16	17	17	18	19	19	20	21	22	23	25	26	27	29	30
890	16	16	16	16	17	17	18	19	19	20	21	22	23	24	26	27	28	29
900	16	16	16	17	17	18	18	19	20	20	21	22	23	24	25	26	28	29
910	16	16	16	17	17	18	18	19	20	20	21	22	23	24	25	26	27	28
920	16	16	17	17	17	18	18	19	20	20	21	22	23	24	25	26	27	28
930	16	16	17	17	17	18	18	19	20	20	21	22	23	24	25	26	27	28
940	16	17	17	17	18	18	19	19	20	21	21	22	23	24	25	25	26	27
950	17	17	17	17	18	18	19	19	20	21	21	22	23	24	24	25	26	27
960	17	17	17	18	18	18	19	19	20	21	21	22	23	24	24	25	26	27
970	17	17	17	18	18	19	19	20	20	21	21	22	23	24	24	25	26	27
980	17	17	18	18	18	19	19	20	20	21	21	22	23	23	24	25	26	26
990	17	17	18	18	18	19	19	20	20	21	22	22	23	23	24	25	26	26

Appendix B. Heat Exchanger Design Calculations

Constants and Unit Conversions

$bar := 14.503773773021psi$ $kJ := 1000J$ $kmol := mol$ $MJ := 10^6 J$

$R := 8.314\frac{kJ}{mol \cdot K}$ $\sigma := 5.67 \cdot 10^{-8}\frac{W}{m^2 \cdot K^4}$

Assumed Heat Exchanger Inlet and Outlet Temperatures

$T_{fluidin} := 290K$ $T_{fluidout} := 530K$

Ambient Temperature

$T_{amb} := 290K$

Inner Tube Dimensions

$d_{ii} := 2.067in$ $d_{io} := 2.375in$ $l := 30in$

Outer Tube Dimensions

$d_{oi} := 2.635in$ $d_{oo} := 2.875in$

Fuel Properties

Choose your detonation fuel
For Hydrogen FUEL=1
For JP8 FUEL=2

$FUEL := 2$

PDE Operating Parameters

$frequency := 15Hz$ $Vol_{tube} := 245in^3$ $FF := 1$

$Tubes := 2$ $P_{atm} := 1atm$ $T_{mix} := 394K$ $\phi := 1.05$

Heat Transfer Parameters

Turbulent Reynolds Number

$Re_{turb} := 2300$

Laminar Nusselt Number

$Nu_{lam} := 3.66$

Programming Parameters

$dl := .001m \quad q_{tol} := .1W \quad dT := .1K$

For Turbulent Flow Effects when $Re_{turb} = 2300$ Set TURB to 1

For Purely Laminar Flow Effects Set TURB to 0

$TURB := 1$

For a Non-Adiabatic Outer Wall (includes Free Convection and Radiation) Set FCR to 1.
For an Adiabatic Outer Wall Set FCR to 0.

$FCR := 1$

Choose Your Cooling Fluid

For Water	FLUID=1
For Nitrogen	FLUID=2
For JP8 Surrogate	FLUID=3
For JP8	FLUID=4

$FLUID := 3$

Stainless Steel Material Properties

From Introduction to Heat Transfer (Third Edition), Frank P. Incropera, David P. DeWitt, John Wiley & Sons, Inc. Copyright 1996

Appendix A Table A.1

$$T_{ss} := \begin{pmatrix} 100 \\ 200 \\ 400 \\ 600 \\ 800 \\ 1000 \\ 1200 \\ 1500 \end{pmatrix} \cdot K \qquad k_{ss} := \begin{pmatrix} 9.2 \\ 12.6 \\ 16.6 \\ 19.8 \\ 22.6 \\ 25.4 \\ 28.0 \\ 31.7 \end{pmatrix} \cdot \frac{W}{m \cdot K}$$

From Introduction to Heat Transfer (Third Edition), Frank P. Incropera, David P. DeWitt, John Wiley & Sons, Inc. Copyright 1996

Appendix A Table A.8 (Lightly Oxidized Stainless Steel)

$$T_{\varepsilon} := \begin{pmatrix} 300 \\ 400 \\ 600 \\ 800 \\ 1000 \end{pmatrix} \cdot K \qquad \varepsilon_{ss} := \begin{pmatrix} .22 \\ .22 \\ .24 \\ .33 \\ .40 \end{pmatrix}$$

Water Properties

Heat of Formation for Water. From Combution (Third Edition), Irvin Glassman, Academic Press, Copyright 1997, Chap 1, Table 1, pg 6.

$$HOF_{water} := 13.44\frac{kJ}{gm}$$

From Introduction to Heat Transfer (Third Edition), Frank P. Incropera, David P. DeWitt, John Wiley & Sons, Inc. Copyright 1996

Appendix A Table A.6

$$T_{water} := \begin{pmatrix} 273.15 \\ 275 \\ 280 \\ 285 \\ 290 \\ 295 \\ 300 \\ 305 \\ 310 \\ 315 \\ 320 \\ 325 \\ 330 \\ 335 \\ 340 \\ 345 \\ 350 \\ 355 \\ 360 \\ 365 \\ 370 \\ 373.15 \\ 375 \\ 380 \\ 385 \\ 390 \\ 400 \\ 410 \end{pmatrix} \cdot K \quad \upsilon_{water} := \begin{pmatrix} 1 \\ 1 \\ 1 \\ 1 \\ 1.001 \\ 1.002 \\ 1.003 \\ 1.005 \\ 1.007 \\ 1.009 \\ 1.011 \\ 1.013 \\ 1.016 \\ 1.018 \\ 1.021 \\ 1.024 \\ 1.027 \\ 1.030 \\ 1.034 \\ 1.038 \\ 1.041 \\ 1.044 \\ 1.045 \\ 1.049 \\ 1.053 \\ 1.058 \\ 1.067 \\ 1.077 \end{pmatrix} \cdot 10^{-3} \cdot \frac{m^3}{kg} \quad \rho_{water} := \frac{1}{\upsilon_{water}} \quad c_{pwater} := \begin{pmatrix} 4.217 \\ 4.211 \\ 4.198 \\ 4.189 \\ 4.184 \\ 4.181 \\ 4.179 \\ 4.178 \\ 4.178 \\ 4.179 \\ 4.180 \\ 4.182 \\ 4.184 \\ 4.186 \\ 4.188 \\ 4.191 \\ 4.195 \\ 4.199 \\ 4.203 \\ 4.209 \\ 4.214 \\ 4.217 \\ 4.220 \\ 4.229 \\ 4.232 \\ 4.239 \\ 4.256 \\ 4.278 \end{pmatrix} \cdot \frac{kJ}{kg \cdot K}$$

420	1.088		4.302
430	1.099		4.331
440	1.110		4.36
450	1.123		4.40
460	1.137		4.44
470	1.152		4.48
480	1.167		4.53
490	1.184		4.59
500	1.203		4.66
510	1.222		4.74
520	1.244		4.84
530	1.268		4.95
540	1.294		5.08
550	1.323		5.24
560	1.355		5.43
570	1.392		5.68
580	1.433		6.00
590	1.482		6.41
600	1.541		7.00
610	1.612		7.85
620	1.705		9.35
625	1.778		10.6
630	1.856		12.6
635	1.935		16.4
640	2.075		26
645	2.351		90
647.3	3.170		200

$$\mu_{water} := \begin{pmatrix} 1750 \\ 1652 \\ 1422 \\ 1225 \\ 1080 \\ 959 \\ 855 \\ 769 \\ 695 \\ 631 \\ 577 \\ 528 \\ 489 \\ 453 \\ 420 \\ 389 \\ 365 \\ 343 \\ 324 \\ 306 \\ 289 \\ 279 \\ 274 \\ 260 \\ 248 \\ 237 \\ 217 \\ 200 \\ 185 \\ 173 \\ 162 \\ 152 \\ 143 \\ 136 \\ 129 \\ 124 \\ 118 \\ 113 \end{pmatrix} \cdot 10^{-6} \frac{N \cdot s}{m^2} \qquad Pr_{water} := \begin{pmatrix} 12.99 \\ 12.22 \\ 10.26 \\ 8.81 \\ 7.56 \\ 6.62 \\ 5.83 \\ 5.20 \\ 4.62 \\ 4.16 \\ 3.77 \\ 3.42 \\ 3.15 \\ 2.88 \\ 2.66 \\ 2.45 \\ 2.29 \\ 2.14 \\ 2.03 \\ 1.91 \\ 1.80 \\ 1.76 \\ 1.70 \\ 1.61 \\ 1.53 \\ 1.47 \\ 1.34 \\ 1.24 \\ 1.16 \\ 1.09 \\ 1.04 \\ .99 \\ .95 \\ .92 \\ .89 \\ .87 \\ .86 \\ .85 \end{pmatrix} \qquad k_{water} := \begin{pmatrix} 569 \\ 574 \\ 582 \\ 590 \\ 598 \\ 606 \\ 613 \\ 620 \\ 628 \\ 634 \\ 640 \\ 645 \\ 650 \\ 656 \\ 660 \\ 668 \\ 668 \\ 671 \\ 674 \\ 677 \\ 679 \\ 680 \\ 681 \\ 683 \\ 685 \\ 686 \\ 688 \\ 688 \\ 688 \\ 685 \\ 682 \\ 678 \\ 673 \\ 667 \\ 660 \\ 651 \\ 642 \\ 631 \end{pmatrix} \cdot 10^{-3} \cdot \frac{W}{m \cdot K}$$

108	.84	621
104	.85	608
101	.86	594
97	.87	580
94	.90	563
91	.94	548
88	.99	528
84	1.05	513
81	1.14	497
77	1.30	467
72	1.52	444
70	1.65	430
67	2.0	412
64	2.7	392
59	4.2	367
54	12	331
45	100	238

Air Properties

From Introduction to Heat Transfer (Third Edition), Frank P. Incropera, David P. DeWitt, John Wiley & Sons, Inc. Copyright 1996

Appendix A Table A.4

$$T_{air} := \begin{pmatrix} 100 \\ 150 \\ 200 \\ 250 \\ 300 \\ 350 \\ 400 \\ 450 \\ 500 \\ 550 \\ 600 \\ 650 \\ 700 \\ 750 \\ 800 \\ 850 \\ 900 \\ 950 \\ 1000 \\ 1100 \\ 1200 \\ 1300 \\ 1400 \\ 1500 \\ 1600 \end{pmatrix} \cdot K \qquad \nu_{air} := \begin{pmatrix} 2.00 \\ 4.426 \\ 7.590 \\ 11.44 \\ 15.89 \\ 20.92 \\ 26.41 \\ 32.9 \\ 38.79 \\ 45.57 \\ 52.69 \\ 60.21 \\ 68.10 \\ 76.37 \\ 84.93 \\ 93.8 \\ 102.9 \\ 112.2 \\ 121.9 \\ 141.8 \\ 162.9 \\ 185.1 \\ 213 \\ 240 \\ 268 \end{pmatrix} \cdot 10^{-6} \frac{m^2}{s} \qquad k_{air} := \begin{pmatrix} 9.34 \\ 13.8 \\ 18.1 \\ 22.3 \\ 26.3 \\ 30.0 \\ 33.8 \\ 37.3 \\ 40.7 \\ 43.9 \\ 46.9 \\ 49.7 \\ 52.4 \\ 54.9 \\ 57.3 \\ 59.6 \\ 62 \\ 64.3 \\ 66.7 \\ 71.5 \\ 76.3 \\ 82 \\ 91 \\ 100 \\ 106 \end{pmatrix} \cdot 10^{-3} \frac{W}{m \cdot K}$$

$$\alpha_{air} := \begin{pmatrix} 2.54 \\ 5.84 \\ 10.3 \\ 15.9 \\ 22.5 \\ 29.9 \\ 38.3 \\ 47.2 \\ 56.7 \\ 66.7 \\ 76.9 \\ 87.3 \\ 98 \\ 109 \\ 120 \\ 131 \\ 143 \\ 155 \\ 168 \\ 195 \\ 224 \\ 238 \\ 303 \\ 350 \\ 390 \end{pmatrix} \cdot 10^{-6} \cdot \frac{m^2}{s} \qquad Pr_{air} := \begin{pmatrix} .786 \\ .758 \\ .737 \\ .720 \\ .707 \\ .7 \\ .69 \\ .686 \\ .684 \\ .683 \\ .685 \\ .690 \\ .695 \\ .702 \\ .709 \\ .716 \\ .720 \\ .723 \\ .726 \\ .728 \\ .728 \\ .719 \\ .703 \\ .685 \\ .688 \end{pmatrix}$$

Air density and expansion coefficent for Ideal Gas

$$R_{air} := 287 \frac{J}{kg \cdot K} \qquad P_{air} := 1atm \qquad \rho_{air} := \frac{P_{air}}{R_{air} \cdot T_{air}} \qquad \beta_{air} := \frac{1}{T_{air}}$$

Tables of Thermodynamic and Transport Properties of Air, Argon, Carbon Dioxide, Carbon Monoxide, Hydrogen, Nitrogen, Oxygen, and Steam; Hilsenrath, Hoge, Beckett, Masi, Benedict, Nuttall, Fano, Touloukian, Woolley; Pergamon Press Inc.; 1960

$$conv_{\eta} := 5.985 \cdot 10^{-2} \cdot \frac{kg}{hr \cdot m}$$

$$conv_{\rho} := 1.25046 \cdot 10^{-3} \cdot \frac{gn}{cm}$$

$$conv_{cp} := .296774 \frac{J}{gm \cdot K}$$

$$conv_{k} := 2.41 \cdot 10^{-4} \cdot \frac{W}{cm \cdot K}$$

T_{N2} :=	ρ_{N2} :=	c_{pN2} :=
250	79.528	4.124
260	75.689	4.056
270	72.254	4.000
280	69.172	3.953
290	66.376	3.913
300	63.810	3.878
310	61.475	3.848
320	59.311	3.822
330	57.320	3.799
340	55.470	3.779
350	53.747	3.7619
360	52.141	3.7466
370	50.632	3.7331
380	49.213	3.7215
390	47.881	3.7113
400	46.625	3.7023
410	45.434	3.6948
420 ·K	44.309 ·$conv_{\rho}$	3.6882 ·$conv_{cp}$
430	43.215	3.6829
440	42.229	3.6784
450	41.267	3.6746
460	40.346	3.6720
470	39.473	3.6698
480	38.631	3.6685
490	37.832	3.6679
500	37.065	3.6680
510	36.327	3.6685
520	35.625	3.6695
530	34.950	3.6712
540	34.296	3.6733
550	33.669	3.6759
560	33.068	3.6788
570	32.488	3.6823
580	31.927	3.6859
590	31.386	3.6900

$$\mu_{N60} := \begin{pmatrix} 1.127 \\ 1.248 \\ 1.362 \\ 1.472 \\ 1.578 \\ 1.680 \\ 1.778 \\ 1.868 \\ 1.955 \end{pmatrix}$$

$$\mu_{N80} := \begin{pmatrix} 1.154 \\ 1.269 \\ 1.380 \\ 1.487 \\ 1.591 \\ 1.692 \\ 1.789 \\ 1.879 \\ 1.965 \end{pmatrix}$$

$$T_{\mu N2} := \begin{pmatrix} 300 \\ 350 \\ 400 \\ 450 \\ 500 \\ 550 \\ 600 \\ 650 \\ 700 \end{pmatrix} \cdot K$$

$$k_{N2} := \begin{pmatrix} .924 \\ .957 \\ .990 \\ 1.021 \\ 1.051 \\ 1.081 \\ 1.111 \\ 1.141 \\ 1.172 \\ 1.202 \\ 1.232 \\ 1.262 \\ 1.292 \\ 1.321 \\ 1.349 \\ 1.377 \\ 1.405 \\ 1.433 \\ 1.460 \\ 1.487 \\ 1.513 \\ 1.540 \\ 1.566 \\ 1.592 \\ 1.619 \\ 1.645 \\ 1.671 \\ 1.697 \\ 1.722 \\ 1.747 \\ 1.771 \\ 1.795 \\ 1.819 \\ 1.843 \\ 1.867 \end{pmatrix} \cdot conv_k$$

$$\mu_{N2} := \frac{\mu_{N60} + \mu_{N80}}{2} \cdot conv_\eta$$

$$length(T_{N2}) = 35$$

$$i := 0 .. 34$$

$$\mu_{intN2_i} := linterp(T_{\mu N2}, \mu_{N2}, T_{N2_i})$$

AFRL SUPERTRAPP JP-8 Surrogate Properties

Temperature Range for data

$T_{surlow} := 273K \qquad T_{surhigh} := 998K$

$i := 0 .. \frac{T_{surhigh} - T_{surlow}}{K} \qquad T_{sur_i} := T_{surlow} + i \cdot K$

Fuel Pressure for Test

$Pressure := round\left(\frac{700psi}{atm}, 0\right)$

Assinging Surrogate Thermodynamic Properties

$\mu_{surjp8} :=$ ...\mujp8.xls $\quad \mu_{sur_i} := \mu_{surjp8_{i, Pressure-1}} \cdot \frac{N \cdot s}{m^2}$

$\rho_{surjp8} :=$ ...\rojp8.xls $\quad \rho_{sur_i} := \rho_{surjp8_{i, Pressure-1}} \cdot \frac{kg}{m^3}$

$k_{surjp8} :=$ ...\kjp8.xls $\quad k_{sur_i} := k_{surjp8_{i, Pressure-1}} \cdot \frac{W}{m \cdot K}$

$cp_{surjp8} :=$ ...\cpjp8.xls $\quad cp_{sur_i} := cp_{surjp8_{i, Pressure-1}} \cdot \frac{kJ}{kg \cdot K}$

From U.S. Oil and Refining Co., https://www.usor.com/pdfs/specs/lpd/finished/JP-8.pdf

$$HOC_{jp8} := 42.8\,\frac{MJ}{kg}$$

AFRL Provided PPDS JP-8 Surrogate Data @ 1000 psia

$$T_{jp8} := \left[\begin{pmatrix} .1 \\ 100 \\ 200 \\ 300 \\ 400 \\ 500 \\ 600 \\ 700 \\ 800 \\ 900 \\ 1000 \\ 1100 \end{pmatrix} + 459.67\right]\cdot\frac{5}{9}\,K \qquad \rho_{jp8} := \begin{pmatrix} 51.963 \\ 49.438 \\ 46.798 \\ 43.996 \\ 40.953 \\ 37.521 \\ 33.352 \\ 27.108 \\ 27.811 \\ 22.672 \\ 17.557 \\ 13.995 \end{pmatrix}\cdot\frac{lb}{ft^3} \qquad c_{pjp8} := \begin{pmatrix} .436 \\ .499 \\ .563 \\ .626 \\ .689 \\ .752 \\ .815 \\ .876 \\ .821 \\ .873 \\ .891 \\ .89 \end{pmatrix}\cdot\frac{BTU}{lb\cdot\frac{5}{9}\cdot K}$$

$$k_{jp8} := \begin{pmatrix} .0761 \\ .0706 \\ .0651 \\ .0596 \\ 0.0541 \\ .0486 \\ .0431 \\ .0376 \\ .041 \\ .0408 \\ .0412 \\ .0429 \end{pmatrix}\cdot\frac{BTU}{ft\cdot hr\cdot\frac{5}{9}K} \qquad \mu_{jp8} := \begin{pmatrix} 5.849 \\ 2.303 \\ 1.278 \\ .845 \\ .619 \\ .479 \\ .378 \\ .282 \\ .13 \\ .0995 \\ .0766 \\ .0644 \end{pmatrix}\cdot\frac{lb}{ft\cdot hr}$$

Assign Cooling Fluid Properties

$Z :=$ if FLUID = 1

$Z^{\langle 0 \rangle} \leftarrow \frac{T_{water}}{K}$

$Z^{\langle 1 \rangle} \leftarrow \frac{\mu_{water}}{\frac{N \cdot s}{m^2}}$

$Z^{\langle 2 \rangle} \leftarrow \frac{k_{water}}{\frac{W}{m \cdot K}}$

$Z^{\langle 3 \rangle} \leftarrow \frac{c_{pwater}}{\frac{kJ}{kg \cdot K}}$

$Z^{\langle 4 \rangle} \leftarrow \frac{\rho_{water}}{\frac{kg}{m^3}}$

if FLUID = 2

$Z^{\langle 0 \rangle} \leftarrow \frac{T_{N2}}{K}$

$Z^{\langle 1 \rangle} \leftarrow \frac{\mu_{intN2}}{\frac{N \cdot s}{m^2}}$

$Z^{\langle 2 \rangle} \leftarrow \frac{k_{N2}}{\frac{W}{m \cdot K}}$

$Z^{\langle 3 \rangle} \leftarrow \frac{c_{pN2}}{\frac{kJ}{kg \cdot K}}$

$Z^{\langle 4 \rangle} \leftarrow \frac{\rho_{N2}}{\frac{kg}{m^3}}$

if FLUID = 3

$Z^{\langle 0 \rangle} \leftarrow \frac{T_{sur}}{K}$

$Z^{\langle 1 \rangle} \leftarrow \frac{\mu_{sur}}{N \cdot s}$

$$\frac{\quad}{m^2}$$

$$Z^{\langle 2\rangle} \leftarrow \frac{k_{sur}}{\frac{W}{m\cdot K}}$$

$$Z^{\langle 3\rangle} \leftarrow \frac{c_{psur}}{\frac{kJ}{kg\cdot K}}$$

$$Z^{\langle 4\rangle} \leftarrow \frac{\rho_{sur}}{\frac{kg}{m^3}}$$

if FLUID = 4

$$Z^{\langle 0\rangle} \leftarrow \frac{T_{jp8}}{K}$$

$$Z^{\langle 1\rangle} \leftarrow \frac{\mu_{jp8}}{\frac{N\cdot s}{m^2}}$$

$$Z^{\langle 2\rangle} \leftarrow \frac{k_{jp8}}{\frac{W}{m\cdot K}}$$

$$Z^{\langle 3\rangle} \leftarrow \frac{c_{pjp8}}{\frac{kJ}{kg\cdot K}}$$

$$Z^{\langle 4\rangle} \leftarrow \frac{\rho_{jp8}}{\frac{kg}{m^3}}$$

$$T_{fluid} := Z^{\langle 0\rangle}\cdot K$$

$$\rho_{fluid} := Z^{\langle 4\rangle}\cdot\frac{kg}{m^3}$$

$$\mu_{fluid} := Z^{\langle 1\rangle}\cdot\frac{N\cdot s}{m^2}$$

$$k_{fluid} := Z^{\langle 2\rangle}\cdot\frac{W}{m\cdot K}$$

$$c_{pfluid} := Z^{\langle 3\rangle}\cdot\frac{kJ}{kg\cdot K}$$

$$j := 0..last\left(\rho_{fluid}\right) - 2 \qquad d\rho_j := \frac{\rho_{fluid_{j+1}} - \rho_{fluid_j}}{T_{fluid_{j+1}} - T_{fluid_j}} \qquad \rho_{\beta_j} := \rho_{fluid_j}$$

$$\beta_j := \frac{-1}{\rho_{\beta_j}}\cdot d\rho_j \qquad T_{\beta_j} := T_{fluid_j}$$

Mass Flow Calculator

$$C := \begin{cases} 0 & \text{if FUEL} = 1 \\ 10.9 & \text{if FUEL} = 2 \end{cases}$$

$$H := \begin{cases} 2 & \text{if FUEL} = 1 \\ 20.9 & \text{if FUEL} = 2 \end{cases}$$

$$Fuel_{moles} := \begin{cases} 1mol & \text{if FUEL} = 1 \\ 1mol & \text{if FUEL} = 2 \end{cases}$$

Stoichiometric Calculations

$CO_2 := C \qquad Water := \frac{H}{2} \qquad Water = 10.45$

$$Moles_{air} := \left(CO_2 + \frac{Water}{2}\right)mol$$

$$mw_{fuel} := \left(C \cdot 12.01 \cdot \frac{kg}{mol}\right) + \left(H \cdot 1.01 \frac{kg}{mol}\right) \qquad m_{fuel} := Fuel_{moles} \cdot mw_{fuel}$$

$$mw_{air} := \frac{32 \cdot \frac{kg}{mol} + \frac{79}{21} \cdot 28.02 \cdot \frac{kg}{mol}}{1 + \frac{79}{21}} \qquad m_{air} := Moles_{air} \cdot \left(32 \cdot \frac{kg}{mol} + \frac{79}{21} \cdot 28.02 \cdot \frac{kg}{mol}\right)$$

$$\frac{m_{air}}{m_{fuel}} = 14.575 \qquad \frac{m_{fuel}}{m_{air}} = 0.068609$$

Mixture Calculations for Operating Paramaters

$$fueltoair := \phi \cdot \frac{m_{fuel}}{m_{air}} \qquad airtofuel := \frac{1}{fueltoair}$$

Volumetric and Mass Flow Rate Calculations

$V_{dot} := frequency \cdot Vol_{tube} \cdot FF \cdot Tubes$

$m_{adot} := 15 \frac{lb}{min}$ $m_{fdot} := 1 \frac{lb}{min}$ $V_{adot} := V_{dot}$ $V_{fdot} := \frac{1}{100} \cdot V_{dot}$

Given

$V_{dot} = V_{adot} + V_{fdot}$

$m_{adot} = \frac{V_{adot} \cdot P_{atm}}{\frac{R}{mw_{air}} \cdot T_{mix}}$ $m_{fdot} = \frac{V_{fdot} \cdot P_{atm}}{\frac{R}{mw_{fuel}} \cdot T_{mix}}$

$\frac{m_{fdot}}{m_{adot}} = fueltoair$

$Y := Find(V_{adot}, V_{fdot}, m_{adot}, m_{fdot})$

$V_{adot} := Y_0$

$V_{fdot} := Y_1$

$m_{adot} := Y_2$

$m_{fdot} := Y_3$ $m_{dot} := m_{fdot}$

$m_{dottot} := m_{adot} + m_{fdot}$

$Nitrogen := Moles_{air} \cdot \frac{79}{21}$

$$m_{dotwater} := m_{dottot} \frac{Water \cdot mol \cdot 18 \cdot \frac{kg}{mol}}{\left(Water \cdot mol \cdot 18 \cdot \frac{kg}{mol}\right) + \left(Nitrogen \cdot 28.02 \cdot \frac{kg}{mol}\right)}$$

$$m_{dotnitrogen} := m_{dottot} \cdot \frac{Nitrogen \cdot 28.02 \cdot \frac{kg}{mol}}{\left(Water \cdot mol \cdot 18 \cdot \frac{kg}{mol}\right) + Nitrogen \cdot 28.02 \cdot \frac{kg}{mol}}$$

Calculation of specific energy and power required for inlet and outlet temperatures

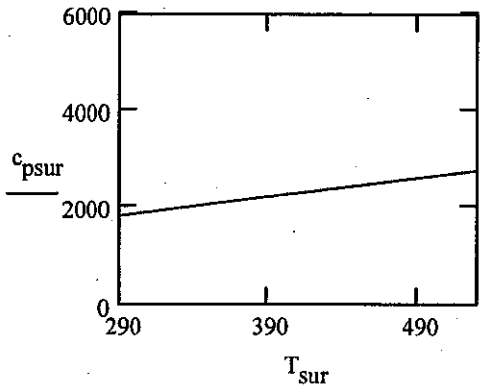

Area Under Cp vs. T curve is the required specific energy required to raise the cooling fluid temperature across the required range.

$n := 10000$

$dt := \frac{T_{fluidout} - T_{fluidin}}{n - 1}$ $dt = 0.024\,K$ $i := 0..n - 1$

$T_{er_i} := T_{fluidin} + i \cdot dt$ $c_{p_i} := linterp(T_{jp8}, c_{pjp8}, T_{er_i})$

$SpecificEnergy := \sum_{i=0}^{n-1} \left(c_{p_i} \cdot dt\right)$ $EnergyRequired := m_{dot} \cdot SpecificEnergy$

$$EnergyReleased := \begin{cases} m_{dotwater} \cdot HOF_{water} & \text{if } FUEL = 1 \\ m_{dot} \cdot HOC_{jp8} & \text{if } FUEL = 2 \end{cases}$$

$$PercentRequired := \frac{EnergyRequired}{EnergyReleased} \cdot 100$$

Calculating average heat transfer coefficient and temperature inside the PDE tube during test

From Steady State Tube Free Convection and Radiation Test

$T_{surf} := 1005K$

$T_{inf} := 290K$

Film Temperature

$$T_f := \frac{T_{surf} + T_{inf}}{2}$$ EQ 7.2, pg 326, Introduction to Heat Transfer (Third Edition)

Tube Dimensions

$D_o := 2.375in$

$D_i := 2.157in$

Free Convection Heat Transfer Coefficient Calculation

$$Ra := \frac{g \cdot linterp(T_{air}, \beta_{air}, T_f) \cdot (T_{surf} - T_{inf}) \cdot D_o^{\,3}}{linterp(T_{air}, \nu_{air}, T_f) \cdot linterp(T_{air}, \alpha_{air}, T_f)}$$ EQ 9.24, pg 456, Introduction to Heat Transfer (Third Edition)

$Ra = 4.58 \times 10^5$

$$Nu := \left[.6 + \frac{.387 \cdot Ra^{\frac{1}{6}}}{\left[1 + \left(\frac{.559}{linterp(T_{air}, Pr_{air}, T_f)} \right)^{\frac{9}{16}} \right]^{\frac{8}{27}}} \right]^2$$ EQ 9.27, pg 457, Introduction to Heat Transfer (Third Edition)

$Nu = 11.658$

$$h := \frac{linterp(T_{air}, k_{air}, T_f) \cdot Nu}{D_o} \qquad h = 9.577 \frac{kg}{s^3 K}$$ EQ 6.58, pg 307, Introduction to Heat Transfer (Third Edition)

Heat Transfer from Surface of Tube Due to Free Convection and Radiation

General Convective Heat Transfer $q_{fc} = \left[h_{fc} \cdot \pi \cdot dia_{outer} \cdot \left(T_{surf} - T_{amb}\right)\right]$

General Radiative Heat Transfer $q_{rad} = \varepsilon \cdot \sigma \cdot dia_{outer} \cdot \pi \cdot \left(T_{surf}^{4} - T_{amb}^{4}\right)$

$$q := \left[h \cdot \pi \cdot D_o \cdot \left(T_{surf} - T_{inf}\right)\right] + linterp\left(T_\varepsilon, \varepsilon_{ss}, T_f\right) \cdot \pi \cdot D_o \cdot \sigma \cdot \left(T_{surf}^{4} - T_{inf}^{4}\right)$$

$$q = 4.143 \times 10^{3} \frac{W}{m}$$

Solving For Inner Tube Wall Temperature

Guess Value

$T_{is} := 1200K$

Given

$$q = \frac{2 \cdot \pi \cdot linterp\left(T_{ss}, k_{ss}, T_{surf}\right) \cdot \left(T_{surf} - T_{is}\right)}{\ln\left(\frac{\frac{D_i}{2}}{\frac{D_o}{2}}\right)}$$

EQ 3.27, pg 91, Introduction to Heat Transfer (Third Edition)

$T_{iwfcrad} := Find\left(T_{is}\right)$

Inner Wall Temperature

$T_{iwfcrad} = 1.007 \times 10^{3} K$

Heat Flux Calculation for Free Convection and Radiation

$$flux_{fcrad} := \left[h \cdot \left(T_{surf} - T_{inf}\right)\right] + linterp\left(T_\varepsilon, \varepsilon_{ss}, T_f\right) \cdot \sigma \cdot \left(T_{surf}^{4} - T_{inf}^{4}\right)$$

From Water Jacket Tests

Operating Parameters

$V_{dotwater} := 6.1\frac{gal}{min}$ $\Delta T := 24\cdot\frac{5}{9}\cdot K$ $\Delta T = 13.333\,K$

Tube Dimensions

$Lengthtube := 36in$ $D_i := 2.067in$ $D_o := 2.375in$

Heat Transfer to Water

$q = m_{dot}\cdot c_p\cdot\left(T_{x+dx} - T_x\right)$ EQ 8.37, pg 399, Introduction to Heat Transfer (Third Edition)

$$q := V_{dotwater}\cdot linterp\left[T_{water}, \rho_{water}, \frac{295\cdot K + (295\cdot K + \Delta T)}{2}\right]\cdot linterp\left[T_{water}, c_{pwater}, \left[\frac{295\cdot K + (295\cdot}{2}\right.\right.$$

Heat Flux to Water

$flux_{wj} := \frac{q}{Lengthtube\cdot D_i\cdot\pi}$ $flux_{wj} = 141.651\frac{kW}{m^2}$

$T_{al} := \begin{pmatrix}100\\200\\400\\600\end{pmatrix}\cdot K$ $k_{al} := \begin{pmatrix}65\\163\\186\\186\end{pmatrix}\cdot\frac{W}{m\cdot K}$

Solving for Inner Wall Temperuture

$q_{prime} := \frac{q}{D_i\cdot\pi}$

$T_{iwwj} := 500K$

Given

$$q_{prime} = \frac{2\cdot\pi\cdot linterp\left(T_{al}, k_{al}, 295\cdot K + \Delta T\right)\cdot\left[T_{iwwj} - (295\cdot K + \Delta T)\right]}{\ln\left(\frac{D_o}{D_i}\right)}$$

$T_{iwwj} := Find\left(T_{iwwj}\right)$ $T_{iwwj} = 324.653\,K$

Two Equations Two Unknowns. Solve for PDE Tube Avg. Heat Transfer Coefficient and Avg. Gas Temperature

Solving for Heat Transfer Coefficient and Avg. Gas Temperature

$h_{flame} := 100 \frac{W}{m^2 K}$ $T_{flame} := 2000K$

Given

$flux_{fcrad} = h_{flame} \cdot (T_{flame} - T_{iwfcrad})$

$flux_{wj} = h_{flame} \cdot (T_{flame} - T_{iwwj})$

$Z := Find(h_{flame}, T_{flame})$

$h_{flame} := Z_0$ $T_{flame} := Z_1$

$h_{flame} = 175.428 \frac{W}{m^2 \cdot K}$ $T_{flame} = 1132.111\,K$

Finite Difference Method Heat Exchanger Design Calculation

Concentric Tube Calculations

$$A_{conc} := \frac{\pi}{4}\cdot\left(d_{oi}^{\ 2} - d_{io}^{\ 2}\right)$$

$$P_{conc} := \pi\cdot\left(d_{oi} + d_{io}\right)$$

Hydraulic Diameter of Concentric Tube Heat Exchanger

$$d_{hconc} := \frac{4\cdot A_{conc}}{P_{conc}}$$ EQ 8.67, pg 417, Introduction to Heat Transfer (Third Edition)

Cooling Fluid Velocity in Concentric Tube

$$u_{conc} := \frac{m_{dot}}{\left(\text{linterp}\left(T_{fluid}, \rho_{fluid}, T_{amb}\right)\cdot A_{conc}\right)} \qquad u_{conc} = 0.551\,\frac{in}{s}$$

Finite Difference Method Heat Transfer Calculations

X :=

$i \leftarrow 0$

$T_i \leftarrow T_{fluidin}$

while $T_i < T_{fluidout}$

$$Re \leftarrow \frac{\text{linterp}\left(T_{fluid}, \rho_{fluid}, T_i\right)\cdot u_{conc}\cdot d_{hconc}}{\text{linterp}\left(T_{fluid}, \mu_{fluid}, T_i\right)}$$

if TURB = 0

$Nu \leftarrow Nu_{lam}$

$$h_o \leftarrow \frac{Nu\cdot\text{linterp}\left(T_{fluid}, k_{fluid}, T_i\right)}{d_{hconc}}$$

if TURB = 1

if $Re < Re_{turb}$

$Nu \leftarrow Nu_{lam}$

$$h_o \leftarrow \frac{Nu\cdot\text{linterp}\left(T_{fluid}, k_{fluid}, T_i\right)}{d_{hconc}}$$

otherwise

$$f \leftarrow (.790\cdot\ln(Re) - 1.64)^{-2}$$

$$Nu \leftarrow \frac{\frac{f}{8}\cdot(Re - 1000)\cdot\frac{\text{linterp}\left(T_{fluid}, c_{pfluid}, T_i\right)\cdot\text{linterp}\left(T_{fluid}, \mu_{fluid}, T_i\right)}{\text{linterp}\left(T_{fluid}, k_{fluid}, T_i\right)}}{\frac{1}{2}\left[\left(\text{linterp}(T\ldots\ldots T)\cdot\text{linterp}(T\ldots\ldots T)\right)^{\frac{2}{3}}\right.}$$

$$1 + 12.7 \cdot \left(\frac{f}{8}\right)^{2} \cdot \left[\left(\frac{\text{linterp}\left(T_{fluid}, c_{pfluid}, T_i\right) \cdot \text{linterp}\left(T_{fluid}, \mu_{fluid}, T_i\right)}{\text{linterp}\left(T_{fluid}, k_{fluid}, T_i\right)}\right) - 1\right]$$

$$h_o \leftarrow \frac{Nu \cdot \text{linterp}\left(T_{fluid}, k_{fluid}, T_i\right)}{d_{hconc}}$$

if FCR = 0

$T_{oo} \leftarrow 0 \cdot K$

$h_{fc} \leftarrow 0 \cdot \frac{W}{m^2 \cdot K}$

$T_{oi} \leftarrow 0 \cdot K$

$q_{w1} \leftarrow 0 \cdot W$

$q_{w2} \leftarrow 0 \cdot W$

if FCR = 1

$T_{oo} \leftarrow T_{amb} + dT$

$T_f \leftarrow \frac{T_{oo} + T_{amb}}{2}$

$$Ra \leftarrow \frac{g \cdot \text{linterp}\left(T_\beta, \beta, T_f\right) \cdot \left(T_{oo} - T_{amb}\right) \cdot {d_{oo}}^3}{\text{linterp}\left(T_{air}, \nu_{air}, T_f\right) \cdot \text{linterp}\left(T_{air}, \alpha_{air}, T_f\right)}$$

$$Nu_{fc} \leftarrow \left[.60 + \frac{.387 \cdot Ra^{\frac{1}{6}}}{\left[1 + \left(\frac{.559}{\text{linterp}\left(T_{air}, Pr_{air}, T_f\right)}\right)^{\frac{9}{16}}\right]^{\frac{8}{27}}}\right]^2$$

$$h_{fc} \leftarrow \frac{Nu_{fc} \cdot \text{linterp}\left(T_{air}, k_{air}, T_f\right)}{d_{oo}}$$

$$q_{w1} \leftarrow h_{fc} \cdot d_{oo} \cdot \pi \cdot dl \cdot \left(T_{oo} - T_{amb}\right) + \text{linterp}\left(T_\varepsilon, \varepsilon_{ss}, T_{oo}\right) \cdot \sigma \cdot \left(d_{oo} \cdot \pi \cdot dl\right) \cdot \left({T_{oo}}^4 - {T_{amb}}^4\right)$$

$$T_{oi} \leftarrow \frac{q_{w1} \cdot \ln\left(\frac{d_{oo}}{d_{oi}}\right)}{2 \cdot \pi \cdot dl \cdot \text{linterp}\left(T_{ss}, k_{ss}, T_{oo}\right)} + T_{oo}$$

$$q_{w2} \leftarrow h_o \cdot \pi \cdot d_{oi} \cdot dl \cdot \left(T_i - T_{oi}\right)$$

while $\left|q_{w2} - q_{w1}\right| > q_{tol}$

$T_{oo} \leftarrow T_{oo} + dT$

$$T_f \leftarrow \frac{T_{oo} + T_{amb}}{2}$$

$$Ra \leftarrow \frac{g \cdot \text{linterp}\left(T_\beta, \beta, T_f\right) \cdot \left(T_{oo} - T_{amb}\right) \cdot {d_{oo}}^3}{\text{linterp}\left(T_{air}, \nu_{air}, T_f\right) \cdot \text{linterp}\left(T_{air}, \alpha_{air}, T_f\right)}$$

$$Nu_{fc} \leftarrow \left[.60 + \frac{.387 \cdot Ra^{\frac{1}{6}}}{\left[1 + \left(\frac{.559}{\text{linterp}\left(T_{air}, Pr_{air}, T_f\right)} \right)^{\frac{9}{16}} \right]^{\frac{8}{27}}} \right]^2$$

$$h_{fc} \leftarrow \frac{Nu_{fc} \cdot \text{linterp}\left(T_{air}, k_{air}, T_f\right)}{d_{oo}}$$

$$q_{w1} \leftarrow h_{fc} \cdot d_{oo} \cdot \pi \cdot dl \cdot \left(T_{oo} - T_{amb}\right) + \text{linterp}\left(T_\varepsilon, \varepsilon_{ss}, T_{oo}\right) \cdot \sigma \cdot \left(d_{oo} \cdot \pi \cdot dl\right) \cdot \left({T_{oo}}^4 - T_{aml}\right.$$

$$T_{oi} \leftarrow \frac{q_{w1} \cdot \ln\left(\frac{d_{oo}}{d_{ii}}\right)}{2 \cdot \pi \cdot dl \cdot \text{linterp}\left(T_{ss}, k_{ss}, T_{oo}\right)} + T_{oo}$$

$$q_{w2} \leftarrow h_o \cdot \pi \cdot d_{oi} \cdot dl \cdot \left(T_i - T_{oi}\right)$$

$$T_{io} \leftarrow T_{fluidin} + dT$$

$$q_{in1} \leftarrow h_o \cdot \pi \cdot d_{io} \cdot dl \cdot \left(T_{io} - T_i\right)$$

$$T_{ii} \leftarrow \frac{q_{in1} \cdot \ln\left(\frac{d_{io}}{d_{ii}}\right)}{2 \cdot \text{linterp}\left(T_{ss}, k_{ss}, T_{io}\right) \cdot dl \cdot \pi} + T_{io}$$

$$q_{in2} \leftarrow h_{flame} \cdot \pi \cdot d_{ii} \cdot dl \cdot \left(T_{flame} - T_{ii}\right)$$

while $\left|q_{in1} - q_{in2}\right| > q_{tol}$

$$T_{io} \leftarrow T_{io} + dT$$

$$q_{in1} \leftarrow h_o \cdot \pi \cdot d_{io} \cdot dl \cdot \left(T_{io} - T_i\right)$$

$$T_{ii} \leftarrow \frac{q_{in1} \cdot \ln\left(\frac{d_{io}}{d_{ii}}\right)}{2 \cdot \text{linterp}\left(T_{ss}, k_{ss}, T_{io}\right) \cdot dl \cdot \pi} + T_{io}$$

$$q_{in2} \leftarrow h_{flame} \cdot \pi \cdot d_{ii} \cdot dl \cdot \left(T_{flame} - T_{ii}\right)$$

$$q_{trans} \leftarrow q_{in2} - q_{w2}$$

$$X_{i,0} \leftarrow \frac{T_i}{K}$$

$$X_{i,1} \leftarrow \frac{T_{ii}}{K}$$

$$X_{i,2} \leftarrow \frac{T_{io}}{K}$$

$$X_{i,3} \leftarrow \frac{T_{oi}}{K}$$

$$X_{i,4} \leftarrow \frac{T_{oo}}{K}$$

$$X_{i,5} \leftarrow \frac{q_{trans}}{dl} \cdot \frac{m}{W}$$

$$X_{i,6} \leftarrow \frac{q_{in2}}{dl} \cdot \frac{m}{W}$$

$$X_{i,7} \leftarrow \frac{q_{w1}}{dl} \cdot \frac{m}{W}$$

$$X_{i,8} \leftarrow \frac{q_{w2}}{dl} \cdot \frac{m}{W}$$

$$X_{i,9} \leftarrow \frac{\text{linterp}\left(T_\varepsilon, \varepsilon_{ss}, T_{oo}\right) \cdot \sigma \cdot \left(d_{oo} \cdot \pi \cdot dl\right) \cdot \left(T_{oo}^{\ 4} - T_{amb}^{\ 4}\right)}{dl} \cdot \frac{m}{W}$$

$$X_{i,10} \leftarrow \frac{h_{fc} \cdot d_{oo} \cdot \pi \cdot dl \cdot \left(T_{oo} - T_{amb}\right)}{dl} \cdot \frac{m}{W}$$

$$X_{i,11} \leftarrow i$$

$$X_{i,12} \leftarrow Re$$

$$X_{i,13} \leftarrow Nu$$

$$X_{i,14} \leftarrow h_o \cdot \frac{m^2 \cdot K}{W}$$

$$X_{i,15} \leftarrow h_{fc} \cdot \frac{m^2 \cdot K}{W}$$

$$T_{i+1} \leftarrow \frac{q_{trans}}{m_{dot} \cdot \text{linterp}\left(T_{fluid}, c_{pfluid}, T_i\right)} + T_i$$

$$i \leftarrow i + 1$$

X

Fluid Temperature

$T_{coolingfluid} := X^{\langle 0 \rangle} \cdot K$

Inner Tube Inner Surface Temperature

$T_{pdeinner} := X^{\langle 1 \rangle} \cdot K$

Inner Tube Outer Surface Temperature

$T_{pdeouter} := X^{\langle 2 \rangle} \cdot K$

Outer Tube Inner Surface Temperature

$T_{oinner} := X^{\langle 3 \rangle} K$

Outer Tube Outer Surface Temperature

$T_{oouter} := X^{\langle 4 \rangle} \cdot K$

Heat Transfer to the cooling fluid

$q_{trans} := X^{\langle 5 \rangle} \cdot \frac{W}{m}$

Heat Transfer into the System

$q_{in} := X^{\langle 6 \rangle} \frac{W}{m}$

Heat Transfer rejected by Free Convection and Radiation

$q_{waste} := X^{\langle 7 \rangle} \cdot \frac{W}{m}$

$q_{waste2} := X^{\langle 8 \rangle} \frac{W}{m}$

Heat Losses due to Radiation

$q_{rad} := X^{\langle 9 \rangle} \cdot \frac{W}{m}$

Heat Losses due to Free Convection

$q_{fc} := X^{\langle 10 \rangle} \cdot \frac{W}{m}$

Tube Length

$Length := X^{\langle 11 \rangle} \cdot mm$

Reynolds Number

$Re := X^{\langle 12 \rangle}$

Nusselt Number

$$Nu := X^{\langle 13 \rangle}$$

Fluid Heat Transfer Coefficient

$$h := X^{\langle 14 \rangle} \cdot \frac{W}{m^2 \cdot K}$$

Free Convection Heat Transfer Coefficient on Outside of Outer Tube

$$h_{fc} := X^{\langle 15 \rangle} \cdot \frac{W}{m^2 \cdot K}$$

$x := \text{length}(Length)$ $\quad x = 742$

$$LengthRequired := Length_{(x-1)}$$

$$ResidenceTime := \frac{(LengthRequired \cdot A_{conc}) \cdot linterp(T_{fluid}, \rho_{fluid}, T_{amb})}{m_{dot}}$$

$$FluidVelocity := \frac{LengthRequired}{ResidenceTime}$$

$$T_{heatexchangerexit} := T_{coolingfluid_{x-1}}$$

$$q_{transtotal} := \sum q_{trans} \cdot dl$$

$$q_{intotal} := \sum q_{in} \cdot dl$$

$$Percentloss := \left| 1 - \frac{q_{transtotal}}{q_{intotal}} \right| \cdot 100$$

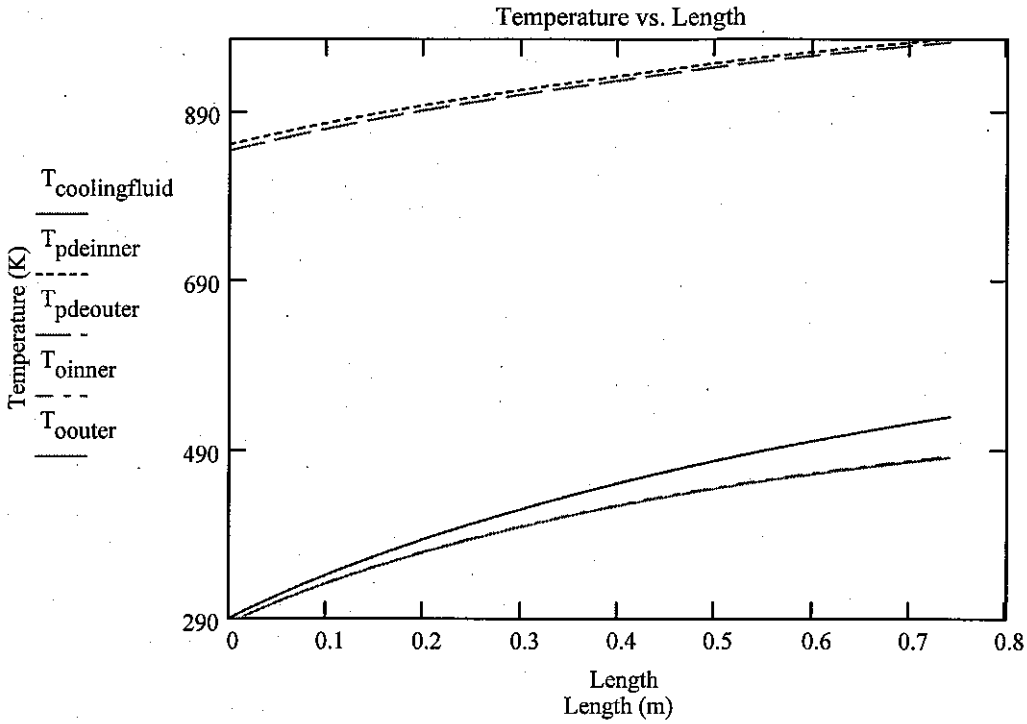
Temperature vs. Length
Temperature (K)
$T_{coolingfluid}$
$T_{pdeinner}$
$T_{pdeouter}$
T_{oinner}
T_{oouter}
890
690
490
290
0
0.1
0.2
0.3
0.4
0.5
0.6
0.7
0.8
Length
Length (m)

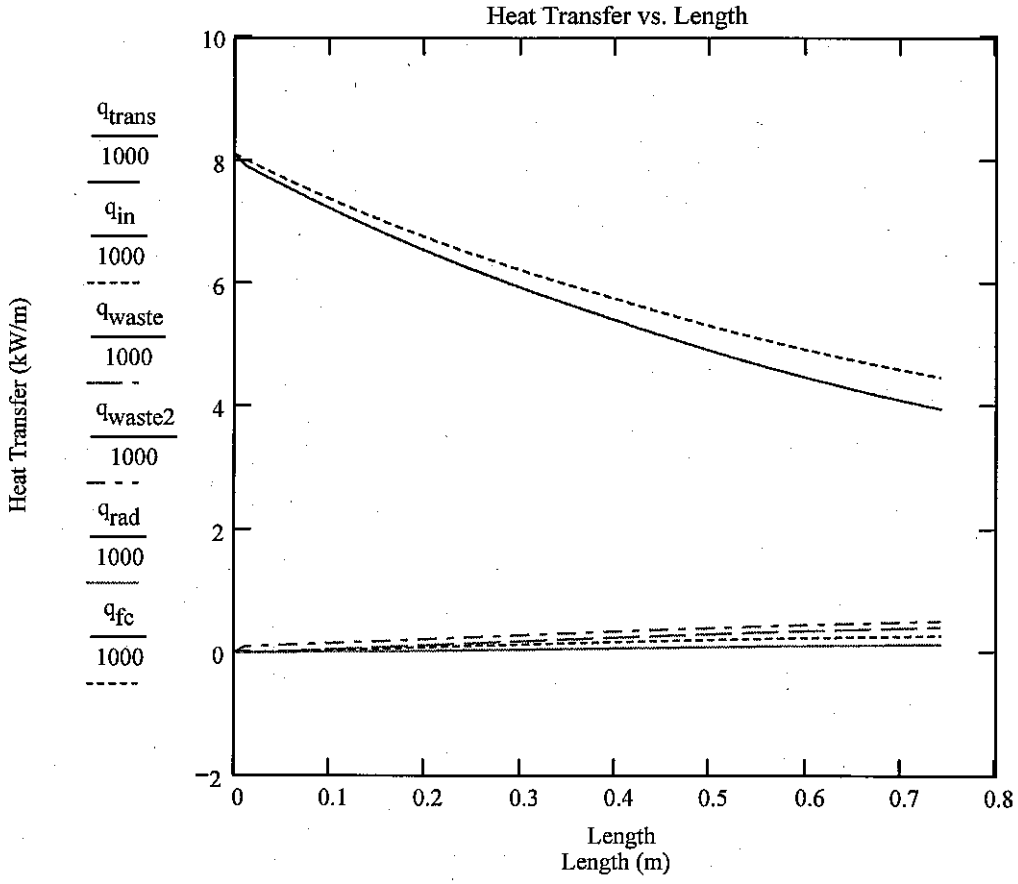
Heat Transfer vs. Length
Heat Transfer (kW/m)
$\frac{q_{trans}}{1000}$
$\frac{q_{in}}{1000}$
$\frac{q_{waste}}{1000}$
$\frac{q_{waste2}}{1000}$
$\frac{q_{rad}}{1000}$
$\frac{q_{fc}}{1000}$
10
8
6
4
2
0
−2
0
0.1
0.2
0.3
0.4
0.5
0.6
0.7
0.8
Length
Length (m)

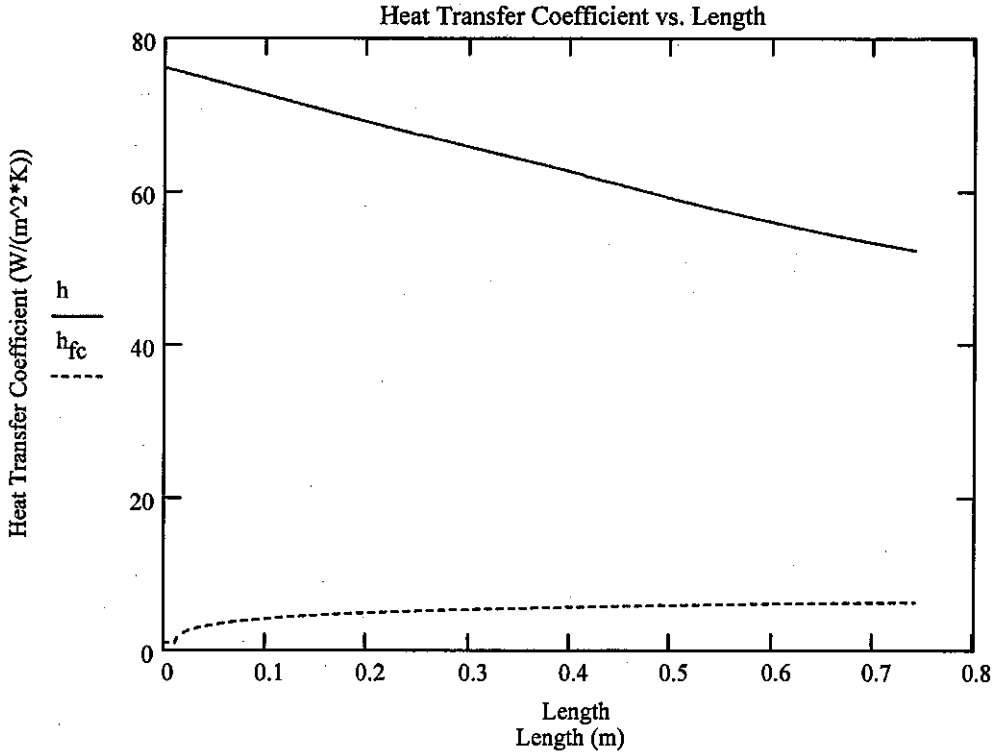
Heat Transfer Coefficient vs. Length
Heat Transfer Coefficient (W/(m^2*K))
h
h_fc
80
60
40
20
0
0
0.1
0.2
0.3
0.4
0.5
0.6
0.7
0.8
Length
Length (m)

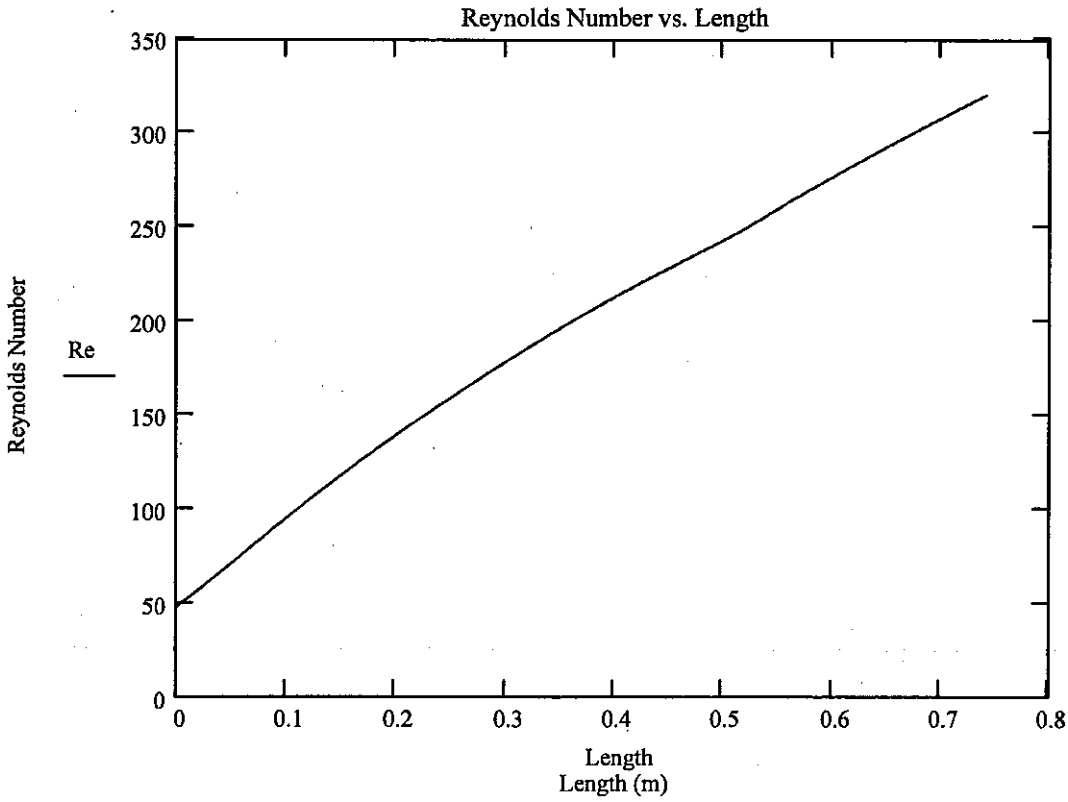
Reynolds Number vs. Length
Reynolds Number
Re
350
300
250
200
150
100
50
0
0
0.1
0.2
0.3
0.4
0.5
0.6
0.7
0.8
Length
Length (m)

Final Results

Stochiometric Values

$Moles_{air} = 16.125\,mol$

Stochiometric Fuel and Air Molecular Weight

$mw_{fuel} = 152.018\,\frac{kg}{mol}$ $mw_{air} = 28.856\,\frac{kg}{mol}$

Mixture Values for Operating Parameters

$fueltoair = 0.07204$ $airtofuel = 13.881$

Volumetric and Mass Flow Rate Values

$V_{dot} = 0.12\,\frac{m^3}{s}$ $V_{adot} = 0.119\,\frac{m^3}{s}$ $V_{fdot} = 1.625 \times 10^{-3}\,\frac{m^3}{s}$

$m_{adot} = 0.106\,\frac{kg}{s}$

$m_{fdot} = 1.011\,\frac{lb}{min}$

Energy Required to Raise Cooling Fluid Temperature
From $T_{fluidin} = 290\,K$ To $T_{fluidout} = 530\,K$

$SpecificEnergy = 615.163\,\frac{kJ}{kg}$ $EnergyRequired = 4.7\,kW$

$EnergyReleased = 327\,kW$ $PercentRequired = 1.437$

Heat Transfer Coefficient and Inner Tube Temperature Values

$h_{flame} = 175.428\,\frac{W}{m^2K}$ $T_{flame} = 1132.111\,K$

Final Values

$q_{transtotal} = 4.226\,kW$

$q_{intotal} = 4.462\,kW$

$Percentloss = 5.29$

$T_{heatexchangerexit} = 529.928\,K$

$LengthRequired = 29\,in$

$ResidenceTime = 52.901\,s$

Appendix C. Plain Tube Heat Transfer Calculations

Constants and Unit Conversions

$bar := 14.503773773021 psi \qquad kJ := 1000 J \qquad MJ := 10^6 J \qquad MPa := 10^6 Pa \qquad kmol := mol$

$R := 8.314 \frac{kJ}{mol \cdot K} \qquad \sigma := 5.67 \cdot 10^{-8} \frac{W}{m^2 \cdot K^4}$

Material and Air Properties

From Introduction to Heat Transfer (Third Edition), Frank P. Incropera, David P. DeWitt, John Wiley & Sons, Inc. Copyright 1996

Appendix A Table A.1

$$T_{ss} := \begin{pmatrix} 100 \\ 200 \\ 400 \\ 600 \\ 800 \\ 1000 \\ 1200 \\ 1500 \end{pmatrix} \cdot K \qquad k_{ss} := \begin{pmatrix} 9.2 \\ 12.6 \\ 16.6 \\ 19.8 \\ 22.6 \\ 25.4 \\ 28.0 \\ 31.7 \end{pmatrix} \cdot \frac{W}{m \cdot K}$$

From Introduction to Heat Transfer (Third Edition), Frank P. Incropera, David P. DeWitt, John Wiley & Sons, Inc. Copyright 1996

Appendix A Table A.8 (Lightly Oxidized Stainless Steel)

$$T_\varepsilon := \begin{pmatrix} 300 \\ 400 \\ 600 \\ 800 \\ 1000 \end{pmatrix} \cdot K \qquad \varepsilon_{ss} := \begin{pmatrix} .22 \\ .22 \\ .24 \\ .33 \\ .40 \end{pmatrix}$$

Appendix A Table A.4

$$T_{air} := \begin{pmatrix} 100 \\ 150 \\ 200 \\ 250 \\ 300 \\ 350 \\ 400 \\ 450 \\ 500 \\ 550 \\ 600 \\ 650 \\ 700 \\ 750 \\ 800 \\ 850 \\ 900 \\ 950 \\ 1000 \\ 1100 \\ 1200 \\ 1300 \\ 1400 \\ 1500 \\ 1600 \end{pmatrix} \cdot K \qquad \nu_{air} := \begin{pmatrix} 2.00 \\ 4.426 \\ 7.590 \\ 11.44 \\ 15.89 \\ 20.92 \\ 26.41 \\ 32.9 \\ 38.79 \\ 45.57 \\ 52.69 \\ 60.21 \\ 68.10 \\ 76.37 \\ 84.93 \\ 93.8 \\ 102.9 \\ 112.2 \\ 121.9 \\ 141.8 \\ 162.9 \\ 185.1 \\ 213 \\ 240 \\ 268 \end{pmatrix} \cdot 10^{-6} \frac{m^2}{s} \qquad k_{air} := \begin{pmatrix} 9.34 \\ 13.8 \\ 18.1 \\ 22.3 \\ 26.3 \\ 30.0 \\ 33.8 \\ 37.3 \\ 40.7 \\ 43.9 \\ 46.9 \\ 49.7 \\ 52.4 \\ 54.9 \\ 57.3 \\ 59.6 \\ 62 \\ 64.3 \\ 66.7 \\ 71.5 \\ 76.3 \\ 82 \\ 91 \\ 100 \\ 106 \end{pmatrix} \cdot 10^{-3} \frac{W}{m \cdot K}$$

$$\alpha_{air} := \begin{pmatrix} 2.54 \\ 5.84 \\ 10.3 \\ 15.9 \\ 22.5 \\ 29.9 \\ 38.3 \\ 47.2 \\ 56.7 \\ 66.7 \\ 76.9 \\ 87.3 \\ 98 \\ 109 \\ 120 \\ 131 \\ 143 \\ 155 \\ 168 \\ 195 \\ 224 \\ 238 \\ 303 \\ 350 \\ 390 \end{pmatrix} \cdot 10^{-6} \cdot \frac{m^2}{s} \qquad Pr_{air} := \begin{pmatrix} .786 \\ .758 \\ .737 \\ .720 \\ .707 \\ .7 \\ .69 \\ .686 \\ .684 \\ .683 \\ .685 \\ .690 \\ .695 \\ .702 \\ .709 \\ .716 \\ .720 \\ .723 \\ .726 \\ .728 \\ .728 \\ .719 \\ .703 \\ .685 \\ .688 \end{pmatrix}$$

$$\rho_{air} := \frac{1}{\nu_{air}} \qquad \beta_{air} := \frac{1}{T_{air}}$$

5-1-20 Avgas Clean Tube Heat Transfer Calcs

Steady-state data obtained from testing

$$\phi := \begin{pmatrix} .95 \\ 1.02 \\ 1.09 \\ 1.12 \\ 1.22 \\ 1.26 \end{pmatrix} \qquad loc := \begin{pmatrix} 19.685 \\ 46.99 \\ 73.8188 \\ 105.886 \\ 121.761 \\ 137.001 \\ 154.623 \\ 169.863 \end{pmatrix} \cdot cm$$

$$Temp := \begin{pmatrix} 596.51 & 605.4541667 & 601.3773889 & 595.3083889 & 575.4475 & 573.5081111 \\ 692.76 & 705.947 & 669.0364444 & 644.0752778 & 613.7165 & 618.1916111 \\ 763.06 & 781.1624444 & 699.8215 & 691.7939444 & 648.9514444 & 641.4213333 \\ 802.92 & 816.6038889 & 800.0493889 & 796.4642222 & 746.0194444 & 733.0732222 \\ 835.58 & 849.4266667 & 853.8216667 & 846.1422222 & 798.5135556 & 789.2047222 \\ 808.82 & 832.4044444 & 851.9672222 & 846.1422222 & 788.8633889 & 780.444 \\ 842.04 & 869.0783333 & 878.4661111 & 876.4894444 & 803.4879444 & 789.4714444 \\ 814.11 & 835.9805556 & 854.2244444 & 854.985 & 756.0436667 & 738.1221667 \end{pmatrix} \cdot K$$

Outer Tube Diameter

$D_o := 2.375in$

Ambient Air Temperature

$T_{inf} := 290K$

Heat transfer calculation based on radiation and free convection from a long horizontal cyclinder

$$
\begin{aligned}
X := \;& \text{for } y \in 0..5 \\
& \quad \text{for } x \in 0..7 \\
& \quad\quad T_{surf} \leftarrow Temp_{x,y} \\
& \quad\quad T_f \leftarrow \frac{T_{surf} + T_{inf}}{2} \qquad 326) \\
& \quad\quad Ra \leftarrow \frac{g \cdot linterp(T_{air}, \beta_{air}, T_f) \cdot (T_{surf} - T_{inf}) \cdot D_o^{\,3}}{linterp(T_{air}, \nu_{air}, T_f) \cdot linterp(T_{air}, \alpha_{air}, T_f)} \qquad 456) \\
& \quad\quad Nu \leftarrow \left[.6 + \frac{.387 \cdot Ra^{\frac{1}{6}}}{\left[1 + \left(\frac{.559}{linterp(T_{air}, Pr_{air}, T_f)} \right)^{\frac{9}{16}} \right]^{\frac{8}{27}}} \right]^2 \qquad 465) \\
& \quad\quad h \leftarrow \frac{linterp(T_{air}, k_{air}, T_f) \cdot Nu}{D_o} \qquad 465) \\
& \quad\quad q_{x,y} \leftarrow \left[h \cdot \pi \cdot D_o \cdot (T_{surf} - T_{inf}) \right] + linterp(T_\varepsilon, \varepsilon_{ss}, T_f) \cdot \pi \cdot D_o \cdot \sigma \cdot \left(T_{surf}^{\,4} - T_{inf}^{\,4} \right) \\
& q \qquad -10)
\end{aligned}
$$

Heat Transfer Values

$$
X = \begin{pmatrix}
0.803 & 0.839 & 0.823 & 0.798 & 0.721 & 0.714 \\
1.251 & 1.323 & 1.129 & 1.008 & 0.874 & 0.893 \\
1.667 & 1.789 & 1.289 & 1.246 & 1.031 & 0.996 \\
1.944 & 2.047 & 1.923 & 1.897 & 1.558 & 1.479 \\
2.196 & 2.31 & 2.348 & 2.283 & 1.912 & 1.845 \\
1.988 & 2.17 & 2.332 & 2.283 & 1.842 & 1.784 \\
2.249 & 2.481 & 2.566 & 2.548 & 1.948 & 1.847 \\
2.028 & 2.199 & 2.351 & 2.357 & 1.622 & 1.51
\end{pmatrix} \frac{kW}{m}
$$

$q_{prime1} := X^{\langle 0 \rangle}$ $q_{prime2} := X^{\langle 1 \rangle}$ $q_{prime3} := X^{\langle 2 \rangle}$

$q_{prime4} := X^{\langle 3 \rangle}$ $q_{prime5} := X^{\langle 4 \rangle}$ $q_{prime6} := X^{\langle 5 \rangle}$

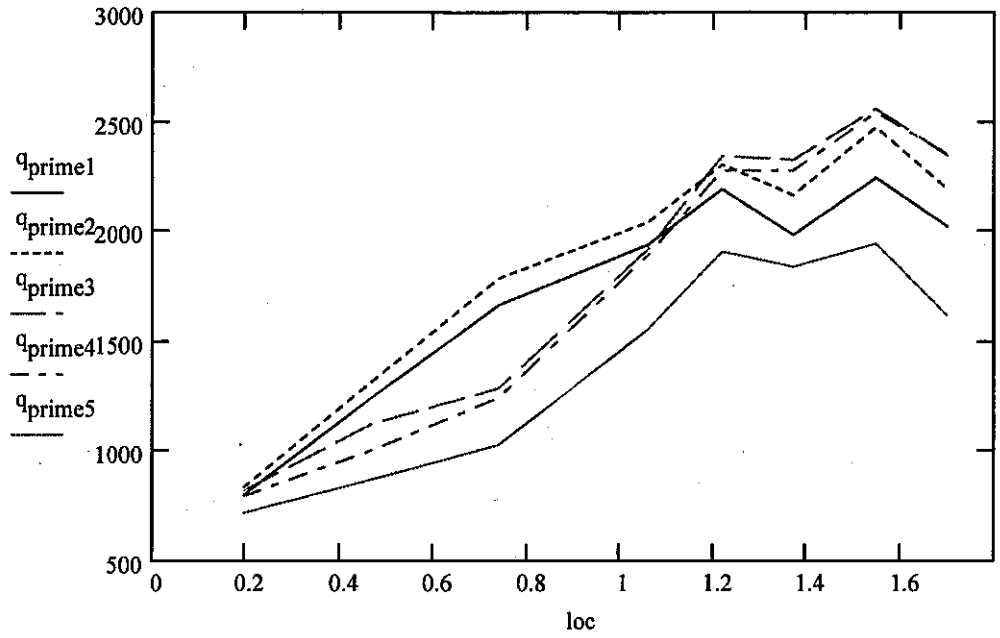
3000
2500
2000
1500
1000
500
0
0.2
0.4
0.6
0.8
1
1.2
1.4
1.6
loc
qprime1
qprime2
qprime3
qprime4
qprime5

5-1-21 JP-8 Clean Tube Heat Transfer Calcs

Steady-state data obtained from testing

$$\phi := \begin{pmatrix} 1.05 \\ 1.07 \\ 1.08 \\ 1.19 \\ 1.26 \end{pmatrix} \qquad loc := \begin{pmatrix} 19.685 \\ 46.99 \\ 73.8188 \\ 105.886 \\ 121.761 \\ 137.001 \\ 154.623 \\ 169.863 \end{pmatrix} \cdot cm$$

$$Temp := \begin{pmatrix} 618.198 & 610.3761667 & 610.3451667 & 607.8732778 & 602.6850556 \\ 764.2152222 & 701.2448333 & 751.4777222 & 676.3736111 & 746.2182222 \\ 838.235 & 809.0104444 & 819.2511111 & 821.0644444 & 777.8316111 \\ 885.5205556 & 866.5633333 & 869.2855556 & 874.6472222 & 864.8983333 \\ 903.9816667 & 878.685 & 887.7288889 & 896.0127778 & 894.4655556 \\ 882.1638889 & 857.4505556 & 868.9688889 & 883.9744444 & 883.1605556 \\ 918.24 & 894.0527778 & 902.6311111 & 911.6044444 & 907.5194444 \\ 858.1288889 & 821.6572222 & 838.5005556 & 850.1838889 & 842.4988889 \end{pmatrix} \cdot K$$

Outer Tube Diameter

$D_o := 2.375in$

Ambient Air Temperature

$T_{inf} := 290K$

From Steady State Tube Free Convection and Radiation Test

$$
\begin{aligned}
Y := \;& \text{for } y \in 0..4 \\
& \quad \text{for } x \in 0..7 \\
& \quad\quad T_{surf} \leftarrow Temp_{x,y} \\
& \quad\quad T_f \leftarrow \frac{T_{surf} + T_{inf}}{2} \qquad \text{(Incropera and Dewitt,1996:326)} \\
& \quad\quad Ra \leftarrow \frac{g \cdot linterp(T_{air}, \beta_{air}, T_f) \cdot (T_{surf} - T_{inf}) \cdot D_o^{\,3}}{linterp(T_{air}, \nu_{air}, T_f) \cdot linterp(T_{air}, \alpha_{air}, T_f)} \qquad \text{(Incropera and Dewitt,1996:456)} \\
& \quad\quad Nu \leftarrow \left[.6 + \frac{.387 \cdot Ra^{\frac{1}{6}}}{\left[1 + \left(\frac{.559}{linterp(T_{air}, Pr_{air}, T_f)} \right)^{\frac{9}{16}} \right]^{\frac{8}{27}}} \right]^2 \qquad \text{(Incropera and Dewitt,1996:465)} \\
& \quad\quad h \leftarrow \frac{linterp(T_{air}, k_{air}, T_f) \cdot Nu}{D_o} \qquad \text{(Incropera and Dewitt,1996:465)} \\
& \quad\quad q_{x,y} \leftarrow \left[h \cdot \pi \cdot D_o \cdot (T_{surf} - T_{inf}) \right] + linterp(T_\varepsilon, \varepsilon_{ss}, T_f) \cdot \pi \cdot D_o \cdot \sigma \cdot \left(T_{surf}^{\,4} - T_{inf}^{\,4} \right) \\
& \quad\quad \text{(Incropera and Dewitt,1996:8-10)} \\
& q
\end{aligned}
$$

Heat Transfer Values

$$
Y = \begin{pmatrix}
0.893 & 0.86 & 0.86 & 0.849 & 0.828 \\
1.675 & 1.297 & 1.592 & 1.166 & 1.559 \\
2.217 & 1.989 & 2.067 & 2.081 & 1.766 \\
2.631 & 2.458 & 2.483 & 2.531 & 2.444 \\
2.809 & 2.568 & 2.652 & 2.731 & 2.716 \\
2.6 & 2.379 & 2.48 & 2.617 & 2.609 \\
2.963 & 2.712 & 2.795 & 2.887 & 2.844 \\
2.385 & 2.085 & 2.22 & 2.317 & 2.252
\end{pmatrix} \frac{kW}{m}
$$

$q_{prime1} := Y^{\langle 0 \rangle}$ $q_{prime2} := Y^{\langle 1 \rangle}$ $q_{prime3} := Y^{\langle 2 \rangle}$ $q_{prime4} := Y^{\langle 3 \rangle}$ $q_{prime5} := Y^{\langle 4 \rangle}$

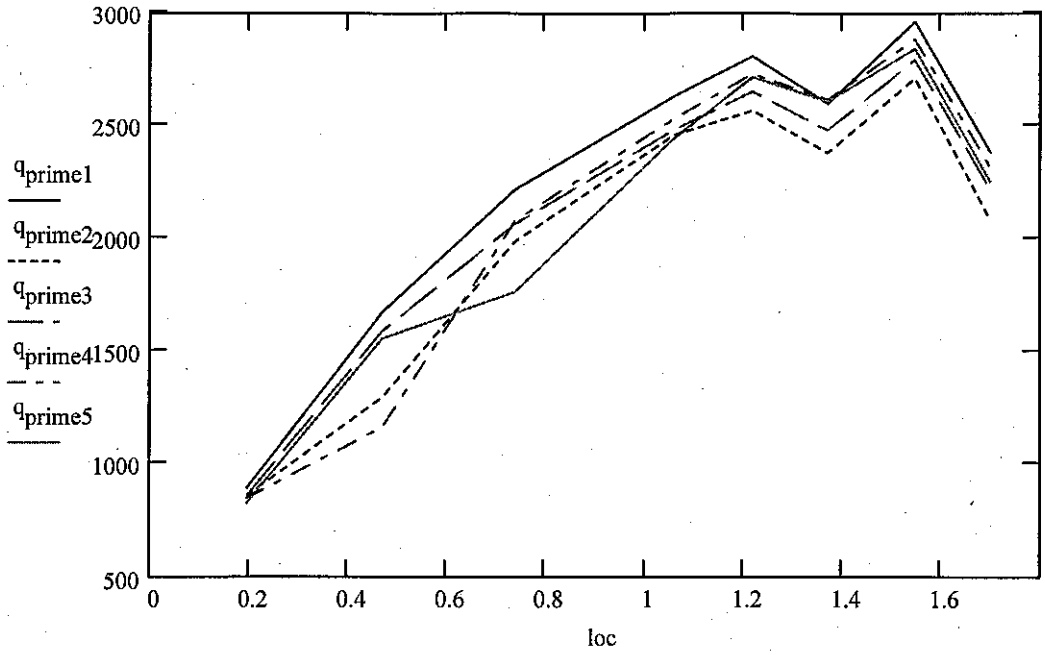
3000
2500
2000
1500
1000
500
0
0.2
0.4
0.6
0.8
1
1.2
1.4
1.6
loc
qprime1
qprime2
qprime3
qprime4
qprime5

Appendix D. Sample Wavespeed Calculation

Constants and Unit Conversions

$bar := 14.503773773021 psi \qquad kJ := 1000 J \qquad kmol := mol \qquad MJ := 10^6 J$

$R := 8.314 \frac{kJ}{mol \cdot K} \qquad \sigma := 5.67 \cdot 10^{-8} \frac{W}{m^2 \cdot K^4} \qquad ms := \frac{1}{1000} s \qquad \mu s := \frac{1}{1000} ms$

Assigning Data

WSIG :=

..\8.xls

Ion Probe Locations

$$ionloc := \begin{pmatrix} 7.75 \\ 18.5 \\ 29.0625 \\ 41.6875 \\ 47.9375 \\ 53.9375 \\ 60.875 \\ 66.875 \end{pmatrix} \cdot in$$

datapoints := 9804

rows := 9804

shift := 11

$col_{shifts} := 0$

Ion probe voltage tolerance for wave time

$ion_{tol} := 4.45$

Spark derivative tolerance for spark time

$spark_{dertol} := -.75$

High and Low Tolerances for spark time

$spark_{tollow} := .5$

$spark_{tolhigh} := 3.5$

skip := 200

$res := \left[\left(WSIG^{\langle 0 \rangle} \right)_1 - \left(WSIG^{\langle 0 \rangle} \right)_0 \right] \cdot s$

Data Resolution

res = 51 μs

Data Column Numbers

timecol := 0 sparkcol := 1 ion1col := 5 ion2col := 6 ion3col := 7 ion4col := 8

ion5col := 9 ion6col := 10 ion7col := 11 ion8col := 12

Assigning Time Data

$time_{vector} :=$ | $z \leftarrow 0$
| while $z \le datapoints$
| for $x \in 0 .. col_{shifts}$
| for $row \in 0 .. rows - 1$
| $col \leftarrow x \cdot shift$
| $time_z \leftarrow WSIG_{row, col}$
| $z \leftarrow z + 1$
| time·s

$i := 0 .. datapoints - 1$

$time_i := time_{vector_i}$

Ion Probe Distance Calculation

$i := 0 .. last(ionloc) - 1 \quad dist_i := ionloc_{i+1} - ionloc_i \quad dist = \begin{pmatrix} 10.75 \\ 10.563 \\ 12.625 \\ 6.25 \\ 6 \\ 6.938 \\ 6 \end{pmatrix}$ in

Assigning Spark Data

$spark_{vec} :=$ | $z \leftarrow 0$
| $channel \leftarrow sparkcol$
| while $z \le datapoints$
| for $x \in 0 .. col_{shifts}$
| for $row \in 0 .. rows - 1$
| $col \leftarrow x \cdot shift + channel$
| $var_z \leftarrow WSIG_{row, col}$
| $z \leftarrow z + 1$
| var

$i := 0 .. datapoints - 1$

$spark_i := spark_{vec_i}$

$i := 1 .. last(time)$

Spark Derivative

$$spark_{der_i} := \frac{spark_i - spark_{i-1}}{time_i - time_{i-1}} \qquad spark_{der} := \frac{spark_{der}}{max(spark_{der})}$$

Assigning Ion Probe Data

$ion1_{vec} :=$
- $z \leftarrow 0$
- $channel \leftarrow ion1col$
- while $z \le datapoints$
  - for $x \in 0 .. col_{shifts}$
    - for $row \in 0 .. rows - 1$
      - $col \leftarrow x \cdot shift + channel$
      - $var_z \leftarrow WSIG_{row, col}$
      - $z \leftarrow z + 1$
- var

$i := 0 .. datapoints - 1$

$ion1_i := ion1_{vec_i}$

$ion2_{vec} :=$
- $z \leftarrow 0$
- $channel \leftarrow ion2col$
- while $z \le datapoints$
  - for $x \in 0 .. col_{shifts}$
    - for $row \in 0 .. rows - 1$
      - $col \leftarrow x \cdot shift + channel$
      - $var_z \leftarrow WSIG_{row, col}$
      - $z \leftarrow z + 1$
- var

$i := 0 .. datapoints - 1$

$ion2_i := ion2_{vec_i}$

$ion3_{vec} :=$
- $z \leftarrow 0$
- $channel \leftarrow ion3col$
- while $z \le datapoints$
  - for $x \in 0 .. col_{shifts}$
    - for $row \in 0 .. rows - 1$
      - $col \leftarrow x \cdot shift + channel$
      - $var_z \leftarrow WSIG_{row, col}$
      - $z \leftarrow z + 1$
- var

$i := 0 .. datapoints - 1$

$ion3_i := ion3_{vec_i}$

$ion4_{vec} :=$
- $z \leftarrow 0$
- $channel \leftarrow ion4col$
- while $z \le datapoints$
  - for $x \in 0 .. col_{shifts}$
    - for $row \in 0 .. rows - 1$
      - $col \leftarrow x \cdot shift + channel$
      - $var_z \leftarrow WSIG_{row, col}$
      - $z \leftarrow z + 1$
- var

$i := 0 .. datapoints - 1$

$ion4_i := ion4_{vec_i}$

$ion5_{vec} :=$
z ← 0
channel ← ion5col
while z ≤ datapoints
  for x ∈ 0.. col_{shifts}
    for row ∈ 0.. rows − 1
      col ← x·shift + channel
      var_z ← $WSIG_{row,col}$
      z ← z + 1
var

i := 0.. datapoints − 1

$ion5_i := ion5_{vec_i}$

$ion6_{vec} :=$
z ← 0
channel ← ion6col
while z ≤ datapoints
  for x ∈ 0.. col_{shifts}
    for row ∈ 0.. rows − 1
      col ← x·shift + channel
      var_z ← $WSIG_{row,col}$
      z ← z + 1
var

i := 0.. datapoints − 1

$ion6_i := ion6_{vec_i}$

$ion7_{vec} :=$
z ← 0
channel ← ion7col
while z ≤ datapoints
  for x ∈ 0.. col_{shifts}
    for row ∈ 0.. rows − 1
      col ← x·shift + channel
      var_z ← $WSIG_{row,col}$
      z ← z + 1
var

i := 0.. datapoints − 1

$ion7_i := ion7_{vec_i}$

$ion8_{vec} :=$
z ← 0
channel ← ion8col
while z ≤ datapoints
  for x ∈ 0.. col_{shifts}
    for row ∈ 0.. rows − 1
      col ← x·shift + channel
      var_z ← $WSIG_{row,col}$
      z ← z + 1
var

i := 0.. datapoints − 1

$ion8_i := ion8_{vec_i}$

Determining Spark Time

$t_{spark} :=$
- $x \leftarrow 0$
- $y \leftarrow 0$
- while $x < last(time)$
  - if $spark_{der_x} \leq spark_{dertol}$
    - if $spark_x \leq spark_{tolhigh}$
      - $t_{spark_y} \leftarrow time_x$
      - $y \leftarrow y + 1$
      - $x \leftarrow x + 1$
    - $x \leftarrow x + 1$ otherwise
  - $x \leftarrow x + 1$ otherwise
- t_{spark}

Determining wave times at each Ion Probe

$t_{ion1} :=$ ion ← ion1
x ← 0
y ← 0
while x < last(time)
  if $ion_x \le ion_{tol}$
    if y < last(t_{spark})
      if $time_x > t_{spark_y}$
        $t_{ion_y} \leftarrow \dfrac{time_{x-1} \cdot ion_{tol} + time_x \cdot ion_{x-1} - time_x \cdot ion_{tol} - ion_x \cdot time_{x-1}}{ion_{x-1} - ion_x}$
        x ← x + skip
        y ← y + 1
      x ← x + 1 otherwise
    x ← x + 1 otherwise
  x ← x + 1 otherwise
a ← 0
b ← 0
while a < last(t_{spark})
  if $t_{ion_b} < t_{spark_{a+1}}$
    $time1_a \leftarrow t_{ion_b}$
    a ← a + 1
    b ← b + 1
  otherwise
    $time1_a \leftarrow .001\mu s$
    a ← a + 1
  time1

$t_{ion2} :=$

ion ← ion2

x ← 0

y ← 0

while x < last(time)

  if $ion_x \le ion_{tol}$

    if y < last(t_{spark})

      if $time_x > t_{spark_y} + 5ms$

        $t_{ion_y} \leftarrow \dfrac{time_{x-1} \cdot ion_{tol} + time_x \cdot ion_{x-1} - time_x \cdot ion_{tol} - ion_x \cdot time_{x-1}}{ion_{x-1} - ion_x}$

        x ← x + skip

        y ← y + 1

      x ← x + 1 otherwise

    x ← x + 1 otherwise

  x ← x + 1 otherwise

a ← 0

b ← 0

while a < last(t_{spark})

  if $t_{ion_b} < t_{spark_{a+1}}$

    $time1_a \leftarrow t_{ion_b}$

    a ← a + 1

    b ← b + 1

  otherwise

    $time1_a \leftarrow .002\mu s$

    a ← a + 1

  time1

$t_{ion3} :=$

ion ← ion3

x ← 0

y ← 0

while x < last(time)

  if $ion_x \le ion_{tol}$

    if y < last(t_{spark})

      if $time_x > t_{spark_y}$

        $t_{ion_y} \leftarrow \dfrac{time_{x-1} \cdot ion_{tol} + time_x \cdot ion_{x-1} - time_x \cdot ion_{tol} - ion_x \cdot time_{x-1}}{ion_{x-1} - ion_x}$

        x ← x + skip

        y ← y + 1

      x ← x + 1 otherwise

    x ← x + 1 otherwise

  x ← x + 1 otherwise

a ← 0

b ← 0

while a < last(t_{spark})

  if $t_{ion_b} < t_{spark_{a+1}}$

    $time1_a \leftarrow t_{ion_b}$

    a ← a + 1

    b ← b + 1

  otherwise

    $time1_a \leftarrow 0.003\mu s$

    a ← a + 1

  time1

$t_{ion4} :=$

ion ← ion4

x ← 0

y ← 0

while x < last(time)

  if $ion_x \le ion_{tol}$

    if y < last(t_{spark})

      if $time_x > t_{spark_y}$

        $t_{ion_y} \leftarrow \dfrac{time_{x-1} \cdot ion_{tol} + time_x \cdot ion_{x-1} - time_x \cdot ion_{tol} - ion_x \cdot time_{x-1}}{ion_{x-1} - ion_x}$

        x ← x + skip

        y ← y + 1

      x ← x + 1 otherwise

    x ← x + 1 otherwise

  x ← x + 1 otherwise

a ← 0

b ← 0

while a < last(t_{spark})

  if $t_{ion_b} < t_{spark_{a+1}}$

    $time1_a \leftarrow t_{ion_b}$

    a ← a + 1

    b ← b + 1

  otherwise

    $time1_a \leftarrow 0.004\mu s$

    a ← a + 1

  time1

$t_{ion5} :=$ | ion ← ion5
| x ← 0
| y ← 0
| while x < last(time)
| | if $ion_x \le ion_{tol}$
| | | if y < last(t_{spark})
| | | | if $time_x > t_{spark_y}$
| | | | | $t_{ion_y} \leftarrow \frac{time_{x-1} \cdot ion_{tol} + time_x \cdot ion_{x-1} - time_x \cdot ion_{tol} - ion_x \cdot time_{x-1}}{ion_{x-1} - ion_x}$
| | | | | x ← x + skip
| | | | | y ← y + 1
| | | | x ← x + 1 otherwise
| | | x ← x + 1 otherwise
| | x ← x + 1 otherwise
| a ← 0
| b ← 0
| while a < last(t_{spark})
| | if $t_{ion_b} < t_{spark_{a+1}}$
| | | $time1_a \leftarrow t_{ion_b}$
| | | a ← a + 1
| | | b ← b + 1
| | otherwise
| | | $time1_a \leftarrow 0.005\mu s$
| | | a ← a + 1
| | time1

$t_{ion6} :=$ ion ← ion6

x ← 0

y ← 0

while x < last(time)

  if $ion_x \le ion_{tol}$

    if y < last(t_{spark})

      if $time_x > t_{spark_y}$

        $t_{ion_y} \leftarrow \dfrac{time_{x-1} \cdot ion_{tol} + time_x \cdot ion_{x-1} - time_x \cdot ion_{tol} - ion_x \cdot time_{x-1}}{ion_{x-1} - ion_x}$

        x ← x + skip

        y ← y + 1

      x ← x + 1 otherwise

    x ← x + 1 otherwise

  x ← x + 1 otherwise

a ← 0

b ← 0

while a < last(t_{spark})

  if $t_{ion_b} < t_{spark_{a+1}}$

    $time1_a \leftarrow t_{ion_b}$

    a ← a + 1

    b ← b + 1

  otherwise

    $time1_a \leftarrow 0.006\mu s$

    a ← a + 1

  time1

$t_{ion7} :=$

ion ← ion7

x ← 0

y ← 0

while x < last(time)

  if $ion_x \le ion_{tol}$

    if y < last(t_{spark})

      if $time_x > t_{spark_y}$

        $t_{ion_y} \leftarrow \dfrac{time_{x-1} \cdot ion_{tol} + time_x \cdot ion_{x-1} - time_x \cdot ion_{tol} - ion_x \cdot time_{x-1}}{ion_{x-1} - ion_x}$

        x ← x + skip

        y ← y + 1

      x ← x + 1 otherwise

    x ← x + 1 otherwise

  x ← x + 1 otherwise

a ← 0

b ← 0

while a < last(t_{spark})

  if $t_{ion_b} < t_{spark_{a+1}}$

    $time1_a \leftarrow t_{ion_b}$

    a ← a + 1

    b ← b + 1

  otherwise

    $time1_a \leftarrow 0.007\mu s$

    a ← a + 1

  time1

$t_{ion8} :=$

ion ← ion8

x ← 0

y ← 0

while x < last(time)

  if $ion_x \le ion_{tol}$

    if y < last(t_{spark})

      if $time_x > t_{spark_y}$

        $t_{ion_y} \leftarrow \dfrac{time_{x-1} \cdot ion_{tol} + time_x \cdot ion_{x-1} - time_x \cdot ion_{tol} - ion_x \cdot time_{x-1}}{ion_{x-1} - ion_x}$

        x ← x + skip

        y ← y + 1

      x ← x + 1 otherwise

    x ← x + 1 otherwise

  x ← x + 1 otherwise

a ← 0

b ← 0

while a < last(t_{spark})

  if $t_{ion_b} < t_{spark_{a+1}}$

    $time1_a \leftarrow t_{ion_b}$

    a ← a + 1

    b ← b + 1

  otherwise

    $time1_a \leftarrow 0.006\mu s$

    a ← a + 1

  time1

Determining Velocities from time and distance

$$v_{12} := \frac{dist_0}{t_{ion2} - t_{ion1}} \quad v_{23} := \frac{dist_1}{t_{ion3} - t_{ion2}} \quad v_{34} := \frac{dist_2}{t_{ion4} - t_{ion3}} \quad v_{45} := \frac{dist_3}{t_{ion5} - t_{ion4}}$$

$$v_{56} := \frac{dist_4}{t_{ion6} - t_{ion5}} \quad v_{67} := \frac{dist_5}{t_{ion7} - t_{ion6}} \quad v_{78} := \frac{dist_6}{t_{ion8} - t_{ion7}}$$

Assign Data to Matrix for Exporting

$$ans_{\langle 0 \rangle} := \frac{t_{spark}}{s} \quad ans_{\langle 1 \rangle} := \frac{t_{ion1}}{s} \quad ans_{\langle 2 \rangle} := \frac{t_{ion2}}{s} \quad ans_{\langle 3 \rangle} := \frac{t_{ion3}}{s} \quad ans_{\langle 4 \rangle} := \frac{t_{ion4}}{s}$$

$$ans_{\langle 5 \rangle} := \frac{t_{ion5}}{s} \quad ans_{\langle 6 \rangle} := \frac{t_{ion6}}{s} \quad ans_{\langle 7 \rangle} := \frac{t_{ion7}}{s} \quad ans_{\langle 8 \rangle} := \frac{t_{ion8}}{s}$$

$$ans_{\langle 9 \rangle} := \frac{v_{12}}{\frac{m}{s}} \quad ans_{\langle 10 \rangle} := \frac{v_{23}}{\frac{m}{s}} \quad ans_{\langle 11 \rangle} := \frac{v_{34}}{\frac{m}{s}} \quad ans_{\langle 12 \rangle} := \frac{v_{45}}{\frac{m}{s}}$$

$$ans_{\langle 13 \rangle} := \frac{v_{56}}{\frac{m}{s}} \quad ans_{\langle 14 \rangle} := \frac{v_{67}}{\frac{m}{s}} \quad ans_{\langle 15 \rangle} := \frac{v_{78}}{\frac{m}{s}}$$

Wavespeed vs. SparkTime

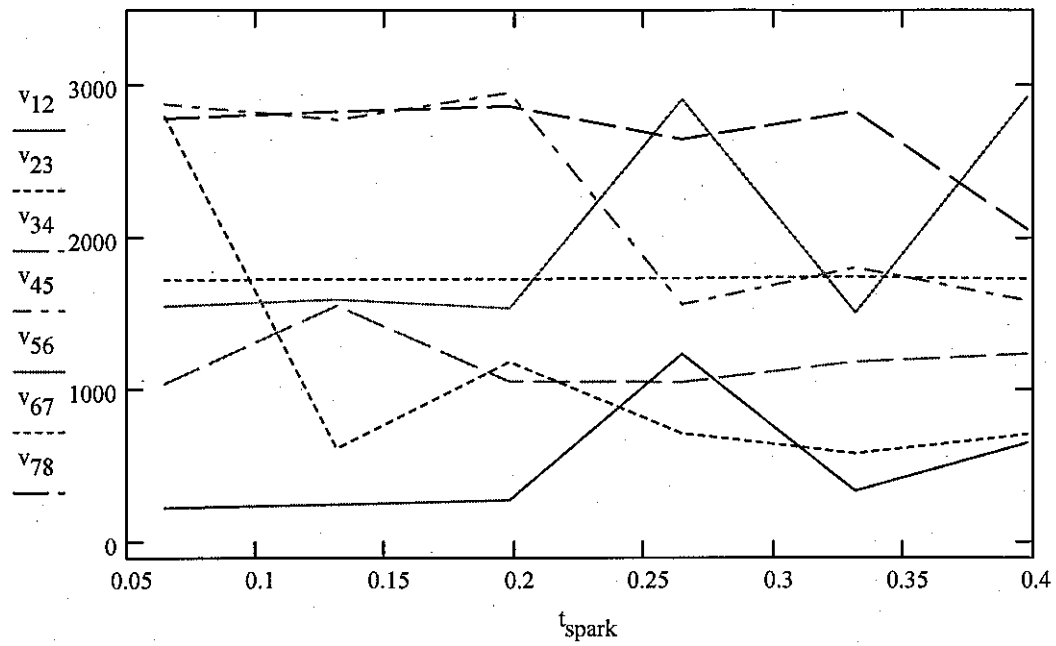

Appendix E. Flash Vaporization System Heat Transfer Calculations

Constants and Unit Conversions

$bar := 14.503773773021psi \qquad kJ := 1000J \qquad MJ := 10^6 J \qquad MPa := 10^6 Pa \qquad kmol := 1000mol$

$R := 8.314\frac{kJ}{mol \cdot K} \qquad \sigma := 5.67 \cdot 10^{-8}\frac{W}{m^2 \cdot K^4}$

Importing surrogate data

$\mu_{surjp8} :=$ ...\mujp8.xls $\qquad k_{surjp8} :=$ ...\kjp8.xls

$\rho_{surjp8} :=$ ...\rojp8.xls $\qquad cp_{surjp8} :=$ ...\cpjp8.xls

6 Dec 04 FN 3.2 H2-AIR EOT

Water volumetric flow

$V_{dottest} := \frac{4L}{7.15min}$

Importing test data

$data :=$ 4-12-6.xls

$T_{amb} := 290K$

$T_{in} := data^{\langle 5 \rangle} \cdot K$

$T_{out} := data^{\langle 6 \rangle} \cdot K$

Max outlet temperature and inlet temperature at same time

$T_{fluidout} := max(T_{out}) \qquad T_{fluidin} := T_{in}|_{match(T_{fluidout}, T_{out})}$

$T_{fluidout} = 512.073\,K \qquad T_{fluidin} = 301.986\,K$

$Time := data^{\langle 0 \rangle} \cdot s$

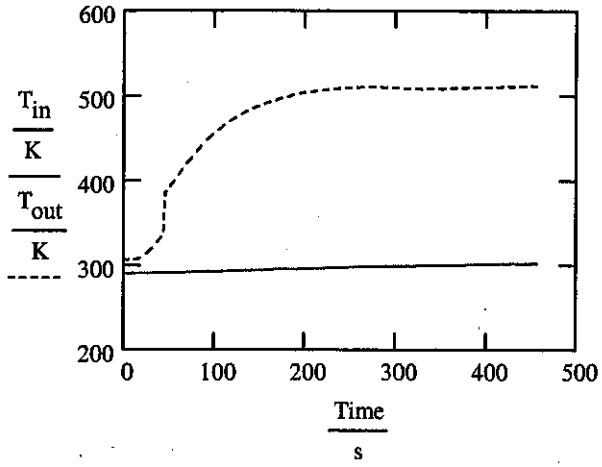

Heat Exchanger Dimensions

$d_{ii} := 2.067in$ $d_{io} := 2.375in$ $l := 30in$ $d_{oi} := 2.635in$ $d_{oo} := 2.875in$

Operating Parameters

$frequency := 10Hz$ $Vol_{tube} := 245in^3$ $FF := 1$ $Tubes := 2$

$P_{atm} := 1atm$ $T_{mix} := 290K$ $\phi := 1.0$

Properties Information

Mass Flow Calculator

Energy Required

Data Analysis

$\rho_{test} := linterp(T_{water}, \rho_{water}, T_{fluidin})$

$m_{dottest} := \rho_{test} \cdot V_{dottest}$

$$HeatTransfer := \left[m_{dottest} \cdot linterp\left[T_{water}, c_{pwater}, \frac{(T_{in} + T_{out})}{2} \right] \cdot ((T_{out} - T_{in})) \right]$$

$m_{dottest} = 0.557 \frac{kg}{min}$

$m_{fdot} = 0.401 \frac{kg}{min}$

$EnergyRequired = 3.211\,kW$

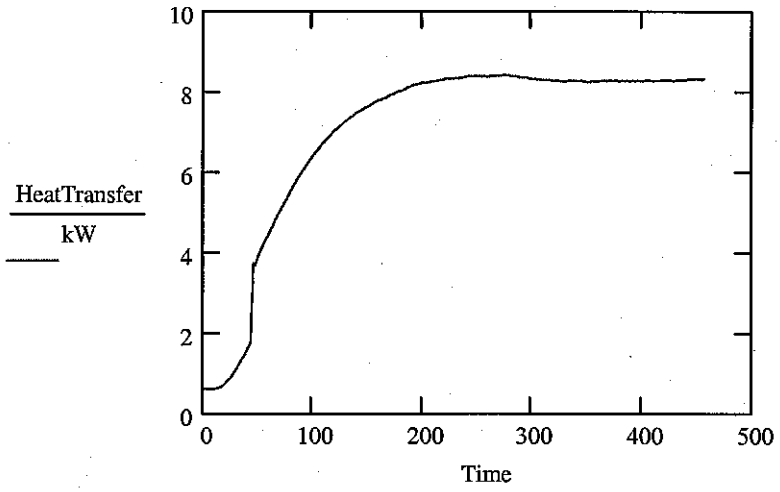

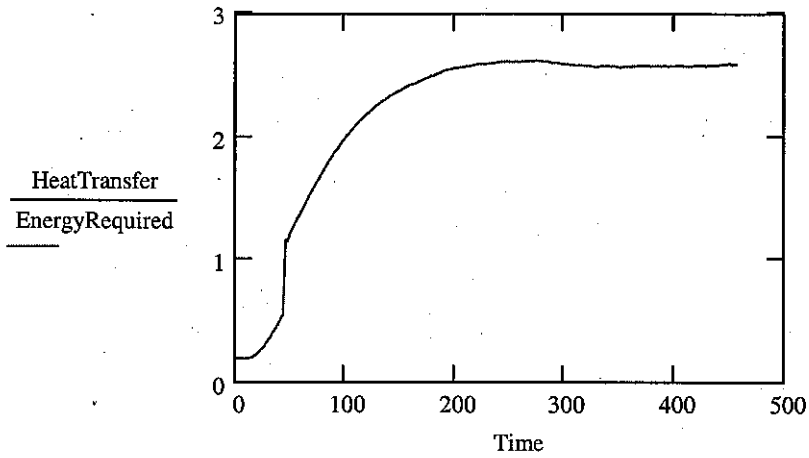

Data Analysis

10 Dec 04 FN 2.4 H2-AIR BOT

$V_{dottest} := \frac{4L}{12min}$

data :=
4-12-10.xls

$T_{amb} := 290K$

$T_{in} := data^{\langle 9 \rangle} \cdot K$

$T_{out} := data^{\langle 10 \rangle} \cdot K$

$T_{fluidout} := \max(T_{out})$ $T_{fluidin} := T_{in}\left|_{match(T_{fluidout}, T_{out})}\right.$

$T_{fluidout} = 531.207\ K$ $T_{fluidin} = 291.961\ K$

$Time := data^{\langle 0 \rangle} \cdot s$

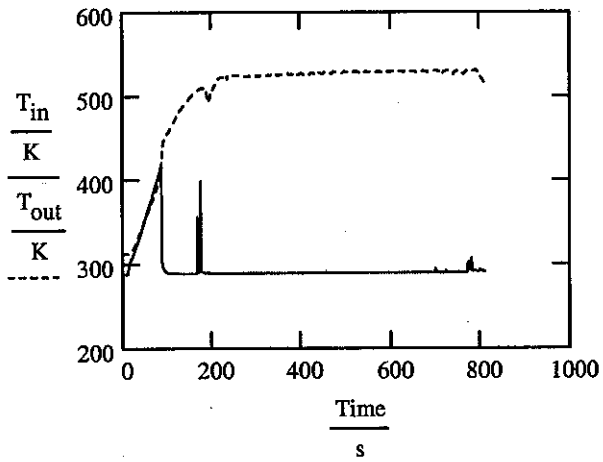

$d_{ii} := 2.067in$ $d_{io} := 2.375in$ $l := 30in$ $d_{oi} := 2.635in$ $d_{oo} := 2.875in$

$frequency := 10Hz$ $Vol_{tube} := 245in^3$ $FF := 1$

$Tubes := 2$ $P_{atm} := 1atm$ $T_{mix} := 290K$ $\phi := 1.0$

▶ Properties

▶ Mass Flow Calculator

▶ Energy Required

$\rho_{test} := \text{linterp}(T_{water}, \rho_{water}, T_{fluidin})$

$m_{dottest} := \rho_{test} \cdot V_{dottest}$

$$\overrightarrow{\text{HeatTransfer} := \left[m_{dottest} \cdot \text{linterp}\left[T_{water}, c_{pwater}, \frac{(T_{in} + T_{out})}{2} \right] \cdot \left((T_{out} - T_{in}) \right) \right]}$$

$m_{dottest} = 0.333 \frac{kg}{min}$

$m_{fdot} = 0.401 \frac{kg}{min}$

EnergyRequired = 3.693 kW

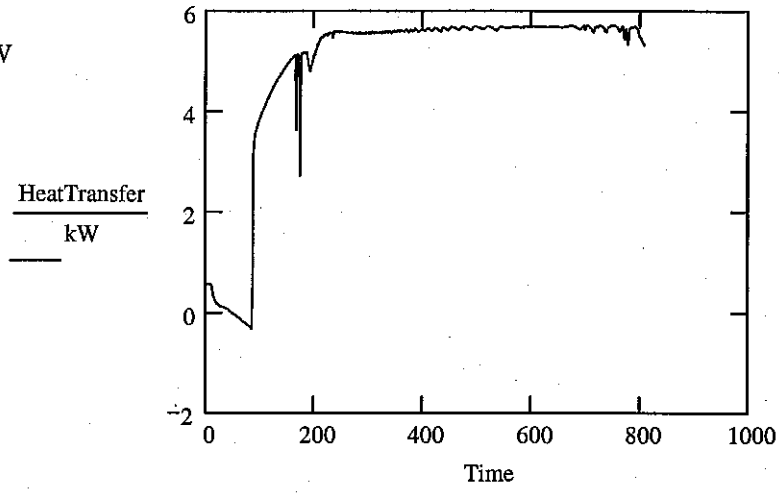

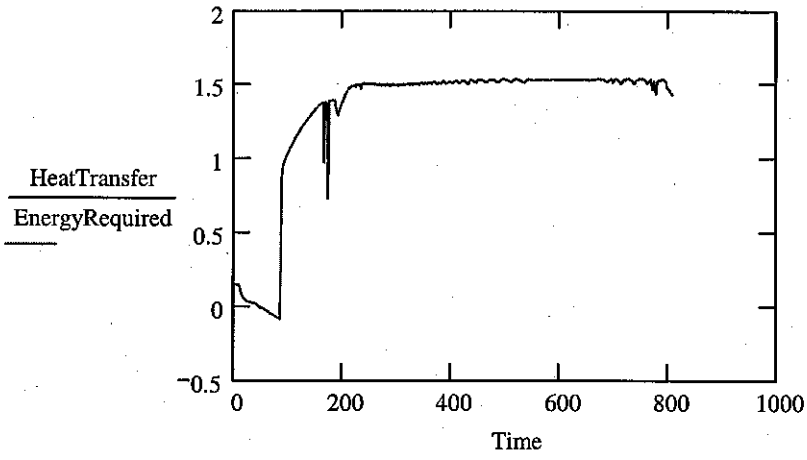

5-1-12 Avgas-H20 phi 1.04-1.1 15hz .837kgmin

data :=

5-1-12.xls

$T_{amb} := 290K$

$T_{in} := data^{\langle 4 \rangle} \cdot K$

$T_{out} := data^{\langle 5 \rangle} \cdot K$

$T_{fluidout} := \max(T_{out})$ $T_{fluidin} := T_{in}|_{match(T_{fluidout}, T_{out})0}$

$T_{fluidout} = 546.773\,K$ $T_{fluidin} = 296.349\,K$

$Time := data^{\langle 0 \rangle} \cdot s$

$m_{dottest} := .837 \cdot \frac{kg}{min}$

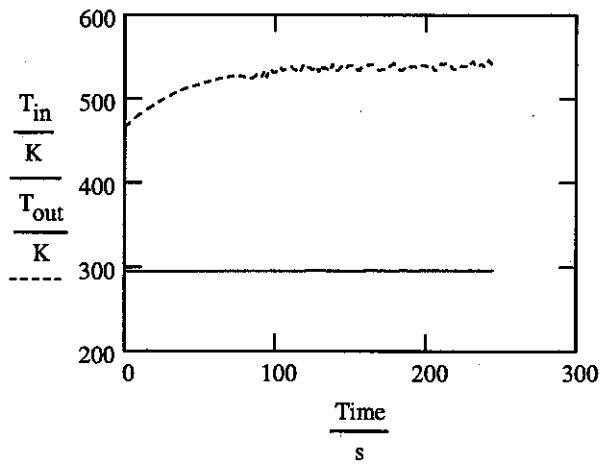

$d_{ii} := 2.067in$ $d_{io} := 2.375in$ $l := 30in$ $d_{oi} := 2.635in$ $d_{oo} := 2.875in$

frequency := 15Hz $Vol_{tube} := 245in^3$ $FF := 1$ $Tubes := 2$ $P_{atm} := 1atm$ $\phi := mean(data^{\langle 1 \rangle})$

$T_{heatedair} := linterp\left[\begin{pmatrix} -459.67 \\ 1340.33 \end{pmatrix}, \begin{pmatrix} 0 \\ 1000 \end{pmatrix} K, 120\right]$ $T_{mix} := \frac{T_{heatedair} \cdot 15 + T_{fluidin} \cdot 1}{16}$

Properties

Mass Flow Calculator

Energy Required

$$\text{HeatTransfer} := \overrightarrow{\left[m_{dottest} \cdot \text{linterp}\left[T_{water}, c_{pwater}, \frac{(T_{in} + T_{out})}{2} \right] \cdot \left((T_{out} - T_{in}) \right) \right]}$$

$$m_{dottest} = 0.837 \frac{kg}{min}$$

$$m_{fdot} = 0.582 \frac{kg}{min}$$

$$\text{EnergyRequired} = 5.693\,kW$$

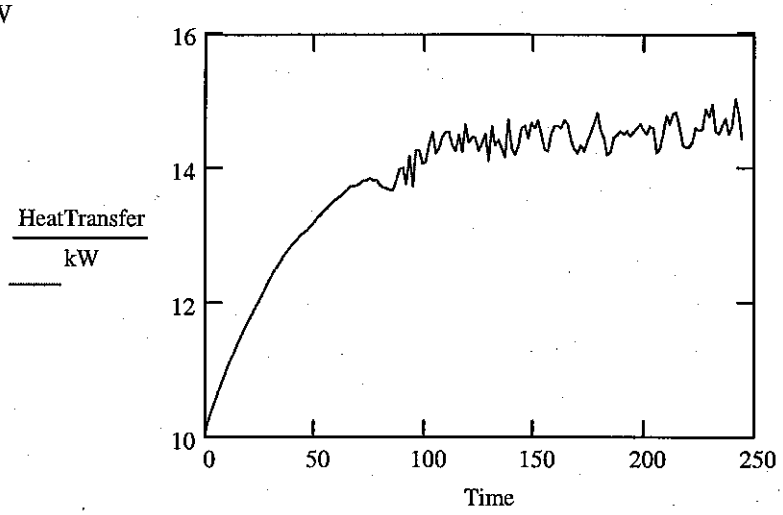

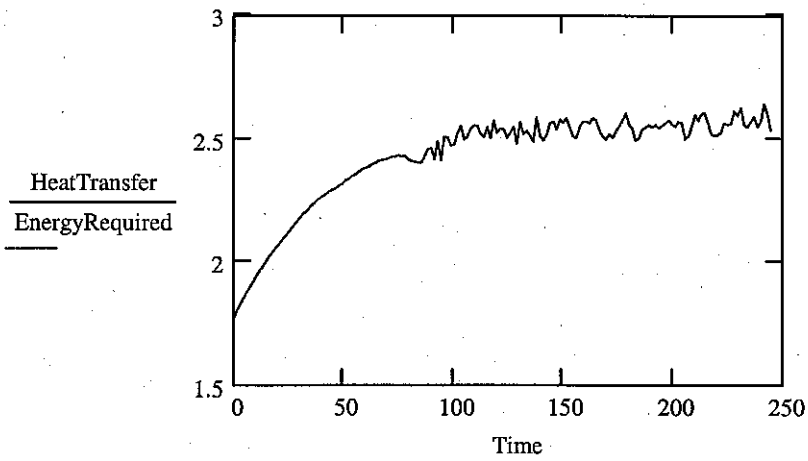

5-1-26 Avgas-H20 phi 1.05-1.1 15hz 1.154lbmin

data :=

5-1-26 1.xls

$T_{amb} := 290K$

$T_{in} := data^{\langle 8 \rangle} \cdot K$

$T_{out} := data^{\langle 9 \rangle} \cdot K$

$T_{fluidout} := \max(T_{out})$ $T_{fluidin} := T_{in}|_{match(T_{fluidout}, T_{out})0}$

$T_{fluidout} = 479.581\,K$ $T_{fluidin} = 289.086\,K$

$Time := data^{\langle 0 \rangle} \cdot s$

$m_{dottest} := 1.154 \cdot \frac{lb}{min}$

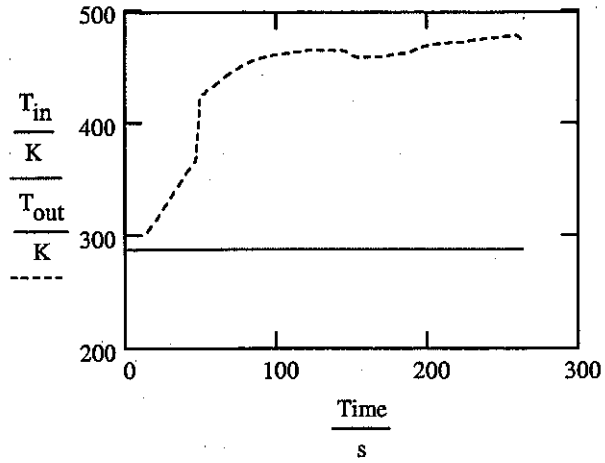

$d_{ii} := 2.067in$ $d_{io} := 2.375in$ $l := 15in$ $d_{oi} := 2.635in$ $d_{oo} := 2.875in$

$frequency := 15Hz$ $Vol_{tube} := 245in^3$ $FF := 1$ $Tubes := 2$ $P_{atm} := 1atm$ $\phi := 1.0$

$T_{air} := linterp\left[\begin{pmatrix} -459.67 \\ 1340.33 \end{pmatrix}, \begin{pmatrix} 0 \\ 1000 \end{pmatrix} K, 120\right]$ $T_{mix} := \frac{T_{air} \cdot 15 + T_{fluidin} \cdot 1}{16}$ $T_{mix} = 319.979\,K$

Properties

Mass Flow Calculator

Energy Required

$$\overrightarrow{\text{HeatTransfer} := \left[m_{dottest} \cdot \text{linterp}\left[T_{water}, c_{pwater}, \frac{(T_{in} + T_{out})}{2} \right] \cdot \left((T_{out} - T_{in}) \right) \right]}$$

$$m_{dottest} = 0.523 \frac{kg}{min}$$

$$m_{fdot} = 0.572 \frac{kg}{min}$$

EnergyRequired = 3.998 kW

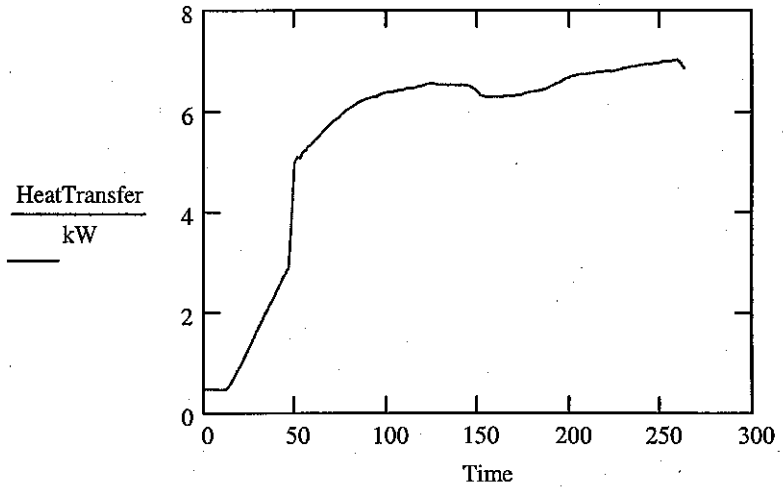

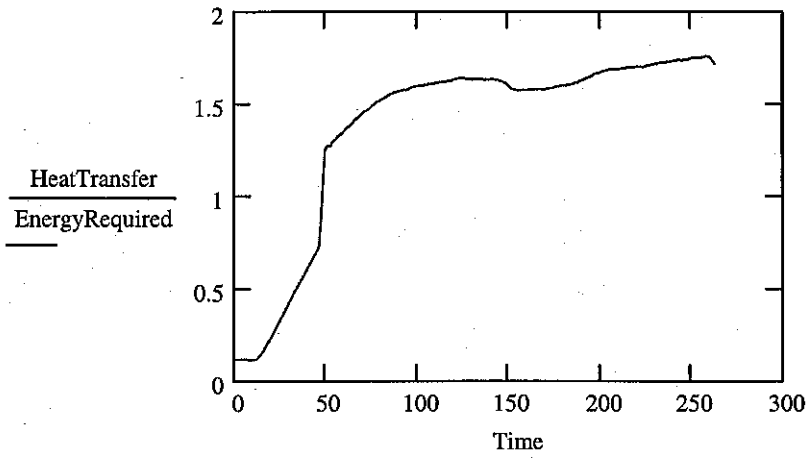

5-1-26 Avgas-H20 phi 1.05-1.1 15hz .802 lbmin

data :=

5-1-26 2.xls

$T_{amb} := 290K$

$T_{in} := data^{\langle 8 \rangle} \cdot K$

$T_{out} := data^{\langle 9 \rangle} \cdot K$

$T_{fluidout} := \max(T_{out})$ $T_{fluidin} := T_{in}\left|_{match(T_{fluidout}, T_{out})0}\right.$

$T_{fluidout} = 538.763\,K$ $T_{fluidin} = 290.763\,K$

$Time := data^{\langle 0 \rangle} \cdot s$

$m_{dottest} := .802 \cdot \frac{lb}{min}$

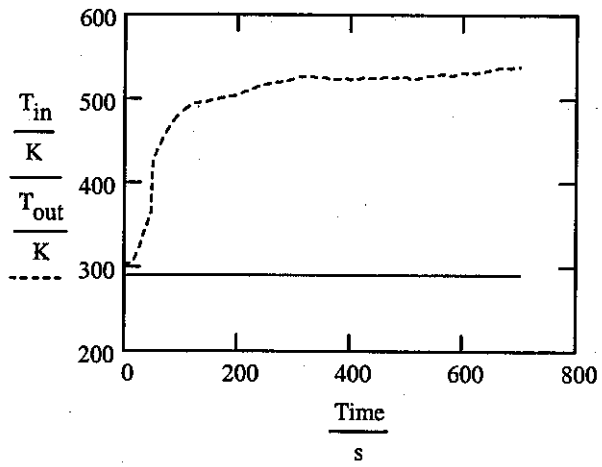

$d_{ii} := 2.067in$ $d_{io} := 2.375in$ $l := 15in$ $d_{oi} := 2.635in$ $d_{oo} := 2.875in$

frequency := 15Hz $Vol_{tube} := 245in^3$ $FF := 1$ $Tubes := 2$ $P_{atm} := 1atm$ $\phi := 1.05$

$T_{air} := linterp\left[\begin{pmatrix} -459.67 \\ 1340.33 \end{pmatrix}, \begin{pmatrix} 0 \\ 1000 \end{pmatrix} K, 120\right]$ $T_{mix} := \frac{T_{air} \cdot 15 + T_{fluidin} \cdot 1}{16}$ $T_{mix} = 320.084\,K$

▶ Properties

▶ Mass Flow Calculator

▶ Energy Required

$$\overrightarrow{\text{HeatTransfer} := \left[m_{dottest} \cdot \text{linterp}\left[T_{water}, c_{pwater}, \frac{(T_{in} + T_{out})}{2} \right] \cdot ((T_{out} - T_{in})) \right]}$$

$$m_{dottest} = 0.364 \frac{kg}{min}$$

$$m_{fdot} = 0.572 \frac{kg}{min}$$

EnergyRequired = 5.478 kW

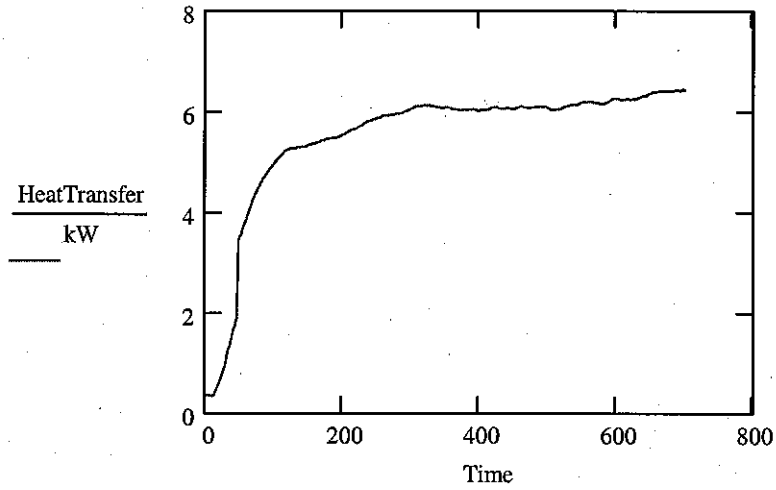

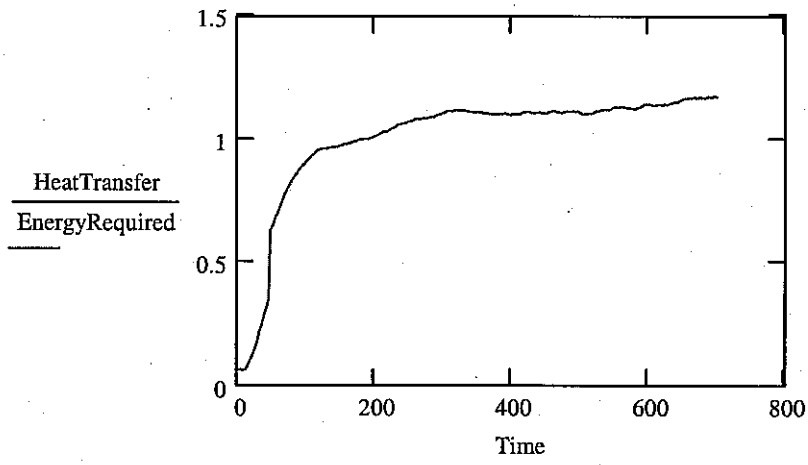

5-2-1 JP8-JP8

data :=

5-2-1.xls

$T_{amb} := 290K$

$T_{in} := data^{\langle 28 \rangle} \cdot K$

$T_{out} := data^{\langle 29 \rangle} \cdot K$

$T_{fluidout} := \max(T_{out})$ $\quad T_{fluidin} := T_{in}\left|_{match(T_{fluidout}, T_{out})0}\right.$

$T_{fluidout} = 632.054\,K$ $\quad T_{fluidin} = 291.548\,K$

$m_{flowmeter} := data^{\langle 33 \rangle} \cdot \frac{lb}{min}$ $\quad T_{fuelinlet} := data^{\langle 30 \rangle} \cdot K$

$\Delta P := \left(data^{\langle 35 \rangle} - data^{\langle 34 \rangle}\right) \cdot psi$

$Time := data^{\langle 0 \rangle} \cdot s$

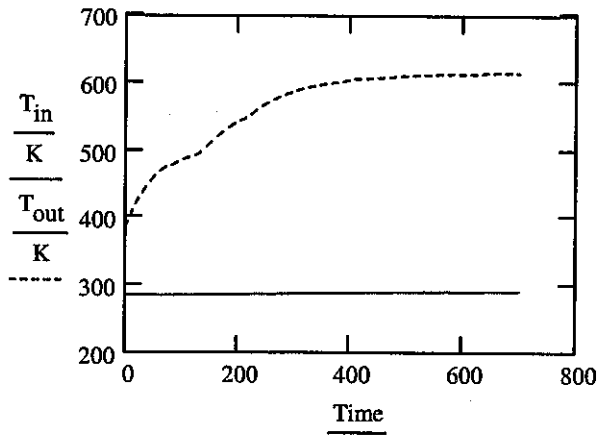

$d_{ii} := 2.067in$ $\quad d_{io} := 2.375in$ $\quad l := 15in$ $\quad d_{oi} := 2.635in$ $\quad d_{oo} := 2.875in$

$frequency := linterp\left[\begin{pmatrix} 9.65 \\ 13.17 \\ 16.7 \end{pmatrix}, \begin{pmatrix} 10 \\ 15 \\ 20 \end{pmatrix}, 10.65\right] Hz$ $\quad Vol_{tube} := 245in^3$ $\quad FF := 1$ $\quad Tubes := 2$

$P_{atm} := 1atm$ $\quad \phi := 1.05$

$T_{air} := linterp\left[\begin{pmatrix} -459.67 \\ 1340.33 \end{pmatrix}, \begin{pmatrix} 0 \\ 1000 \end{pmatrix} K, 250\right]$ $\quad T_{mix} := \frac{T_{air} \cdot 15 + T_{fluidin} \cdot 1}{16}$ $\quad T_{mix} = 387.842\,K$

▶ Properties

▶ Mass Flow Calculator

▶ Energy Required

$$\overrightarrow{\text{HeatTransfer} := \left[m_{fdot} \cdot \text{linterp}\left[T_{sur}, c_{psur}, \frac{(T_{in} + T_{out})}{2} \right] \cdot \left((T_{out} - T_{in}) \right) \right]}$$

$$m_{fdot} = 0.355 \frac{kg}{min}$$

EnergyRequired = 5.073 kW

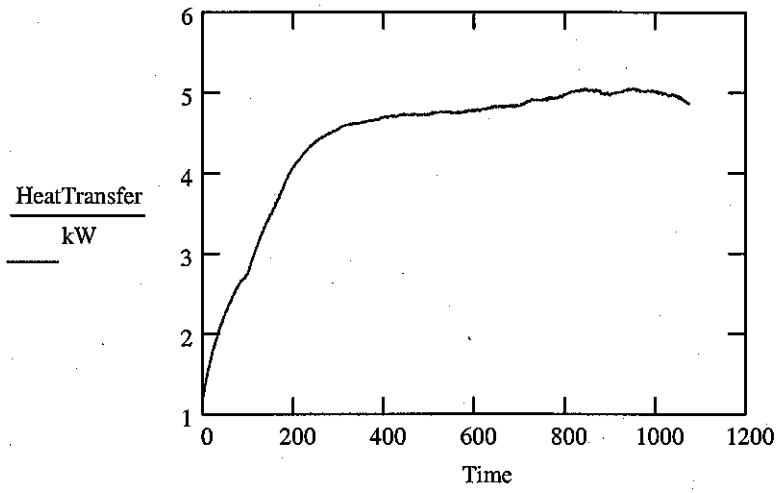

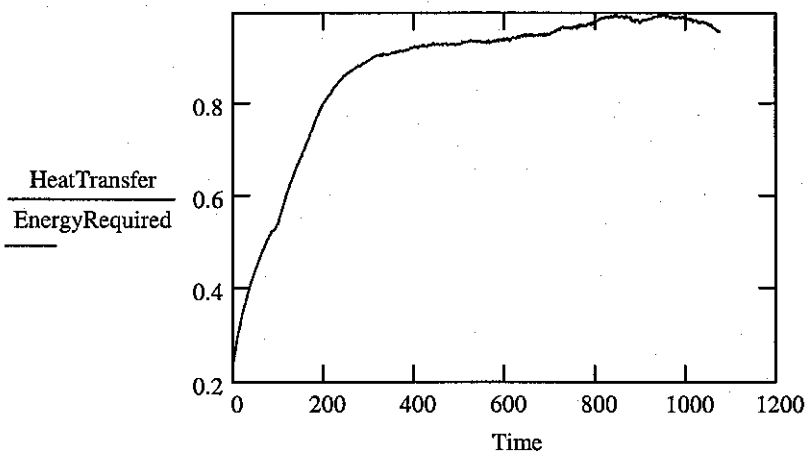

$$\rho_{surr} := \text{linterp}\left(T_{sur}, \rho_{sur}, T_{fuelinlet}\right)$$

$$hi := 20$$

$$lo := 10$$

$$avg := hi - lo + 1$$

CRC density data used for FN calibration

$$\rho_{CRC} := \begin{pmatrix} 805\,\frac{kg}{m^3} \\ 760\,\frac{kg}{m^3} \end{pmatrix} \qquad T_{CRC} := \begin{pmatrix} 293 \\ 358 \end{pmatrix} \cdot K$$

$$\text{linterp}\left(T_{CRC}, \rho_{CRC}, \frac{\sum_{i=lo}^{hi} T_{out_i}}{avg}\right) = 710.775\,\frac{kg}{m^3}$$

$$FN := \frac{\frac{\sum_{i=lo}^{hi} m_{flowmeter_i}}{avg}}{\sqrt{\frac{\sum_{i=lo}^{hi} \Delta P_i}{avg}} \cdot \sqrt{\text{linterp}\left(T_{CRC}, \rho_{CRC}, \frac{\sum_{i=lo}^{hi} T_{out_i}}{avg}\right)}} \qquad FN = 0.0000001478\,m^2$$

Given

$$FN_{xx} = \frac{m_{dotxx}}{\sqrt{dp_{xx}} \cdot \sqrt{\rho_{xx}}}$$

$$\text{Find}\left(\rho_{xx}\right) \rightarrow \frac{m_{dotxx}^{\ 2}}{dp_{xx} \cdot FN_{xx}^{\ 2}}$$

$$\rho_{calc} := \frac{\overrightarrow{m_{flowmeter}^{\ 2}}}{\Delta P \cdot FN^2}$$

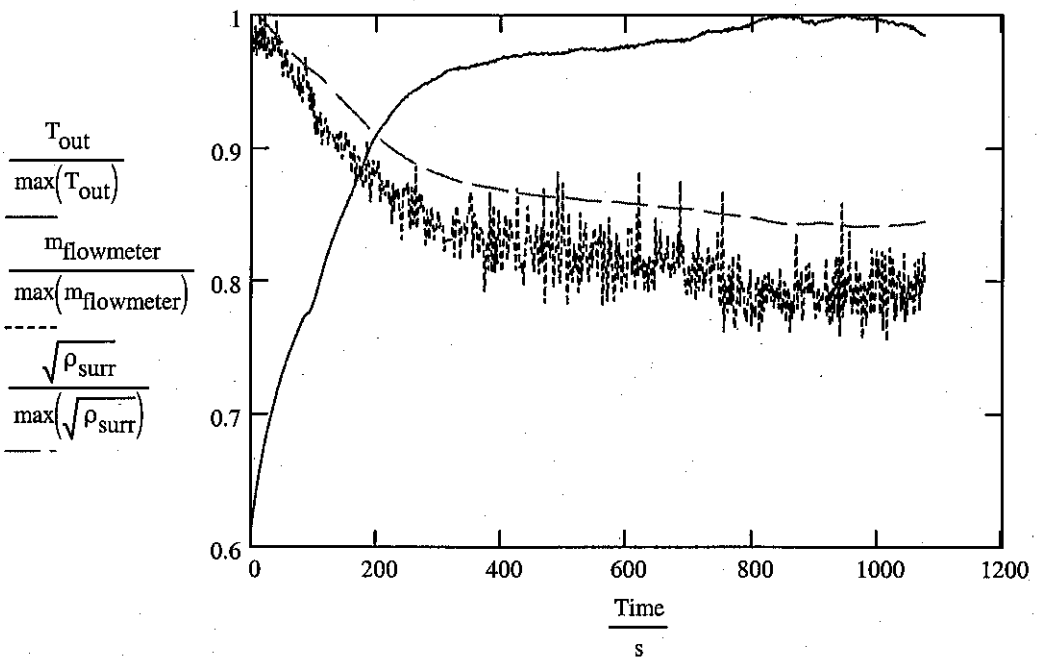
$\frac{T_{out}}{max(T_{out})}$
$\frac{m_{flowmeter}}{max(m_{flowmeter})}$
$\frac{\sqrt{\rho_{surr}}}{max(\sqrt{\rho_{surr}})}$
1
0.9
0.8
0.7
0.6
0
200
400
600
800
1000
1200
Time
s

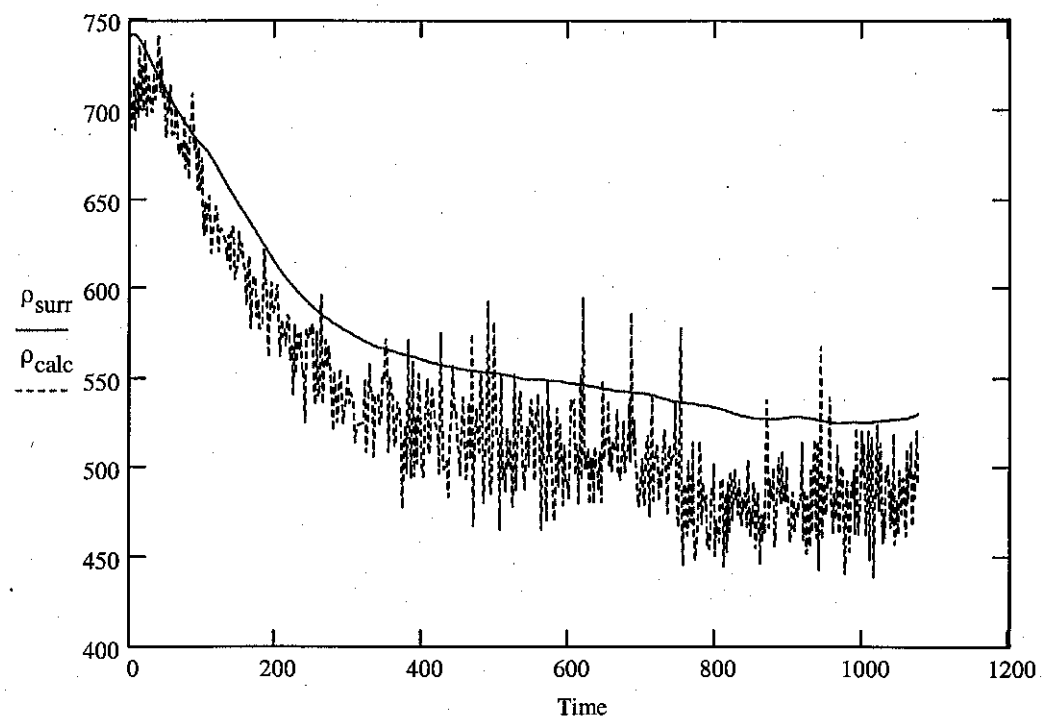
$\frac{\rho_{surr}}{\rho_{calc}}$
750
700
650
600
550
500
450
400
0
200
400
600
800
1000
1200
Time

5-2-3 JP8-JP8

data :=

5-2-3.xls

$T_{amb} := 290K$

$T_{in} := data^{\langle 11 \rangle} \cdot K$

$T_{out} := data^{\langle 14 \rangle} \cdot K$

$T_{fluidout} := \max(T_{out})$ $T_{fluidin} := T_{in}\left|_{match(T_{fluidout}, T_{out})0}\right.$

$T_{fluidout} = 705.424\,K$ $T_{fluidin} = 285.972\,K$

$m_{flowmeter} := data^{\langle 17 \rangle} \cdot \frac{lb}{min}$ $T_{fuelinlet} := data^{\langle 13 \rangle} \cdot K$

$\Delta P := \left(data^{\langle 23 \rangle} - data^{\langle 22 \rangle}\right) \cdot psi$

$Time := data^{\langle 0 \rangle} \cdot s$

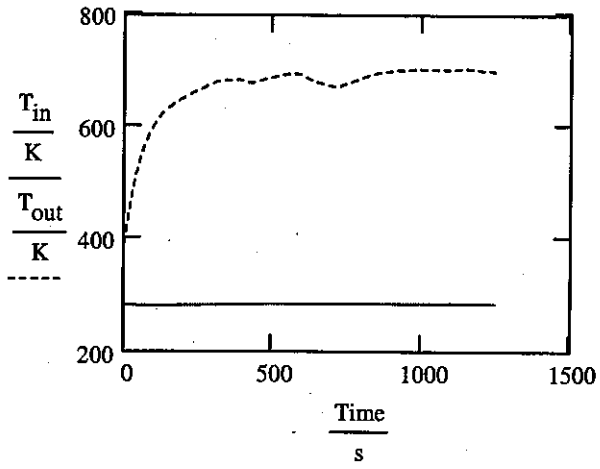

$d_{ii} := 2.067in$ $d_{io} := 2.375in$ $l := 15in$ $d_{oi} := 2.635in$ $d_{oo} := 2.875in$

$frequency := 13.88Hz$ $Vol_{tube} := 245in^3$ $FF := 1$ $Tubes := 2$ $P_{atm} := 1atm$ $\phi := 1.00$

$T_{air} := linterp\left[\begin{pmatrix} -459.67 \\ 1340.33 \end{pmatrix}, \begin{pmatrix} 0 \\ 1000 \end{pmatrix} K, 250\right]$ $T_{mix} := \frac{T_{air} \cdot 15 + T_{fluidin} \cdot 1}{16}$ $T_{mix} = 387.493\,K$

Properties

Mass Flow Calculator

Energy Required

$$\text{HeatTransfer} := \overrightarrow{\left[m_{fdot} \cdot \text{linterp}\left[T_{sur}, c_{psur}, \frac{(T_{in} + T_{out})}{2} \right] \cdot \left((T_{out} - T_{in}) \right) \right]}$$

$$m_{fdot} = 0.906 \frac{lb}{min}$$

EnergyRequired = 7.633 kW

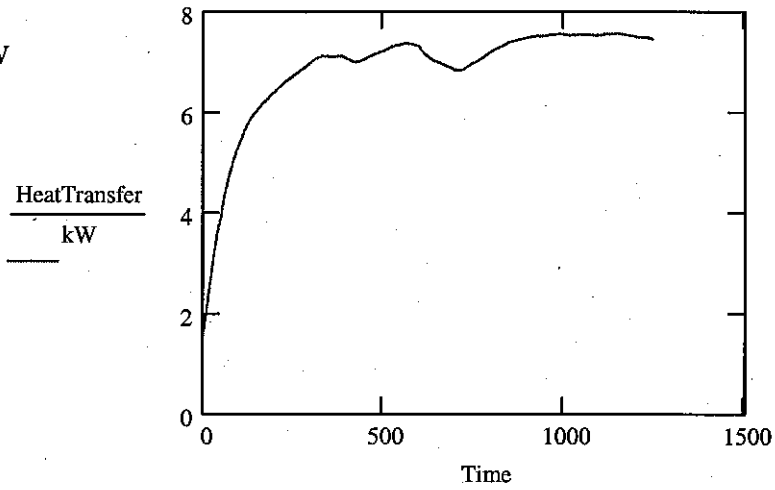

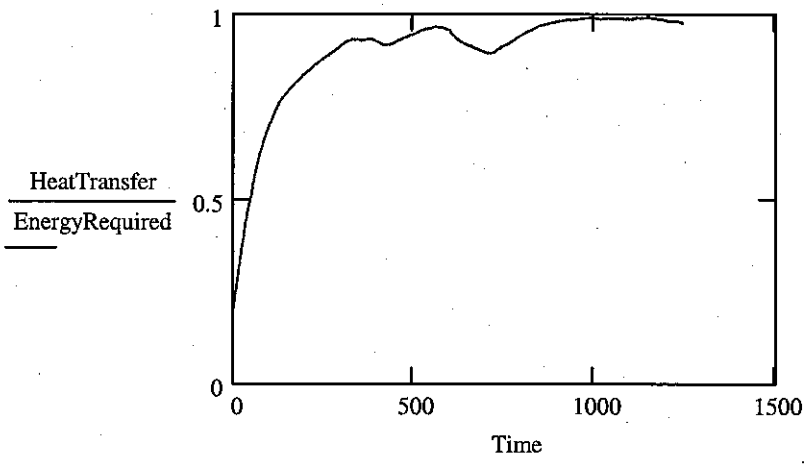

$\rho_{surr} := \text{linterp}(T_{sur}, \rho_{sur}, T_{fuelinlet})$

$hi := 20$

$lo := 10$

$avg := hi - lo + 1$

CRC density data used for FN calibration

$$\rho_{CRC} := \begin{pmatrix} 805\,\frac{kg}{m^3} \\ 760\,\frac{kg}{m^3} \end{pmatrix} \qquad T_{CRC} := \begin{pmatrix} 293 \\ 358 \end{pmatrix} \cdot K$$

$$\text{linterp}\left(T_{CRC}, \rho_{CRC}, \frac{\sum_{i=lo}^{hi} T_{out_i}}{avg}\right) = 684.799\,\frac{kg}{m^3}$$

$$FN := \frac{\frac{\sum_{i=lo}^{hi} m_{flowmeter_i}}{avg}}{\sqrt{\frac{\sum_{i=lo}^{hi} \Delta P_i}{avg}} \cdot \sqrt{\text{linterp}\left(T_{CRC}, \rho_{CRC}, \frac{\sum_{i=lo}^{hi} T_{out_i}}{avg}\right)}} \qquad FN = 0.0000001512\,m^2$$

Given

$$FN_{xx} = \frac{m_{dotxx}}{\sqrt{dp_{xx}} \cdot \sqrt{\rho_{xx}}}$$

$$\text{Find}(\rho_{xx}) \rightarrow \frac{m_{dotxx}^{\ 2}}{dp_{xx} \cdot FN_{xx}^{\ 2}}$$

$$\rho_{calc} := \frac{\overrightarrow{m_{flowmeter}^{\ 2}}}{\Delta P \cdot FN^2}$$

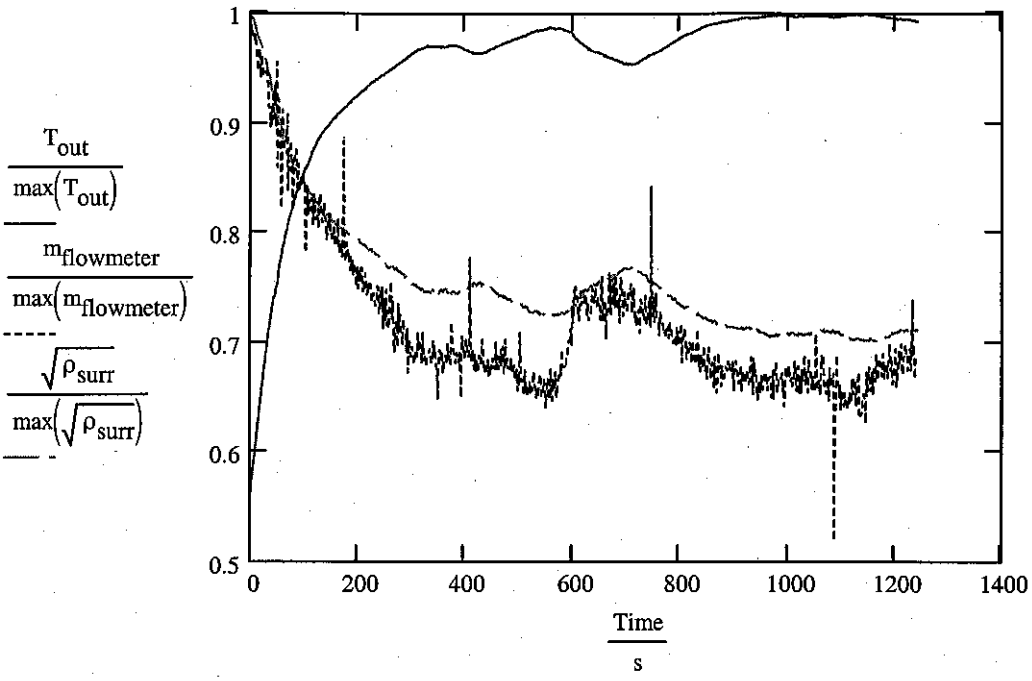
$\frac{T_{out}}{\max(T_{out})}$
$\frac{m_{flowmeter}}{\max(m_{flowmeter})}$
$\frac{\sqrt{\rho_{surr}}}{\max(\sqrt{\rho_{surr}})}$
1
0.9
0.8
0.7
0.6
0.5
0
200
400
600
800
1000
1200
1400
Time
s

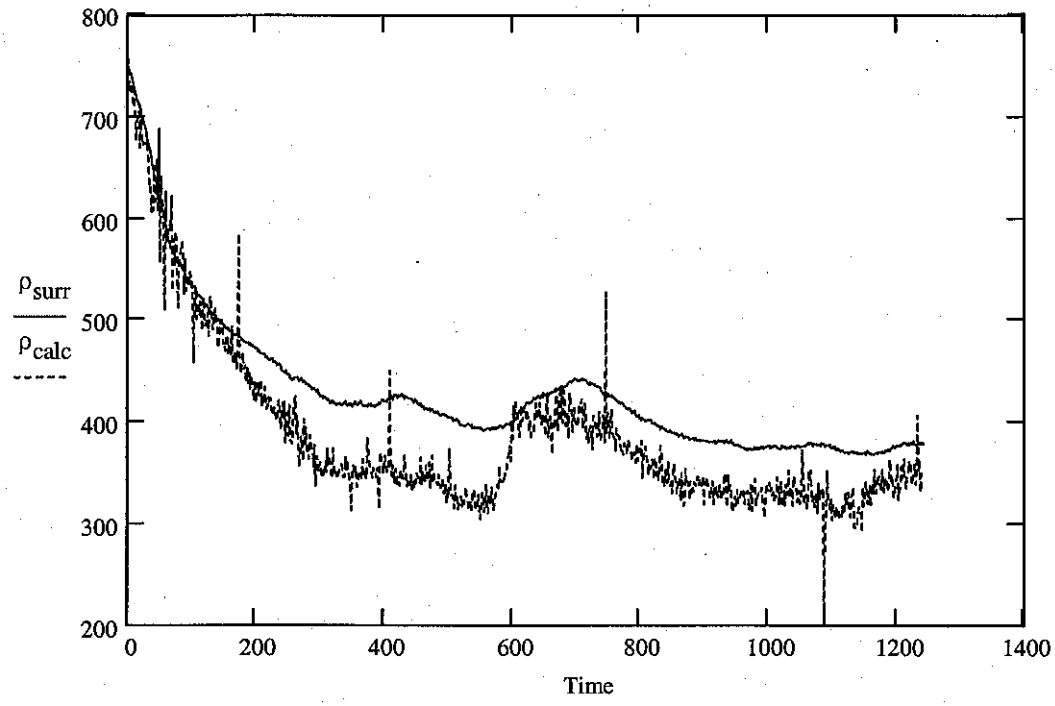
$\frac{\rho_{surr}}{\rho_{calc}}$
800
700
600
500
400
300
200
0
200
400
600
800
1000
1200
1400
Time

5-2-4 JP8-JP8

data :=

5-2-4.xls

$T_{amb} := 290K$

$T_{in} := data^{\langle 15 \rangle} \cdot K$

$T_{out} := data^{\langle 16 \rangle} \cdot K$

$T_{fluidout} := \max(T_{out})$ $T_{fluidin} := T_{in}\left|_{match(T_{fluidout}, T_{out})0}\right.$

$T_{fluidout} = 769.571\,K$ $T_{fluidin} = 293.244\,K$

$m_{flowmeter} := data^{\langle 12 \rangle} \cdot \frac{kg}{min}$ $T_{fuelinlet} := data^{\langle 17 \rangle} \cdot K$

$\Delta P := \left(data^{\langle 6 \rangle} - data^{\langle 5 \rangle}\right) \cdot psi$

$Time := data^{\langle 0 \rangle} \cdot s$

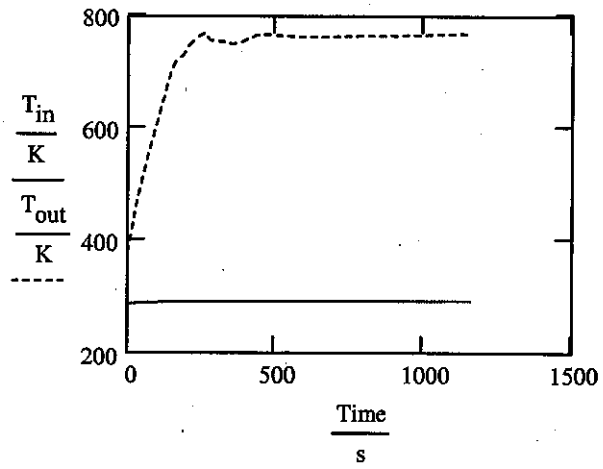

$d_{ii} := 2.067in$ $d_{io} := 2.375in$ $l := 30in$ $d_{oi} := 2.635in$ $d_{oo} := 2.875in$

$frequency := 12Hz$ $Vol_{tube} := 245in^3$ $FF := 1$ $Tubes := 2$

$P_{atm} := 1atm$ $\phi := 1.00$

$T_{air} := linterp\left[\begin{pmatrix} -459.67 \\ 1340.33 \end{pmatrix}, \begin{pmatrix} 0 \\ 1000 \end{pmatrix} K, 250\right]$ $T_{mix} := \frac{T_{air} \cdot 15 + T_{fluidin} \cdot 1}{16}$ $T_{mix} = 387.948\,K$

Properties

Mass Flow Calculator

Energy Required

$$\text{HeatTransfer} := \overrightarrow{\left[m_{fdot} \cdot \text{linterp}\left[T_{sur}, c_{psur}, \frac{(T_{in} + T_{out})}{2} \right] \cdot \left((T_{out} - T_{in}) \right) \right]}$$

$$m_{fdot} = 0.783 \frac{lb}{min}$$

EnergyRequired = 7.985 kW

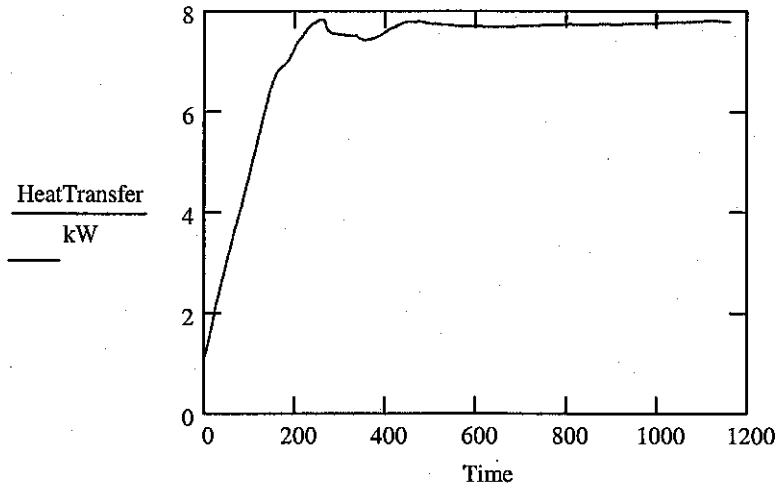

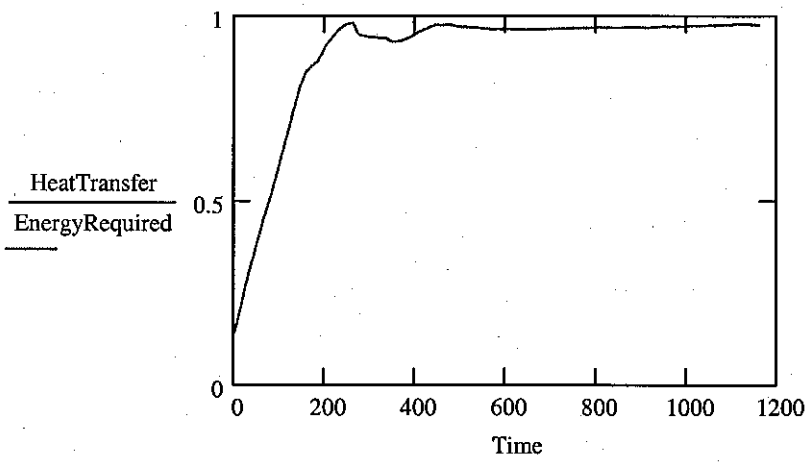

$\rho_{surr} := \text{linterp}(T_{sur}, \rho_{sur}, T_{fuelinlet})$

$hi := 20$

$lo := 10$

$avg := hi - lo + 1$

CRC density data used for FN calibration

$$\rho_{CRC} := \begin{pmatrix} 805 \frac{kg}{m^3} \\ 760 \frac{kg}{m^3} \end{pmatrix} \qquad T_{CRC} := \begin{pmatrix} 293 \\ 358 \end{pmatrix} \cdot K$$

$$\text{linterp}\left(T_{CRC}, \rho_{CRC}, \frac{\sum_{i=lo}^{hi} T_{out_i}}{avg}\right) = 699.549 \frac{kg}{m^3}$$

$$FN := \frac{\frac{\sum_{i=lo}^{hi} m_{flowmeter_i}}{avg}}{\sqrt{\frac{\sum_{i=lo}^{hi} \Delta P_i}{avg}} \cdot \sqrt{\text{linterp}\left(T_{CRC}, \rho_{CRC}, \frac{\sum_{i=lo}^{hi} T_{out_i}}{avg}\right)}} \qquad FN = 0.0000002021\, m^2$$

Given

$$FN_{xx} = \frac{m_{dotxx}}{\sqrt{dp_{xx}} \cdot \sqrt{\rho_{xx}}}$$

$$\text{Find}(\rho_{xx}) \rightarrow \frac{m_{dotxx}^{\ 2}}{dp_{xx} \cdot FN_{xx}^{\ 2}}$$

$$\rho_{calc} := \overrightarrow{\frac{m_{flowmeter}^{\ 2}}{\Delta P \cdot FN^2}}$$

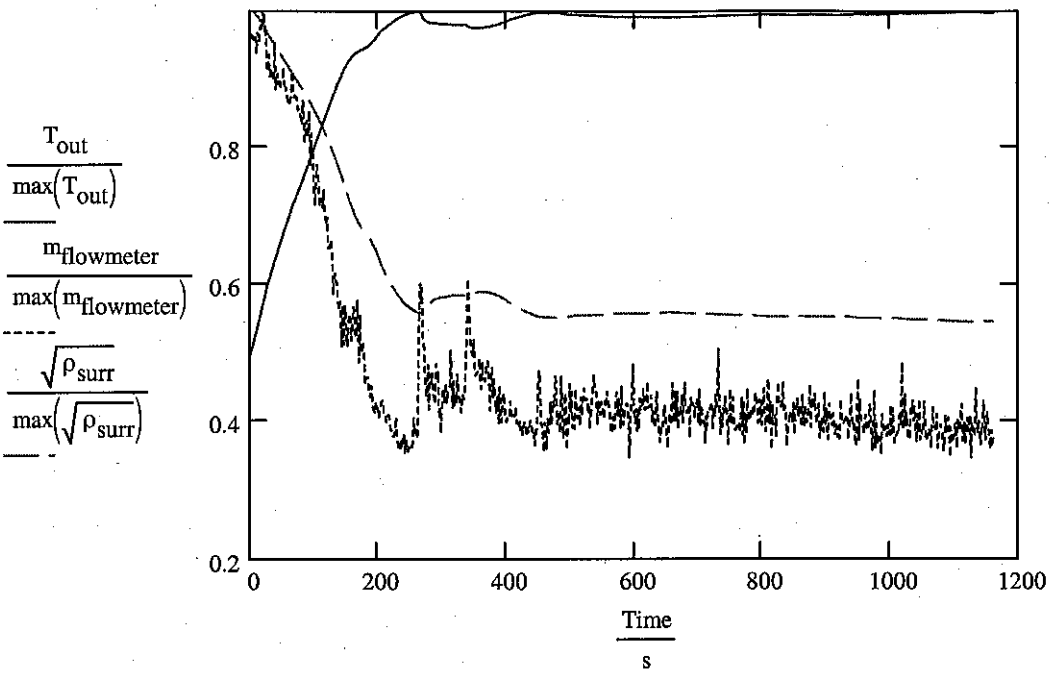
$\frac{T_{out}}{\max(T_{out})}$
$\frac{m_{flowmeter}}{\max(m_{flowmeter})}$
$\frac{\sqrt{\rho_{surr}}}{\max(\sqrt{\rho_{surr}})}$
0.8
0.6
0.4
0.2
0
200
400
600
800
1000
1200
Time
s

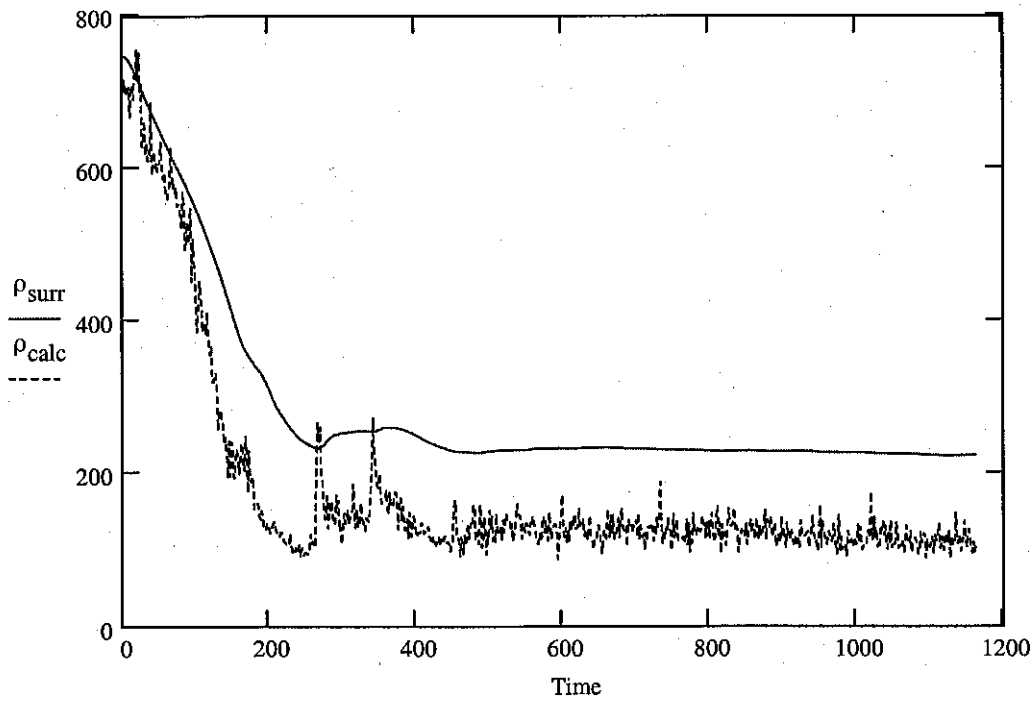
$\frac{\rho_{surr}}{\rho_{calc}}$
800
600
400
200
0
0
200
400
600
800
1000
1200
Time

Bibliography

1. Hoffman, N. *Reaction Propulsion by Intermittent Detonative Combustion.* German Ministry of Supply, AI152365 Volkenrode Translation. 1940.

2. Eidelman, S., Grossman, W., Lottati I. *Review of Propulsion Applications and Numerical Simulations of the Pulsed Detonation Engine Concept.* Journal of Propulsion, Vol. 7, No. 6, Nov-Dec 1991.

3. Kailasanath, K. *Recent Developments in the Research on Pulse Detonation Engines.* AIAA Journal. Vol. 41, No. 2, February 2003.

4. Tucker, K.C., King, P.I., Bradley, R.P., Schauer, F.R. *The Use of Flash Vaporization System with Liquid Hydrocarbon Fuels in a Pulse Detonation Engine.* AIAA 2004-0868. 2004.

5. Radulescu, M.I., Morris, C.I., Hanson, R.K. The Effect of Wall Heat Loss on the Flow Fields in a Pulse-Detonation Wave Engine. AIAA-2004-1124. 42nd Aerospace Sciences Meeting and Exhibit. 5-8 January 2004, Reno, NV.

6. Hoke, J.L., Bradley, R.P., Schauer, F.R. Heat Transfer and Thermal Management in a Pulsed Detonation Engine. AIAA-2003-0852. 41st AIAA Aerospace Sciences. 6-9 January 2003, Reno, NV.

7. Hoke, J.L., Bradley, R.P., Schauer, F.R. *Impact of DDT Mechanism, combustion Wave speed, Temperature, and Charge Quality on Pulsed-Detonation-Engine Performance.* AIAA 2005-1342, 43rd AIAA Aerospace Sciences Meeting, 10-13 January 2005, Reno, NV.

8. Eidelman, S., Sharov, D., Book, D. Aerothermodynamics of Pulsed Detonation Engines. AIAA-2000-3892. 36th AIAA/ASME/SAE/ASEE Joint Propulsion Conference and Exhibit. 16-19 July 2000. Huntsville, AL.

9. Paxson, D.E., Perkins D.H. *Thermal Load Considerations for Detonative Combustion-Based Gas Turbine Engines.* AIAA-2004-3396. 40th Joint Propulsion Conference and Exhibit. 11-14 July 2004. Fort Lauderdale, FL.

10. Szetela, E.J. and TeVelde, J.A. *External Fuel Vaporization Study, Phase II Final Report.* UTRC, NASA CR 165513, November 1981.

11. Bartok, W. and Sarofim, A. *Fossil Fuel Combustion – A Source Book.* New York: John Wiley & Sons, 1991.

12. Coordinating Researcy Council (CRC), Inc. *Handbook of Aviation Fuel Properties* (2004 Third Edition). CRC Report No. 635. 2004.

13. PPDS website. *http://www.ppds.co.uk/products/ppds.asp.*

14. National Institute of Standards and Technology. *NIST Thermophysical Properties of Hydrocarbon Mixtures Database (SUPERTRAPP) Users Guide* (Version 3.1). February 2003

15. Henegan, S.P. and Schulz, W.D. *Static Tests of Jet Fuel Thermal and Oxidative Stability*. Journal of Propulsion and Power. Vol. 9, No. 1, Jan-Feb 1993.

16. Spadaccini, L.J., Sobel, D.R., Haung, H., Dardas, Z., Coke *Deposition/Mitigation in Endothermic Fuels – Advanced Fuel Development and Fuel Combustion.* AFRL-PR-WP-TR-1998-2098. June 1998

17. Shchelkin, K.L. *Soviet Journal of Technical Physics*. Vol. 10, pg. 823-827, 1940.

18. Schauer, F., Stutrud, J., and Bradley, R. *Detonation Initiation Studies and Performance Results for Pulsed Detonation Engine Applications.* AIAA 2001-129, 39th AIAA Aerospace Sciences Meeting & Exhibit, 8-11 January 2001, Reno, NV.

19. Tucker, K.C. *A Flash Vaporization System for Detonation of Hydrocarbon Fuels in a Pulse Detonation Engine.* Air Force Institute of Technology (AU), Wright-Patterson AFB OH. YET TO BE PUBLISHED

20. Incropera, F.P. and DeWitt, D.P. *Introduction to Heat Transfer* (Third Edition). New York: John Wiley & Sons, 1996.

21. Glassman, Irvin. *Combustion* (Third Edition). San Diego: Academic Press, 1996.

REPORT DOCUMENTATION PAGE

Form Approved OMB No. 074-0188

1. REPORT DATE *(DD-MM-YYYY)*	2. REPORT TYPE	3. DATES COVERED *(From – To)*
21-03-2005	Master's Thesis	Aug 2003 – Mar 2005

4. TITLE AND SUBTITLE

Pulse Detonation Engine Thrust Tube Heat Exchanger for Flash Vaporization and Supercritical Heating of JP-8

5a. CONTRACT NUMBER

5b. GRANT NUMBER

5c. PROGRAM ELEMENT NUMBER

6. AUTHOR(S)

Miser, Christen, L., Captain, USAF

5d. PROJECT NUMBER

5e. TASK NUMBER

5f. WORK UNIT NUMBER

7. PERFORMING ORGANIZATION NAMES(S) AND ADDRESS(S)
Air Force Institute of Technology
Graduate School of Engineering and Management (AFIT/EN)
2950 Hobson Way
WPAFB OH 45433-7765

8. PERFORMING ORGANIZATION REPORT NUMBER

AFIT/GAE/ENY/05-M11

9. SPONSORING/MONITORING AGENCY NAME(S) AND ADDRESS(ES)
AFRL/PRTC
Attn: Dr. Frederick R. Schauer
Bldg 71A, D-Bay, 7th Street
WPAFB OH 45433 DSN: 785-7439

10. SPONSOR/MONITOR'S ACRONYM(S)

11. SPONSOR/MONITOR'S REPORT NUMBER(S)

12. DISTRIBUTION/AVAILABILITY STATEMENT
APPROVED FOR PUBLIC RELEASE; DISTRIBUTION UNLIMITED.

13. SUPPLEMENTARY NOTES

14. ABSTRACT

Research has shown that performance of liquid hydrocarbon fueled pulse detonation engines is limited by the time required to evaporate liquid fuel droplets within the mixture. Vaporization of liquid fuels prior to injection has been shown to decrease ignition times and also increases fuel efficiency; however, the size and efficiency of the vaporization system used are not feasible for use in future pulse detonation aircraft concepts. The purpose of this research is to harness the waste heat of pulse detonation engine thrust tubes to generate a steady-state, self-sustained flash vaporization and supercritical heating system using JP-8 as the working fluid and fuel.

Using a pulse detonation engine thrust tube mounted heat exchanger, the successful flash vaporization of JP-8 has been demonstrated. Additional testing demonstrated the successful heating of JP-8 to supercritical conditions with fuel injection temperatures over 760 K. All JP-8 flash vaporization and supercritical heating tests were sustained by the heated fuel and run to steady-state conditions. Heat addition rates to the fuel of up to 7.7 kW were achieved during superheated testing. A method for experimentally determining supercritical fluid density is presented based on the findings of the supercritical heating tests.

15. SUBJECT TERMS

Flash vaporize, flash vaporization, supercritical, pulse detonation engine, heat exchanger, JP-8, JP8, liquid hydrocarbon, vaporization, thrust tube, fuel injection, supercritical density, fuel heater, endothermic, finite difference method, waste heat, SUPERTRAPP, surrogate, concentric tube

16. SECURITY CLASSIFICATION OF:			17. LIMITATION OF ABSTRACT	18. NUMBER OF PAGES	19a. NAME OF RESPONSIBLE PERSON
REPORT	ABSTRACT	c. THIS PAGE			Dr. Paul I. King
U	U	U	UU	202	19b. TELEPHONE NUMBER *(Include area code)* (937) 255-6565, ext 4628; e-mail: pking@afit.edu